Pathogenic Mediators in Multiple Sclerosis: GM-CSF and Other T_H Cell-Derived Cytokines

Dissertation

zur

Erlangung der naturwissenschaftlichen Doktorwürde

(Dr. sc. nat.)

vorgelegt der

Mathematisch-naturwissenschaftlichen Fakultät

der

Universität Zürich

von

Felix Jerg Hartmann

aus

Deutschland

Promotionskomitee

Prof. Dr. Burkhard Becher

(Vorsitz und Leitung der Dissertation)

Prof. Dr. Christian Münz

Prof. Dr. Roland Martin

Zürich, 2016

Disclaimer

The thesis was based upon and partly adapted from the following publications:

Multiple sclerosis-associated *IL2RA* polymorphism controls GM-CSF production in human T_H cells
Felix J. Hartmann, Mohsen Khademi, Jehan Aram, Sandra Ammann, Ingrid Kockum, Cris Constantinescu, Bruno Gran, Fredrik Piehl, Tomas Olsson, Laura Codarri & Burkhard Becher

The End of Gating? An introduction to automated analysis of high dimensional cytometry data
Florian Mair*, **Felix J. Hartmann*,** Dunja Mrdjen, Vinko Tosevski, Carsten Krieg and Burkhard Becher. ***Contributed equally**

And partially from the following manuscripts in preparation:

High-Dimensional Mass Cytometry for Extensive Profiling of Pathogenic Mediators in Multiple Sclerosis (working title)
Felix J. Hartmann, Dunja Mrdjen, Edoardo Galli, Lukas Weber, Mark Robinson, Mohsen Khademi, Carsten Krieg, Fredrik Piehl, Tomas Olsson and Burkhard Becher

Immune-Activation in Narcolepsy Revealed by High-Dimensional Mass Cytometry (working title)
Felix J. Hartmann, Raphael Bernard-Valnet, Dunja Mrdjen, Edoardo Galli, Lukas Weber, Mark Robinson, Carsten Krieg, Roland Liblau and Burkhard Becher

Table of Contents

Zusammenfassung

Autoimmunerkrankungen wie Multiple Sklerose (MS) entstehen durch eine deregulierte Immunantwort, bei der Gewebe des eigenen Körpers durch eine Abwehrreaktion angegriffen werden. Im Falle der MS ist das zentrale Nervensystem betroffen was zu einer Vielfalt an neurologischen Symptomen führt. Zur Immunreaktion in MS tragen vielerlei verschiedene Zelltypen bei, wobei sogenannte T-Helfer Zellen eine zentrale Rolle spielen. T-Helfer Zellen schütten eine Reihe unterschiedlicher Substanzen aus, sogenannte Botenstoffe oder Zytokine, um mit anderen Zellen zu kommunizieren und so die Immunantwort zu koordinieren. Durch Forschung im Mausmodell der Multiplen Sklerose konnte gezeigt werden, dass besonders ein Zytokin namens „Granulocyte Macrophage-Colony Stimulating Factor“ (GM-CSF) einen essentiellen Beitrag in der Entstehung dieser Autoimmunerkrankung übernimmt.

In der hier vorliegenden Arbeit konnten wir zeigen, dass T-Helfer Zellen in Multiple Sklerose Patienten vermehrt GM-CSF ausschütten und dass dies mit einem verschlechtertem Krankheitsverlauf einhergeht. Die Produktion von GM-CSF in T-Helfer Zellen wird hauptsächlich durch das Zytokin Interleukin-2 angeregt. Des weiteren zeigt diese Arbeit, dass eine Genvariante im Rezeptor für Interleukin-2 zu einer gesteigerten GM-CSF Produktion führt. Diese Erkenntnis stellt somit einen möglichen molekularen Mechanismus dar, wie diese genetische Variante das Risiko an Multipler Sklerose zu erkranken erhöht.

Im weiteren Verlauf dieser Arbeit wurde die Zytokin-Produktion der T-Helfer Zellen von MS Patienten anhand der neu entwickelten Methode der sogenannten Massen-Zytometrie in einer zuvor unerreichten Dimensionalität untersucht. Dadurch konnten wir einerseits die erhöhte GM-CSF Produktion in MS Patienten bestätigen und zusätzlich eine spezifische Charakterisierung dieser T-Helfer Zellen erstellen. GM-CSF-produzierende T-Helfen Zellen lassen sich in mehrere Subtypen unterteilen, von denen eine spezifische Gruppe, nicht aber die anderen, in MS Patienten erhöht sind.

Zusammengefasst sollen diese Erkenntnisse somit zu einem verbesserten Verständnis der Entstehung der Multiplen Sklerose, sowie möglicherweise zu neuen Therapiemöglichkeiten in deren Behandlung beitragen.

Summary

Autoimmune diseases such as multiple sclerosis (MS) are a result of dysregulated immune mechanisms, leading to the destruction of tissues by the immune system. In the case of MS, the targeted organ is the central nervous system, which leads to the establishment of a heterogeneous set of neurological symptoms in the patients. Multiple lineages of immune cells are involved in this process and especially T-helper (T_H) cells have been shown to play a crucial role. T_H cells are able to direct immune responses and communicate with other cell types via soluble mediators, termed cytokines. Research using an animal model of MS has shown that the initiation of neuro-inflammation is dependent on the T_H cell-derived cytokine "granulocyte macrophage-colony stimulating factor" (GM-CSF).

In this thesis, we report an increased frequency of GM-CSF-producing by T_H cells in MS patients. This elevated GM-CSF production was associated with several biomarkers of disease activity and severity. Further, we found that GM-CSF secretion in human T_H cells is strongly induced by interleukin 2. Additionally, we here show that an MS-associated genetic polymorphism in the interleukin 2 receptor gene specifically increases the frequency of GM-CSF producing T_H cells, thus proposing a possible molecular mechanism of how an immunologically relevant genetic risk factor might translate into an increased risk of multiple sclerosis.

Extending these studies, we employed the recently developed mass cytometry technology to further analyze T_H cell cytokine production in MS patients with a unprecedented high-dimensionality. Firstly, we could validate the increased GM-CSF production in MS patients and further, we were able to perform an in-depth description of these cells. This characterization revealed that GM-CSF producing T_H cell can be divided into several subsets which have been associated with distinct T_H cell lineages. Moreover, we could show that only specific subtypes of these GM-CSF producing T_H cells are elevated in MS patients, thus further refining our understanding of the role of this cytokine in MS.

Together, we hope that these results will add to our knowledge of T_H cell biology in general and especially to our understanding of the pathogenic role of these cells in autoimmune diseases such as MS.

Abbreviations

AML	acute myeloid leukemia
APC	antigen-presenting cell
BSA	bovine serum albumin
CCR	chemokine (C-C motif) receptor
CD	cluster of differentiation
CFSE	carboxyfluorescein succinimidyl ester
CIA	collagen-induced arthritis
CIS	clinically isolated syndrome
CNS	central nervous system
CSF	cerebrospinal fluid
CSF2	colony-stimulating factor 2
CSM	cell staining medium
CyTOF	cytometry by time-of-flight
DC	dendritic cell
DMSO	dimethyl sulfoxide
DNA	deoxyribonucleic acid
DOTA	1,4,7,10-tetraazacyclododecane-1,4,7,10-tetraacetic acid
DTPA	diethylene triamine pentaacetic acid
EAE	experimental autoimmune encephalomyelitis
EBV	Epstein-Barr virus
EDTA	ethylenediaminetetraacetic acid
ELISA	enzyme-linked immunosorbent assay
FACS	fluorescence-activated cell sorting
FCS	fetal calf serum
GM-CSF	granulocyte-macrophage colony stimulating factor
GWAS	genome-wide association study
HLA	histocompatibility leukocyte antigen
ICP	inductively coupled plasma
IFN-γ	interferon gamma
Ig	immunoglobulin
IL	interleukin
K	Kelvin
k-NNG	k nearest neighbor graph
LPS	lipopolysaccharide
MAPK	mitogen-activated protein kinase
MHC	major histocompatibility complex
MMP9	matrix metalloproteinase 9
MRI	magnetic resonance imaging
MS	multiple sclerosis
NFκB	nuclear factor kappa-light-chain-enhancer of activated B cells
NFL	neurofilament-light chain
NK cell	natural killer cells
NLDR	non-linear dimensionality reduction
OND	other neurological diseases
PAP	pulmonary alveolar proteinosis
PBMC	peripheral mononuclear cells
PBS	phosphate buffered saline
PCA	principle component analysis
PCR	polymerase chain reaction
PFA	paraformaldehyde
PMA	phorbol 12-myristate 13-acetate
PPMS	primary-progressive MS
QC	quality control
RA	rheumatoid arthritis
RNA	ribonucleic acid
ROS	reactive oxygen species
RRMS	relapse-remitting MS
SNP	single-nucleotide polymorphism
SPADE	spanning-tree progression analysis of density-normalized events
SPMS	secondary-progressive MS
STAT	signal transducer and activator of transcription
t-SNE	t-stochastic neighbor embedding
TCR	T cell receptor
TGF-β	transforming growth factor beta
TH	T-helper
TNF-α	tumor necrosis factor alpha
TOF	time-of-flight

1. Introduction

1.1. Clinical features of multiple sclerosis

First described almost 180 years ago (Carswell 1838), multiple sclerosis (MS) is one of today's most prevalent autoimmune diseases, affecting almost 10'000 patients in Switzerland (Pugliatti et al. 2006) and about 2.5 million worldwide. MS is a chronic inflammatory disorder of the central nervous system (CNS) i.e. the brain and spinal cord. A hallmark of MS are so called lesions or plaques which are found in the white and grey matter of the CNS and which represent areas of demyelination and loss of oligodendrocytes (Figure 1). These lesions are caused by immune infiltration and inflammation, resulting in demyelination, gliosis and ultimately neuroaxonal degeneration (Dendrou et al. 2015).

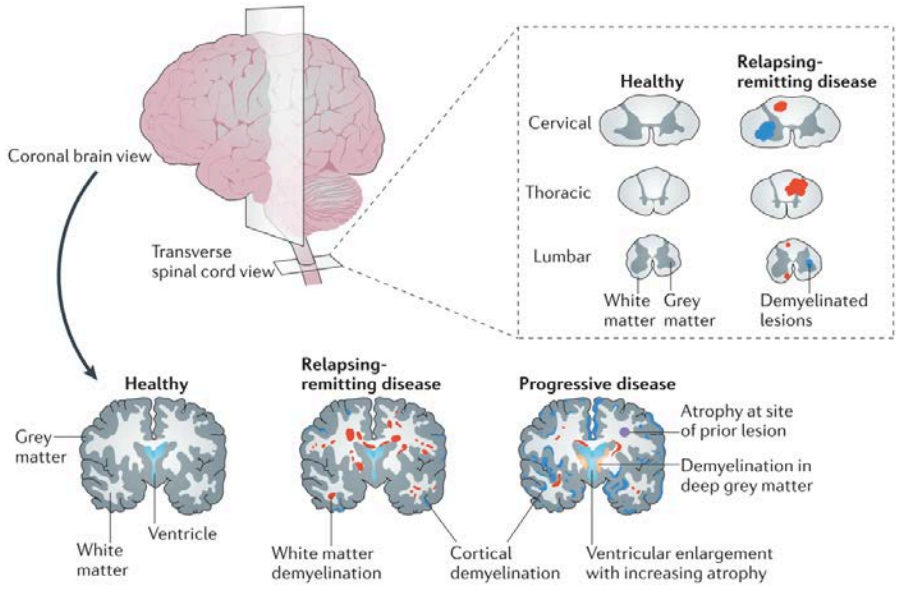

Figure 1. Pathological lesions in the CNS are a hallmark of MS. Multiple sclerosis pathology is characterized by confluent demyelinated areas in the white and grey matter of the brain and spinal cord that are called plaques or lesions and that indicate a loss of myelin sheaths and oligodendrocytes. Figure and legend adapted from (Dendrou et al. 2015).

MS presents with a heterogeneous set of clinical features. Frequently observed signs are cognitive impairments like attention deficits, fatigue, visual disturbances such as reduced color vision and acuity as well as affection of motor functions manifesting as poor balance, limb incoordination or spasms (Compston and Coles 2008).

1.1.1. Diagnosis and clinical course

The common age of onset for MS is usually around 30 years (McFarlin and McFarland 1982a; McFarlin and McFarland 1982b). The majority of patients present in the clinics with a first acute episode known as the clinically isolated syndrome (CIS; Figure 2). The diagnosis of MS is mostly based on the presented neurological symptoms, however magnetic resonance imaging (MRI) can provide further evidence by detecting the dissemination of white matter lesions in space and time. Additionally, about 90% of MS patients show presence of oligoclonal bands after electrophoresis of the cerebrospinal fluid (CSF), which can be used to support an initial diagnosis.

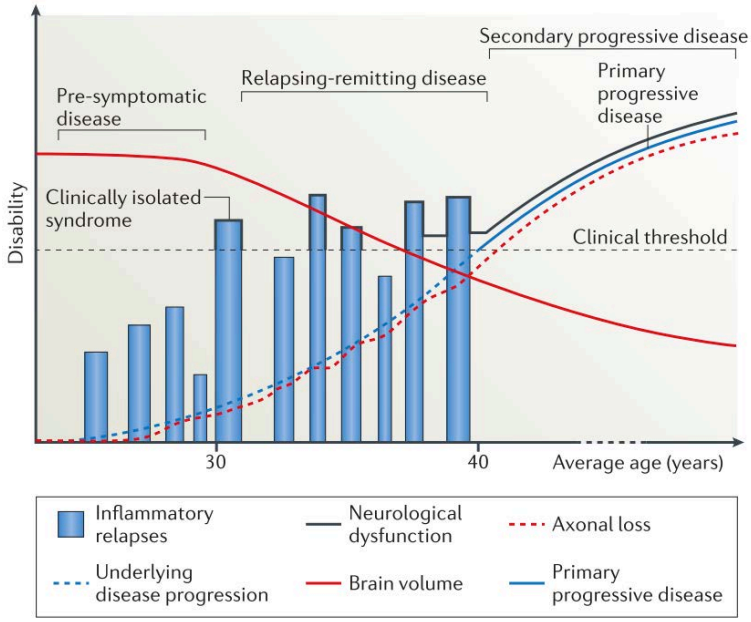

Figure 2. Heterogeneity of multiple sclerosis. Shown are the progression of disability over time for different forms of MS. Figure and legend adapted from (Dendrou et al. 2015).

Following the initial acute episode, most patients (circa 85%) develop a relapse-remitting form of the disease (relapse-remitting MS; RRMS) in which relapses occur erratically and are followed by a period of clinical recovery. However, with time the improvements from these relapses remains incomplete and symptoms accumulate (Figure 2). Eventually, the majority of patients transition to secondary progressive MS (SPMS) which represents a stage of the disease with a more steady progression and less pronounced or no relapses as compared to RRMS. About 10-15% of patients with

MS experience no distinct relapses and instead present with a gradually increasing neurological disability directly from the onset of the disease, thus termed primary-progressive MS (PPMS) (Miller and Leary 2007).

1.1.2. Treatment

Currently approved MS therapeutics mostly are mostly aimed at reducing immune activation and infiltration into the CNS. Early drugs such as interferon-β (Ebers 1998), glatiramer acetate (Comi et al. 2001) and the more recently approved dimethyl fumarate (Fox et al. 2012) are general immunomodulators with unclear mechanisms of action. Glucocorticoids have general anti-inflammatory and immunosuppressive properties and are thus used to treat acute attacks. Two other approved therapeutics, mitoxantrone (Hartung et al.) and teriflunomide (O'Connor et al. 2011) interfere with DNA synthesis and thus probably limit T cell proliferation. Acting more specific, natalizumab is an approved mAb directed against the integrin VLA4 (Polman et al. 2006). It effectively inhibits T cell infiltration into the CNS (>65% reduction of relapses and >90% reduction of new inflammatory lesions) but bears the risk of opportunistic John Cunningham (JC) virus reactivation which leads to potentially life-threatening progressive multifocal leukoencephalopathy (PML) (Bloomgren et al. 2012). Fingolimod (Cohen et al. 2010), a functional antagonist of the sphingosine 1-phospate (S1P) receptor inhibits lymphocyte egress from the lymph nodes. Recently, a humanized monoclonal α-CD52 antibody (termed alemtuzumab) has been approved for MS therapy (Cohen et al. 2012). Alemtuzumab depletes T as well as B cells and is highly effective in suppressing MS inflammatory activity. To date, there are however no effective drugs for the treatment of SPMS or PPMS.

Taken together, the newly approved therapies have a good efficacy, however they are often accompanied by side effect such as PML or other flu like infections. Thus research into more specific therapies is still essential.

1.2. Risk factors of multiple sclerosis

1.2.1. Genetic risk factors

MS is a multifactorial disease triggered by environmental factors in individuals with genetic predisposition. For example the substantially increased risk among relatives and the concordance rate of 30% between identical twins indicate that genetic factors strongly influence the disease susceptibility (Oksenberg et al. 2008). Recent genome wide association studies (GWAS) have identified around 110 distinct genetic regions to be reliably associated with multiple sclerosis (Figure 3a) (Hafler et al. 2007; Sawcer et al. 2011; Beecham et al. 2013). Together, genetic variation accounts for approximately 30% of the total disease risk (Beecham et al. 2013).

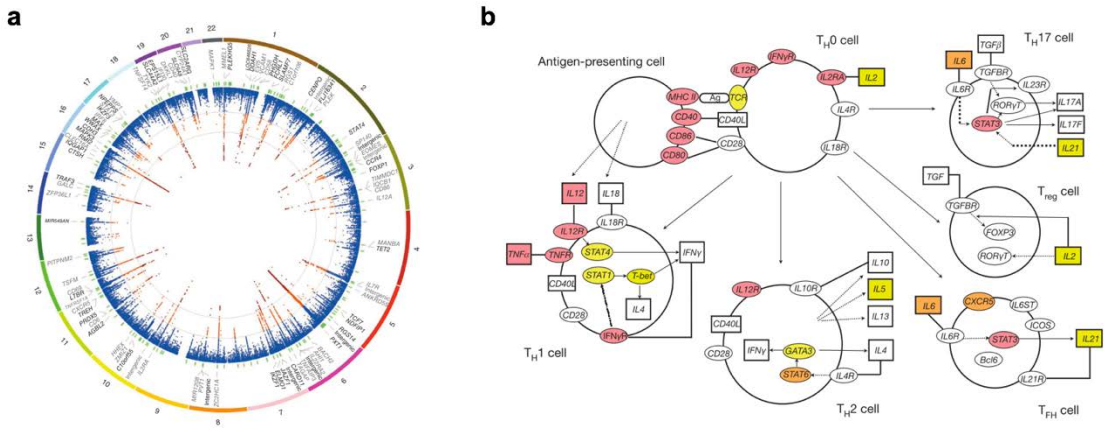

Figure 3. Genetic risk factors for multiple sclerosis. a) Discovery phase results. Circos plot showing primary association analysis of 161,311 autosomal variants in the discovery phase (14,498 cases and 24,091 healthy controls). The outermost track shows the numbered autosomal chromosomes. The second track indicates the gene closest to the most associated SNP meeting all replication criteria. The third track indicates the physical position of the 184 fine-mapping intervals (green). The innermost track indicates −log(P) (two-sided) for each SNP (scaled from 0–12, which truncates the signal in several regions; Additionally, contour lines are given at the a priori discovery (−log(P) = 4) and genome-wide significance (−log(P) = 7.3) thresholds. Orange indicates −log(P) ≥ 4 and <7.3, and red indicates −log(P) ≥ 7.3. b) Graphic representation of the T_H-cell differentiation pathway. Colored nodes are those containing a gene implicated by proximity to an SNP showing evidence of association. Red, strong evidence; orange discovery P value < 1 x $10^{-4.5}$; yellow discovery P value < 1 x 10^{-3}. Figure and legend adapted from a) (Beecham et al. 2013) and b) (Sawcer et al. 2011).

The majority of MS-associated genetic variants are found within immunologically relevant regions. Particularly single-nucleotide polymorphisms (SNPs) in genes involved in T_H cell activation and maturation are over-represented in MS (Figure 3), thus specifically implicating the differentiation and polarization of T_H cells in MS pathogenesis.

1.2.1.1. HLA-DR

As for other autoimmune diseases, the strongest genetic associations found for MS lie within the major histocompatibility complex (MHC; histocompatibility leukocyte antigen (HLA) in humans). The contribution of the HLA associations are thought to account for 10%–60% of the genetic risk of MS (Haines et al. 1998). More specifically, the strongest risk factors are found within class II risk genes, especially HLA-DRB1*15:01. This contribution has been observed in many different populations and increases risk for RRMS as well as PPMS (Oksenberg et al. 2008). Risk of MS is increased approximately threefold for heterozygote and sixfold for homozygote carriers (Sadovnick 2012). Weaker contributions stem from HLA-DRB1*03:01 and HLA-DRB1*13:01 as well as some class I alleles (Moutsianas et al. 2015). How these HLA genes confer risk for MS on a mechanistical level remains elusive.

1.2.1.2. Interleukin 2 receptor alpha (*IL2RA*)

Besides the HLA region, polymorphisms in the *IL2RA* are the most strongly associated factors in MS (Figure 3, p.4). IL-2 is a 15-kDa cytokine with pleiotropic functions in promoting T_H cell differentiation and effector responses, as well as mediating immune tolerance via regulatory T (T_{reg}) cells. IL-2 can bind either to its high-affinity receptor, which is composed of three subunits, IL-2Rα (CD25), IL-2Rβ (CD122) and the common γ-chain (γ_c or CD132), or to the intermediate affinity receptor consisting of the heterodimer of the IL-2Rβ and γ_c (Rochman et al. 2009). Importantly, IL-2 signaling has been explored a potential target for MS therapy. Attenuation of IL-2 receptor signaling by monoclonal antibodies against the IL-2Rα (daclizumab) was shown to be effective by reducing annualized relapse rate and the number of gadolinium-enhanced lesions and ameliorating clinical symptoms in clinical trials for MS (Bielekova et al. 2004; Rose 2012; Wiendl and Gross 2013; Pfender and Martin 2014).

Polymorphisms in the *IL2RA* and especially one variant located in the first intron (rs2104286) have repeatedly been shown to be associated MS and also other autoimmune diseases such as rheumatoid arthritis (RA) and type 1 diabetes (T1D). For MS, the odds ratio has been reported to be around 1.2 (Hafler et al. 2007). A second polymorphism within the *IL2RA* (rs12722489) has been implicated previously

but dismissed by recent fine mapping studies (Beecham et al. 2013). Both SNPs have been previously shown to be associated with serum concentrations of soluble IL-2RA (sIL-2RA) (Maier et al. 2009b). However, the correlation was inconsistent with differential modifications of risk for different associated autoimmune diseases, thus most likely not providing a possible pathogenic mechanism for how this genetic variant increases risk of MS.

1.2.2. Environmental risk factors

Besides genetic factors, environmental, lifestyle and dietary factors have been identified as risk factors for MS (Ascherio et al. 2012). One specific risk factor is chronic infection with the Epstein-Barr virus (EBV), a human herpes virus. This infection is common and usually happens early in life without displaying major symptoms. When primary infection occurs later in life, it causes acute febrile illness, known as infectious mononucleosis. A history of infectious mononucleosis has been reported to increase the risk for MS approximately two- to threefold (Thacker et al. 2006). It is however unknown whether these two phenomena might have a common origin, such as good hygiene in childhood, commonly referred to as the hygiene hypothesis (Bach 2002). The possible mechanisms which could link EBV infection and MS are still unknown, however multiple scenarios such as increased activation and survival of B and T cells or immortalization of B cells and autoantibody production have been proposed (Ascherio et al. 2012). Another environmental factor influencing MS risk is lack of sunlight exposure and thus lack of vitamin D production. Vitamin D in turn has been shown to posses multiple effects on various parts of the immune system, *e.g.* regulatory T cells (Ascherio and Munger 2007). Lastly, cigarette smoking increases MS risk approximately by 50%, directly correlating with smoking intensity and duration (Riise et al. 2003).

1.3. The immune system in multiple sclerosis

MS is strongly considered to be an autoimmune disease and various leukocyte populations have been shown to be involved in its pathogenesis.

1.3.1. Helper T cells

T_H cells are at the center of the adaptive immune response. They recognize antigens presented on MHC class II molecules on the surface of professional antigen presenting cells (APCs). Once activated, they can execute multiple functions such as providing help to activate B cells to secrete antibodies (see 1.3.4), activating and maturing other myeloid cells to sustain the immune response (see 1.3.5) or assist in the activation of cytotoxic T cells to kill infected target cells (see 1.3.2). In order to perform this plethora of functions, naive T_H cells undergo a functional diversification, which is usually dependent on the cytokine signals which they receive during their activation by APCs (O'Shea and Paul 2010). An overview of different proposed T_H cell subsets and a simplified list of associated cytokines is shown in Figure 4.

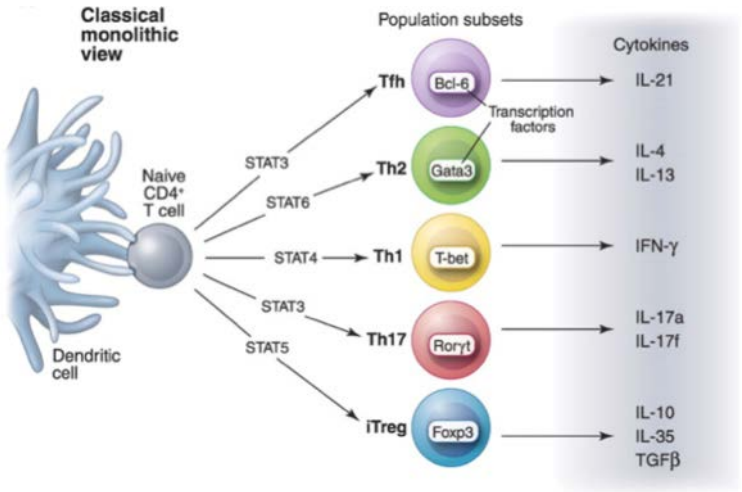

Figure 4. T_H cell differentiation and cytokine production. The classical monolithic view: lineages and master regulators. Initial studies arising from in vitro cultured T_H1 and T_H2 cells led to the idea that these subsets behaved like lineages, meaning that their phenotype (i.e., selective cytokine production) was inflexible. Accordingly, these subsets expressed lineage-defining transcription factors that were sufficient to impart this selective cytokine production. As newer subsets of cytokine producing cells were identified, they too were viewed as stable lineages. Figure and legend adapted from (O'Shea and Paul 2010).

Initially, T_H cells were roughly distinguished into T_H1 cells which in turn activate myeloid and cytotoxic T cells and T_H2 cells which help stimulate B cells to produce a wide range of antibodies. These different lineages are defined by the pattern of the soluble cytokines which they produce. T_H1 cells were found to express interferon gamma (IFN-γ), interleukin-2 (IL-2) and tumor necrosis factor-beta (TNF-β). On the other hand, T_H2 cells were reported to express cytokines such as IL-4 and IL-13, but also IL-5, IL-6, IL-9 and IL-10 (Romagnani 2000). Subsequently, further T_H cell subsets have been proposed. Induced regulatory T (iT_{REG}) cells were found to express transforming growth factor beta (TGF-β) and IL-10 while T_H17 cells were reported to produce IL-17A, IL-17F, IL-21 and IL-22 as well as GM-CSF. More recently, it has been shown that T_H17 cells also express cytokines traditionally associated with other T_H subsets, such as IFN-γ and IL-10 (Zielinski et al. 2012). Additionally, further subsets have been described: T_H9 cells (Schmitt et al. 2014), expressing mainly IL-9 as well as IL-10 and IL-21, and follicular T helper (T_{FH}) cells (Crotty 2011) expressing IL-21, but also an array of cytokines associated with other T_H cell subsets. Lastly, a subset of T_H22 cells has been proposed, characterized by the expression of IL-22 and TNF-α (Eyerich et al. 2009).

In MS, T_H cell activation, differentiation and cytokine production are believed to be the key pathogenic mechanisms. Evidence for this includes the fact that transfer of $CD4^+$ T cells from diseased mice is sufficient to initiate EAE in healthy recipient animals (Ben-Nun et al. 1981), the strong genetic connection with the MHC class II locus and other T_H cell-associated genes (see 1.2.1) and the effectiveness of several T cell directed therapies (see 1.1.2). It is hypothesized that autoreactive T_H cells become activated, either by molecular mimicry, bystander activation or the co-expression of T cell receptors (TCRs) with different specificities and then migrate to the CNS (Dendrou et al. 2015). The exact nature of the T_H cell polarization pattern following activation in MS has been the focus of intense research for several decades (Becher and Segal 2011). Initially T_H1 cells had been identified as potential pathogenic mediators, followed by T_H17 cells. Surprisingly however, both signature cytokines IFN-γ and IL-17A are not essential for the development of neuroinflammation in animal models (Codarri et al. 2011).

1.3.2. Cytotoxic T cells

Cytotoxic T cells are MHC class I restricted cells which protect against viruses or other intracellular pathogens by killing infected cells. Interestingly, $CD8^+$ T-cells are abundantly found in human MS lesions (Booss et al. 1983) and thus believed to be involved in MS pathology (Salou et al. 2015). MHC class I alleles are also associated with MS, although to a lesser extent than MHC class II. The functional roles of $CD8^+$ T cells in MS remain controversial and research in animal models has mostly focused on $CD4^+$ T cells. Several reports exist showing that similar to $CD4^+$ T cells, myelin-specific $CD8^+$ T cells were also able to induce CNS autoimmunity in mice (Sun et al. 2001; Huseby et al. 2001). However, $CD8^+$ T cells might also exert regulatory functions in the context of multiple sclerosis as has been suggested by several studies (Sinha et al. 2015).

1.3.3. γδ T cells

γδ T cells are cells with features of both, the innate as well as the adaptive arm of the immune system. They are found in human blood to some extent, but in much higher frequencies in several other sites such as mucosal tissues or dermis where they produce cytokines that regulate pathogen clearance, inflammation and tissue homeostasis (Bonneville et al. 2010). γδ T cells have been implicated in several autoimmune diseases, such as systemic lupus erythematosus (SLE), RA (Su et al. 2013) and also in models of psoriasis (Cai et al. 2011; Pantelyushin et al. 2012). In MS patients, γδ T cells were also found in CNS lesions, however whether this has functional consequences for the disease development remains unclear (Blink and Miller 2009).

1.3.4. B cells

B cells represent the humoral arm of the adaptive immune system. Their main function is the production of antibodies which then specifically bind their antigen, thus either directly neutralizing pathogenic particles or indirectly facilitating the phagocytosis of microbes by other immune cells. Additionally, B cells can perform further effector functions such as antigen presentation and cytokine production.

Increasing evidence suggests that B cells also partake in MS pathogenesis. Their levels are elevated in both, the CNS and the CSF of MS patients (Cepok et al. 2001). Oligoclonal bands derived from CSF IgG are a hallmark of MS diagnosis and IgG is also frequently found in MS lesions (Lucchinetti et al. 2000). Additionally, highly B cells-enriched, germinal center-like structures have been observed in the meninges of RRMS and SPMS patients (Magliozzi et al. 2007). A critical functional role for B cells is also supported by clinical trials directly targeting B cells. Firstly, depletion of B cells using the anti-CD20 monoclonal antibody rituximab has shown significant clinical activity in MS patients (Hauser et al. 2008). Similarly, the follow-up α-CD20 antibody ocrelizumab (Kappos et al. 2011) is currently being investigated in phase III trials, again showing substantial clinical efficacy.

1.3.5. Mononuclear phagocytes

The mononuclear-phagocyte system (MPS) comprises cells of the myeloid lineage, specifically macrophages, dendritic cells (DCs) and monocytes (Hume 2006; Guilliams et al. 2014). Collectively, they perform various functions such as tissue remodeling and homeostasis as well as antigen presentation and other stimulatory or regulatory immune influences (Yona and Jung 2010). Antigen-presentation is essential for the initial activation of T_H cells in animal models of neuroinflammation and myeloid cells constitute a large fraction of CNS invading cells in EAE as well as in MS, suggesting local re-activation of infiltrating lymphocytes. Additionally, monocyte-derived cells were suggested to actively participate in demyelinative processes (Yamasaki et al. 2014). Neuronal function can also directly be impaired by reactive oxygen species (ROS) or other oxidative stress and mononuclear cells of MS patients have been shown to produce increased amounts of ROS (Vladimirova et al. 1999).

1.3.6. Other innate immune cells

Neutrophils are an abundant type of granulocyte which quickly traffic to sites of infection where they perform antimicrobial functions and contribute to the activation of other immune cells. They have been shown to posses an activated phenotype in MS

(Naegele et al. 2012) and several neutrophil-related factors have been proposed as potential biomarkers in MS (Rumble et al. 2015).

Natural killer (NK) cells are cells of the innate immune system which can release cytokines and perform cytotoxic functions such as killing of virally infected cells and tumor cells. Changes of NK cell functionality in MS were associated with MS activity, and depletion of NK cells exacerbated EAE (Zhang et al. 1997). Additionally, it has been reported that several MS therapies, such as interferon-β, glatiramer acetate, fingolimod, daclizumab, or mitoxantrone seem to affect NK cell functionality (Chanvillard et al. 2013).

1.4. Granulocyte-macrophage colony stimulating factor

1.4.1. The biology of GM-CSF

Granulocyte-macrophage colony stimulating factor (GM-CSF) or CSF2 is a pleiotropic cytokine that belongs to the CSF family of growth factors. Secreted by different cell types, GM-CSF can affect a variety of cells such as hematopoietic progenitor cells and many innate immune populations (Wicks and Roberts 2015). It is part of the colony-stimulating factor (CSF) family of growth factors. Initially, it was described to induce in vitro differentiation of hematopoietic progenitor cells into colonies comprising granulocytes and macrophages. Mice deficient in the *Csf2* gene develop normally apart from lacking alveolar macrophages (Guilliams et al. 2013), a reduction in the number of eosinophils (Becher et al. 2014) and reduced CD103 expression by BATF3 dependent dendritic cells (Edelson et al. 2011). The lack of lung alveolar macrophages leads to surfactant deposition in the lungs, a phenotype which resembles human pulmonary alveolar proteinosis (PAP) and which has also been linked with GM-CSF specific autoantibodies (Sakagami et al. 2009).

1.4.2. Cellular sources of GM-CSF

GM-CSF can be produced by a wide array of different immune cells, among them most prominently T cells and B cells, but also non-hematopoietic cells such as endothelial and pulmonary epithelial cells (LeVine et al. 1999) or osteoblasts and

tumor cells. The factors driving the production of GM-CSF by T cells are not yet fully understood and reports have been contradictory. Early studies indicated that IL-2 or IL-1β could increase GM-CSF production by human T cells (Burdach et al. 1991; Kruger et al. 1996). Using murine T cells, two studies demonstrated that IL-23 might be able to induce GM-CSF (Codarri et al. 2011; El-Behi et al. 2011), whereas later reports indicate the involvement of STAT5-inducing cytokines such as IL-7 (Sheng et al. 2014) or STAT4 inducers like IL-12 (McWilliams et al. 2015). Additionally, the transcription factor basic helix–loop–helix (bHLH) 40 (Bhlhe40) has been proposed to regulate GM-CSF production by murine T_H cells (Lin et al. 2014).

1.4.3. GM-CSF receptor signaling

GM-CSF binds to the heterodimeric GM-CSF receptor (GM-CSFR) which is mainly found on cells of the myeloid lineage and their progenitors. The GM-CSFR is comprised of a low affinity ligand-binding α-chain and a signal-transducing β-chain, which is shared with the receptors for IL-3 and IL-5 (together known as the β-chain family of cytokines). GM-CSF binding to its receptor induces signal transducer and activator of transcription 5 (STAT5) and STAT3 phosphorylation (Hercus et al. 2013). Further downstream, activation of mitogen-activated protein kinases (MAPKs), phosphatidylinositol 3 kinase (PI3K)–Akt and NFκB can occur.

1.4.4. Cellular targets and effects of GM-CSF

As indicated above, GM-CSF acts on a variety of cells (Figure 5). Firstly, it has been shown to promote bone marrow production of neutrophils and eosinophils (Metcalf 2008) as well as activation of neutrophils and induction of several neutrophil effector functions. Other prominent cell types sensing GM-CSF are monocytes and macrophages. Again, GM-CSF stimulates their production in the bone marrow and regulates functions of differentiated cells such as maturation, survival and proliferation (Hamilton 2008). In the context of autoimmune neuroinflammation, GM-CSF has been recently demonstrated to be critical in driving an inflammatory signature in monocytes (Croxford et al. 2015). GM-CSF has also been shown to stimulate phagocytosis, induce upregulation of MHC class II and pattern recognition

receptors (PPRs), stimulate antigen processing and presentation and promote cell adhesion and chemotaxis (Wicks and Roberts 2015). Furthermore, GM-CSF has been shown to control the homeostasis of non-lymphoid tissue DCs (Greter et al. 2012). Systemic administration of GM-CSF leads to the mobilization of monocytes and other myeloid populations from the bone marrow to the blood and also primes them for an increased *in vitro* response to other stimuli, such as LPS (Hamilton 2008).

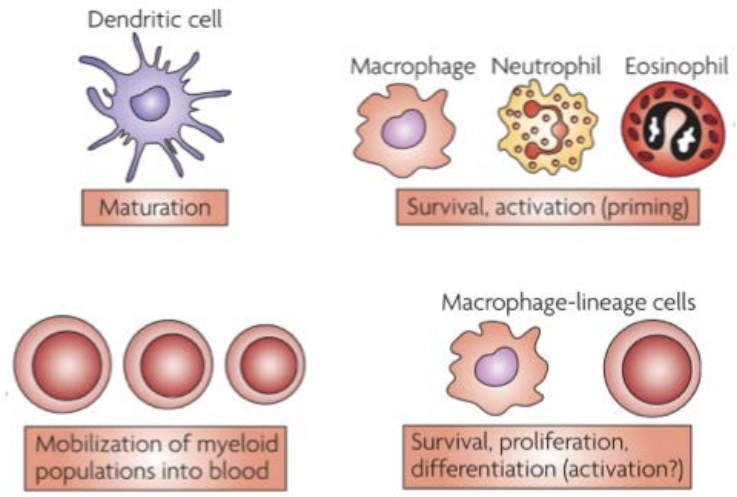

Figure 5. The main functions of GM-CSF in the steady state and during inflammation. In vitro, in addition to the different effects of GM-CSF on immature myeloid precursor cells, GM-CSF can promote the survival and activation of macrophages, neutrophils and eosinophils, as well as dendritic-cell maturation. Data from GM-CSF-deficient indicate that in the steady state GM-CSF, although restricted in expression, is crucial for the maturation of alveolar macrophages and invariant natural killer T (iNKT) cells.. Upon systemic administration or when the levels of these CSFs are increased, for example during inflammation or in response to infection, the CSFs can mimic their in vitro effects but also mobilize myeloid populations and their precursors into the blood, as well as precursor populations from other lineages (not shown). Figure and legend modified from (Hamilton 2008).

1.4.5. GM-CSF in autoimmune neuroinflammation

GM-CSF has also been proposed to be an important cytokine in autoimmune neuroinflammation. Firstly, cerebrospinal fluid (CSF) levels of GM-CSF have been shown to be increased in MS patients (Carrieri et al. 1998). Critically, administration of recombinant human GM-CSF to MS patients worsened their symptoms and induced relapses (Openshaw et al. 2000). Investigating the role of GM-CSF in murine models of neuroinflammation, it was shown that animals deficient in the GM-CSF (*Csf2*) gene are resistant to experimental autoimmune encephalomyelitis (EAE) (McQualter et al. 2001). Subsequent reports demonstrated that it is GM-CSF production by T cells which is critical for the establishment of the disease (Marusic et

al. 2002; Ponomarev et al. 2007; Codarri et al. 2011; El-Behi et al. 2011). Treatment of mice with neutralizing antibodies against GM-CSF (α-GM-CSF) ameliorated the disease (McQualter et al. 2001) and protected against relapses (Codarri et al. 2011). Early-phase clinical trials with α-GM-CSF antibodies in MS patients showed first indications of potential therapeutic effects (Constantinescu et al. 2015).

1.4.6. GM-CSF in rheumatic and other autoimmune diseases

GM-CSF levels are increased in the synovial fluid and blood of rheumatoid arthritis (RA) patients (Fiehn et al. 1992) and administration of GM-CSF to RA patients worsened the symptoms (Hazenberg et al. 1989). Additionally, recent reports have shown an increased risk for RA with genetic variants of the *CSF2* gene (Okada et al. 2014). Mice deficient in the *Csf2* gene are protected from collagen-induced arthritis (CIA) (Campbell et al. 1998) and antibodies against GM-CSF or its receptor have been shown to reduce disease symptoms in the preclinical model as well as in RA patients (Burmester et al. 2011; Burmester et al. 2013).
Furthermore, GM-CSF has been implicated to play a critical role in the pathogenesis of myocarditis (Sonderegger et al. 2008), as well as interstitial lung disease, colitis (Benham et al. 2014) and allergic airway disease (Ritz et al. 2002).

1.5. Emerging cytometry technologies

1.5.1. History developments in flow cytometry

2015 marked the 50-year anniversary of the publication of the first cell sorter, a device that was able to separate cells in suspension based on their difference in volume (Fulwyler 1965) as well as the first cytometry-based cell analyzer (Kamentsky et al. 1965). Shortly after that, the first sorter that could discriminate cells based on fluorescence was developed (Gödhe 1968; Wilder and Cram 1977), and this seminal work marked the advent of flow cytometry as a widely used, single-cell analysis technique driving the identification of all major immune cell subsets known today (Wilder and Cram 1977; De Rosa et al. 2001). These days, many laboratories are equipped with flow cytometers capable of detecting 10-20 parameters (Perfetto et al. 2004), revealing an ever-increasing diversity within established cellular subsets. However, traditional flow cytometry is based on fluorochromes and thus limited in the number of antigens to be investigated simultaneously by spectral overlap. To address this issue, an alternative cytometry-based technique has been recently developed and termed mass cytometry.

1.5.2. The principle of mass cytometry

Mass cytometry is based on the idea to couple the single-cell analysis approach of traditional flow cytometry with a mass spectrometric detection system (Bandura et al. 2009; Bendall et al. 2012; Tanner et al. 2013). The general principle of mass cytometry and a typical workflow are outlined in Figure 6. Employing a mass spectroscopy as a quantification system thus eliminates problems in fluorescence-based cytometry which are associated with spectral overlap. With mass cytometry, it is thus possible to simultaneously measure the expression level of approximately 50 proteins on a single cell. Future developments in the available probes would allow theoretically more than 100 parameters/cell.

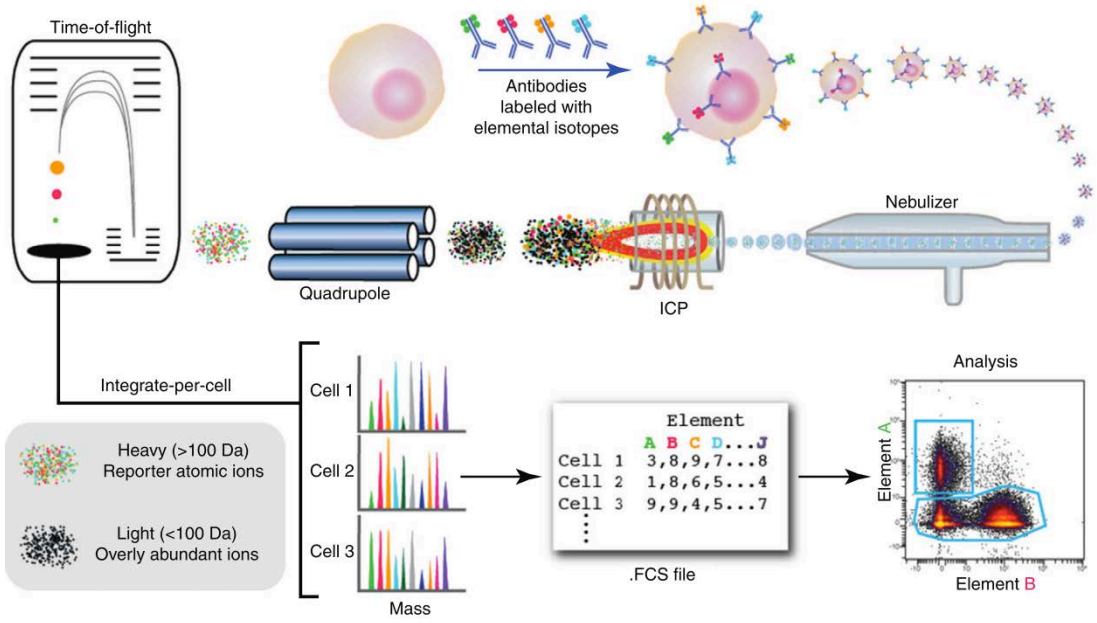

Figure 6. Mass cytometry allows single-cell atomic mass spectrometry of heavy elemental (>100 Da) reporters. Schematic of ICP-MS-based analysis of cellular markers. An affinity product (e.g. antibody) tagged with a specific element binds to the cellular epitope. The cell is introduced into the ICP by droplet nebulization. Each cell is atomized, ionized, overly abundant ions removed, and the elemental composition of remaining heavy elements (reporters) is determined. Signals corresponding to each elemental tag are then correlated with the presence of the respective marker and analyzed using conventional cytometry platforms. Figure and legend taken from (Bendall et al. 2012).

1.5.2.1. Heavy-metal tagged antibodies

In analogy to flourescence cytometry, which mostly uses fluorescently labeled antibodies as probes, mass cytometry probes are commonly antibodies tagged with rare earth metals (Baranov et al. 2002) which are then quantified by time-of-flight (TOF) mass spectroscopy. These elements are stable, non-radioactive and usually not found in biological systems, thus giving virtually no biological background (Figure 7). Tagging of the antibodies is achieved by complexing the desired ions in metal-chelating polymers (Lou et al. 2007; Majonis et al. 2010). Prominent polymeric chelators at the moment are based on DTPA (diethylene triamine pentaacetic acid) and DOTA (1,4,7,10-tetraazacyclodode-cane-1,4,7,10-tetraacetic acid). Polymers can be attached to reduced disulfides in the Fc region of an antibody. Attaching 3-4 polymers to one antibody, about 100 metal ions can be coupled to a single antibody (Ornatsky et al. 2010). The currently used polymers best chelate ions with a positive charge of three, however future developments of chelators for ions with a positive charge of two could further increase the panel of possible elements usable in mass cytometry.

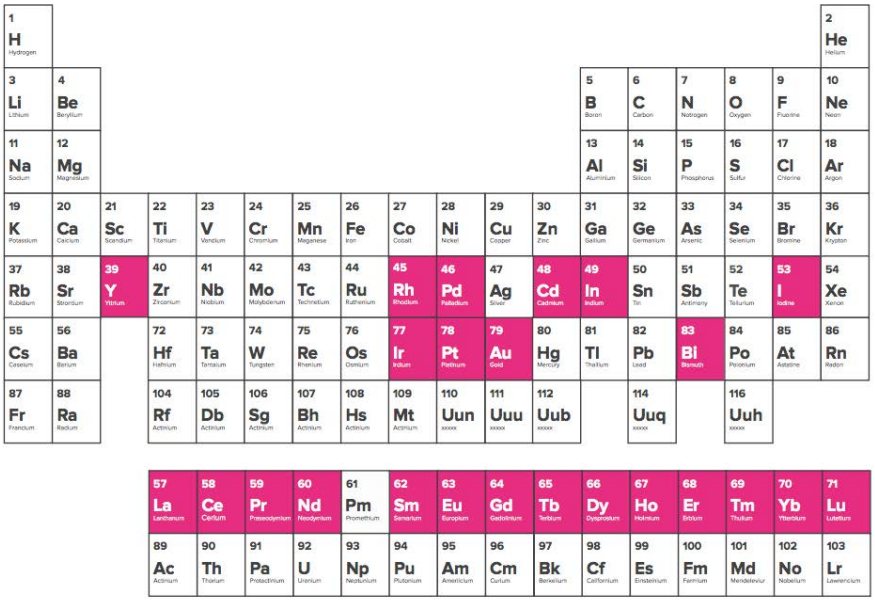

Figure 7. Heavy metal isotopes currently available for mass cytometry. The stable isotopes of these 24 elements provide over 50 unique tags for use in mass cytometry. Figure and legend taken from Fluidigm.

1.5.2.2. Mass spectrometric detection system

Heavy-metal conjugated antibodies can then be used to stain the cells of interest following standard staining procedures. The stained cells are then injected into the mass cytometer where they reach a nebulizer creating single-cell droplets which, are then introduced into an inductively coupled plasma (ICP). This high-temperature ICP (up to 7000°K) vaporizes, atomizes and subsequently ionizes the cells (Bandura et al. 2009). The resulting ion cloud is then filtered through a quadrupole which allows only heavy-metal ions to pass but blocks ions of biological elements commonly found in cells. Lastly, the ion cloud is quantified by a time-of-flight (TOF) mass analyzer and the data is stored in the flow cytometry standard (*.fcs) file format which is compatible with standard flow cytometry data analysis software.

1.6. Analysis of high-dimensional cytometry data

1.6.1. Limitations of manual data analysis

While both fluorescence-based flow cytometry as well as mass cytometry provide a technological platform to interrogate the immune system at a previously unprecedented level (Bendall et al. 2012), scientific progress depends on our ability to analyze and comprehend the resulting data in a meaningful way. Historically, flow cytometric data was - and still is - analyzed using a series of two-dimensional plots and manual gating, i.e. drawing regions of interest (gates) on a plot and either examining that subset on a different bivariate plot, or reporting a certain qualitative measure (cell subset is present or absent, or its relative proportion) or quantitative measure. While this approach is still adequate for many experimental settings, it suffers from several serious shortcomings. First, it is not easily scalable, as the number of two-dimensional plots increases exponentially with the number of measured parameters (i.e. an 18-parameter experiment would require a total of 153 two-dimensional plots to display every marker combination) and thus cannot be easily comprehended anymore. Second, it has been shown by many multi-center studies, such as the Human Immune Genome Project, that manual gating is one of the largest variables in the outcome of a flow cytometry-based experiment (Maecker et al. 2012). Third, every manual gating approach relies on the researcher's prior knowledge, thus introducing a bias towards "expected" results. Due to this focus, much of the potentially relevant and novel information within the dataset might not be recognized and could end up being ignored.

1.6.2. Setting the stage for alternatives

The above-mentioned problems were already recognized some years ago, and several independent groups have started to develop computational methods that automatically identify populations in multidimensional flow cytometry data. First reports on automated cytometry data analysis date back as early as 2007 (Quinn et al. 2007; Lo et al. 2008; Finak et al. 2009), and opened up the field for future developments. With the rapid increase of available tools, in 2010 the first FlowCAP (Flow Cytometry: critical assessment of population identification) challenge was initiated and revealed

that a large number of these automated algorithms perform equally well or even better than a human expert with respect to population identification as well as sample classification (Aghaeepour et al. 2013). The more recent FlowCAP challenges (http://flowcap.flowsite.org/) have seen a number of additional promising automated analysis approaches, among them several novel methods for clustering such as SWIFT (Naim et al. 2014) and immunoCLUST (Sörensen et al. 2015) (for an overview of available tools and their dedicated functions see references (Lugli et al. 2010; Pedreira et al. 2013; Di Palma and Bodenmiller 2015; Kvistborg et al. 2015; Chester and Maecker 2015).

1.6.3. Bioconductor and R provide a versatile analysis platform

As the development of these tools is work in progress, the available packages often lack a user-friendly graphical user interface and instead require at least basic knowledge of one of the programming languages such as R, Python, Java or Matlab. Although possibly sounding like a barrier to any bench scientist, the use of tools written in these programming languages is facilitated by the existence of free, open source repositories containing well-documented and fully functional pieces of code (packages, add-ons, modules) that perform a particular task. Perhaps the best known open source repository is Bioconductor (www.bioconductor.org), a software repository originally developed for the analysis and comprehension of high-throughput genomic data (Gentleman et al. 2004). It uses the statistical programming language R and currently contains 38 packages that deal with the various aspects of cytometry data handling.

1.6.4. Principle component analysis

Early work in analyzing high-dimensional cytometry data often deployed principal component analysis (PCA), a statistical method for reducing the dimensionality of complex datasets to two or three dimensions (Costa et al. 2010; Bendall et al. 2011; Newell et al. 2012). PCA takes all chosen parameters of the higher dimensional data and calculates a smaller number of variable parameters (called principal components) that best preserve most of the variability of the original data and can be more easily

displayed (reviewed in (Genser et al. 2007)). However, PCA is a computational approach that assumes linear relationships between the measured parameters, which is not the case for many biological datasets. As a result, within the past years a variety of new algorithms have been developed which are based on non-linear dimensionality reduction (NLDR) and thus are adequate for the visualization and exploration of single-cell cytometry data.

1.6.5. Recently developed algorithms for automated data analysis

1.6.5.1. SPADE – building a tree of relationships

One of the early tools used to computationally analyze and visualize high-dimensional mass cytometry data is Spanning-tree Progression Analysis of Density-normalized Events (SPADE) (Qiu et al. 2011). SPADE depicts cellular populations in a branched tree structure (dendrogram), thus visualizing high-dimensional data in an intuitive, two-dimensional manner (Figure 8). The SPADE tree consists of connected nodes that represent clusters of cells, thereby also providing information about the relationship of cell types. Typically, the branches of the resulting SPADE tree are manually annotated to give an immediate overview of the main cellular lineages. Further, a third dimension of color can be overlaid onto the tree to depict expression levels of any given marker or fold changes between multiple sample groups. Since the high-dimensional data is visualized as nodes that have undergone a clustering step, and therefore comprise multiple cells, the single-cell resolution of the data is lost at this point and any applied coloring represents subset characteristics.

To create the SPADE tree, the algorithm follows a multi-step process. Briefly, SPADE first performs density-dependent down-sampling. Thus, cells with few similar neighbors in the high-dimensional space will be more likely to be included in the down-sampled dataset than cells with plenty of neighbor cells. This ensures a similar representation of rare and abundant cell types in the down-sampled dataset, and thus facilitates the identification of rare cellular subsets. Second, the algorithm performs hierarchical, agglomerative clustering, grouping cells with its closest neighbors until a user-defined number of clusters is reached. Next, SPADE constructs a minimum spanning tree by randomly choosing an already connected sub-graph and adding an edge to the cluster or sub-graph with the minimum distance to the selected sub-graph.

This process is iterated until all nodes are connected in one minimum spanning tree. Lastly, for all cells in the initial dataset SPADE determines the closest neighbor in the down-sampled data and assigns the cell to the corresponding cluster.

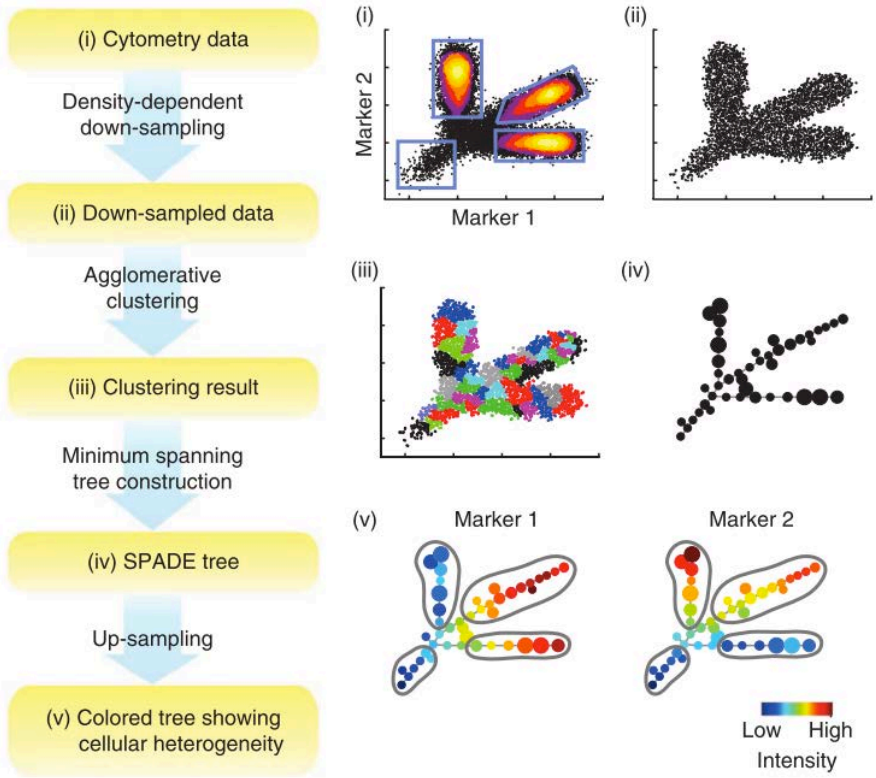

Figure 8. Flowchart of SPADE and SPADE analysis of a simulated data set. (i) A simulated two-parameter flow cytometry data set, with one rare population and three abundant populations. (ii) Result of density- dependent down-sampling of the original data. (iii) Agglomerative clustering result of the down-sampled cells. Adjacent clusters are drawn in alternating colors. (iv) Minimum spanning tree that connects the cell clusters. (v) Colored SPADE trees. Nodes are colored by the median intensities of protein markers of cells in each node, allowing visualization of the behaviors of the two markers across the entire heterogeneous cell population. Figure and legend taken from (Qiu et al. 2011).

The user-defined parameters that are required to construct the SPADE tree, in addition to the choice of cellular markers and the desired number of clusters, are the outlier density and target density. Outlier density is used to exclude cells with very few neighbor cells while the target density determines the outcome of the down-sampling step and therefore modifies the threshold of rare populations that can still be identified. Since SPADE includes steps involving random decisions, it is of a non-deterministic nature. As a consequence, several runs of SPADE will result in differently organized trees, which should be kept in mind when applying SPADE. While the organization of the tree at each individual run might appear distinct, the identified populations have been found to be comparable across several runs. SPADE

has been used in several publications (Bendall et al. 2011; Qiu et al. 2011; Bodenmiller et al. 2012; Lujan et al. 2015), mostly to give an instant overview of different immune populations and their expression of surface markers or intracellular signaling molecules.

1.6.5.2. t-SNE – visualizing the similarity landscape

Another powerful tool to visualize multi-parameter cytometry data is nonlinear dimensionality reduction via t-Stochastic Neighbor Embedding (t-SNE) (Maaten and Hinton 2008; Amir et al. 2013). t-SNE visualizes high-dimensional similarities of cells in an easily understandable two- or three-dimensional scatter plot, the so-called t-SNE map (Figure 9). The proximity of cells in the t-SNE map reflects their distances in the high-dimensional space. Cells that are similar in their analyzed protein-expression pattern will be located closely together in the t-SNE map, thus enabling the visualization of different cellular subpopulations. Importantly, t-SNE has been shown to successfully identify small cellular subpopulations down to 0.25% (Amir et al. 2013) and is able to recognize high-dimensional associations of markers which might be missed when performing conventional, two-dimensional gating.

Briefly, the computational steps underlying t-SNE are: first, the calculation of a pairwise similarity matrix for all data-points, based on their high-dimensional distances. Next, a low-dimensionality similarity matrix is calculated based on initially random locations for each cell in the two (or three) t-SNE dimensions. In an iterative process, the algorithm then tries to minimize the difference between the high- and low-dimensional similarity matrices, thereby adjusting every cell´s position in the two-dimensional space. Recent improvements to t-SNE make use of the Barnes-Hut algorithm (van der Maaten 2014) which uses a tree-like structure to reduce the number of pairwise similarities that actually have to be calculated. This now allows for a higher number of cells to be analyzed and shorter computation time.

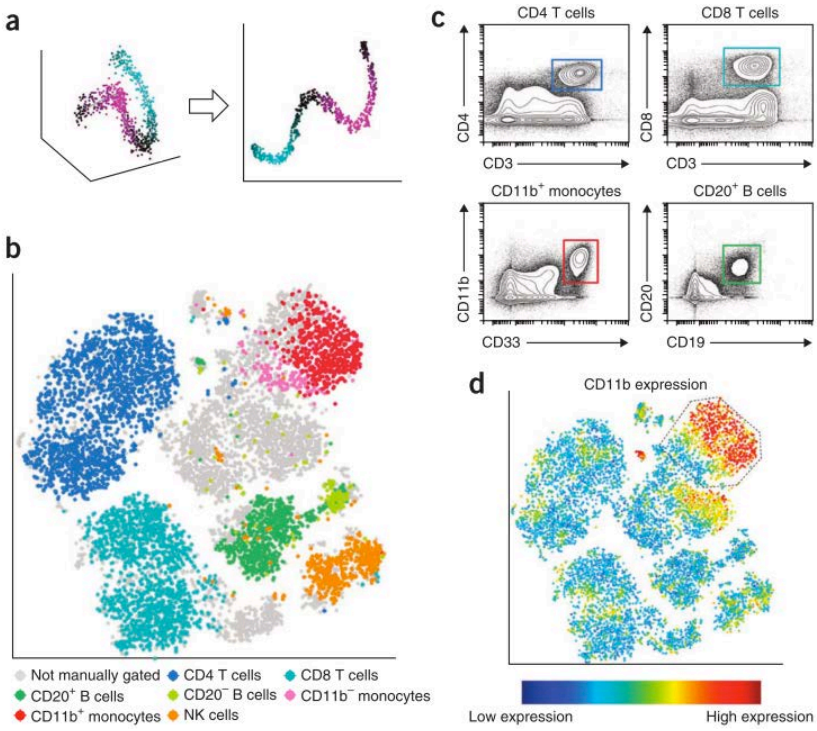

Figure 9. viSNE map of healthy human bone marrow. (a) In a synthetic toy example, (1,000 points randomly distributed with normally distributed noise around a polynomial of the third degree) viSNE projects a one-dimensional curve embedded in three dimensions (left) onto two dimensions (right). The color gradient shows that points that are in close proximity in three dimensions remain in close proximity in two dimensions. (b) Application of viSNE to a healthy human bone marrow sample, stained with 13 markers and measured with mass cytometry, automatically separates cells into spatially distinct subsets based on the combination of markers that they express. Each point in the viSNE map represents an individual cell and its color represents its immune cell subset as designated by independent expert manual gating (manual gates are defined at the bottom). Gray points were not classified by manual gating. The axes are in arbitrary units. (c) Biaxial plots represent the same data shown in b, and show the gates drawn manually by expert operators. The colors of the squares match the colors in b. The actual manual gating used here is more complex and uses a series of biaxial plots to gate each population. Note, that unlike in b, no single biaxial plot spatially separates all subsets. (d) The same viSNE map shown in b is colored according to intensity of CD11b expression. Many of the cells within the dotted line gate were not classified as monocytes by manual gating (gray cells, b). Figure and legend taken from (Qiu et al. 2011).

Similarly to SPADE, t-SNE incorporates random seeds and thus the results from multiple runs may visualize the data differently. This can be prevented by manually defining a random seed. On the resulting t-SNE map, different immune subpopulations will visually appear as distinct clusters, however t-SNE does not per se assign single cells to defined clusters. This can be accomplished either by subsequent manual gating on the t-SNE map or by using automated clustering algorithms. Prominent examples of such clustering methods are ACCENSE (automatic classification of cellular expression by nonlinear stochastic embedding) (Shekhar et al. 2014) or DensVM (Becher et al. 2014), both employing a density-peak detection approach on the two-dimensional t-SNE map.

1.6.5.3. Citrus – Identification of stratifying subpopulations

Visualization of multi-parameter cytometry data is a helpful first step in making high-dimensional data accessible to scientists for further investigation. In many cases, such subsequent questions involve the comparison of two sets of samples in search of cellular subpopulations with distinctive abundance or expression levels. The algorithm named Citrus provides an unsupervised and automated process that combines computational identification of cellular subpopulations with various association models to reveal stratifying clusters and cellular responses that are best predictive, or best correlated with the experimental endpoint (Bruggner et al. 2014). For example, such experimental endpoints can be affiliation to a certain group, good or poor clinical outcomes or even survival time. As an input, Citrus receives cytometry data of two or more sets of samples associated with distinct groups, e.g. patient and control groups or different stimulation regimes. Citrus then automatically defines cellular populations and calculates cluster characteristics. After applying a chosen association model, Citrus provides the user with a list of clusters behaving differentially in the two sample groups, as well as characteristics of these clusters represented in histograms and bar plots (Figure 10). Additionally, Citrus provides a model to predict the affiliation of samples to one of the input groups using regularized classification.

Shortly, the Citrus algorithm combines all samples into one aggregate dataset before identifying cell populations by hierarchical clustering of phenotypically similar cells. Importantly, only clusters of populations that are more abundant than the user-defined minimum cluster-size threshold will be included in the subsequent analysis. Next, cells are assigned back to the individual samples and cluster characteristics, such as median expression level for all markers, are calculated. Subsequently, Citrus employs a regularized classification model to identify stratifying clusters which are used to predict the group of each sample.

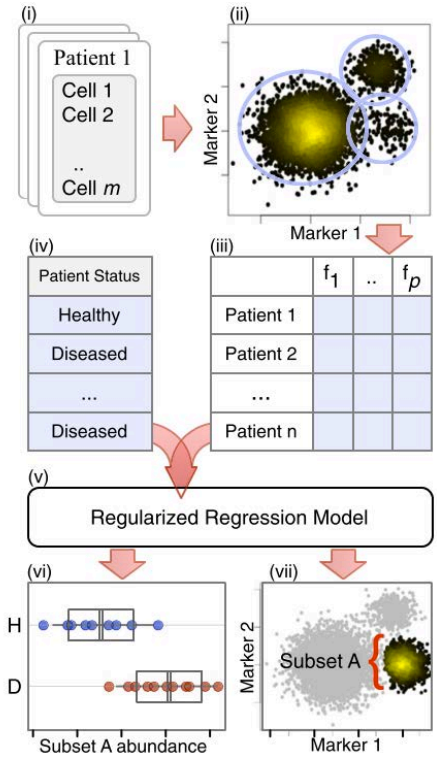

Figure 10. Overview of Citrus. Cells from all samples (i) are combined and clustered by using hierarchical clustering (ii). Descriptive features of identified cell subsets are calculated on a per-sample basis (iii) and used in con- junction with additional experimental metadata (iv) to train a regularized regression model predictive of the experimental endpoint (v). Predictive subset features are plotted as a function of experimental endpoint (vi), along with scatter or density plots of the corresponding informative subset (vii). In this example, the abundance of cells in subset A was found to differ between healthy and diseased samples (vi; H, subset A abundance in healthy patients; D, subset A abundance in diseased patients). Scatter plots show that cells in subset A have high expression of marker 1 and low expression of marker 2 relative to all measured cells (shown in gray). Figure and legend taken from (Bruggner et al. 2014).

1.6.5.4. PhenoGraph – clustering in high-dimensional space

While both t-SNE and SPADE facilitate the visualization of phenotypically similar cell subsets in high-dimensional datasets, these analysis approaches do not directly assign cells to distinct clusters. Also, the density-peak detection algorithms mentioned above (ACCENSE and DensVM) (Shekhar et al. 2014; Becher et al. 2014) do not take the entire dimensionality of a given dataset into account. To do so, a novel algorithm was recently developed and termed PhenoGraph (Levine et al. 2015).

PhenoGraph models the high-dimensional space using a k-NNG, in which each cell is depicted as a node that is connected to its neighbors by edges. In this graph, phenotypically similar clusters of cells will be represented as sets of highly interconnected nodes. These can be seen as neighborhoods or communities of cells, and can be partitioned in high-dimensional space using similar community-detection algorithms which are being used for the analysis of social networks. The resulting

clusters can then be visualized on a t-SNE map, which often corresponds well with the PhenoGraph clustering, or alternatively on a heat map, which will show the expression levels of selected marker across all found clusters (Figure 11).

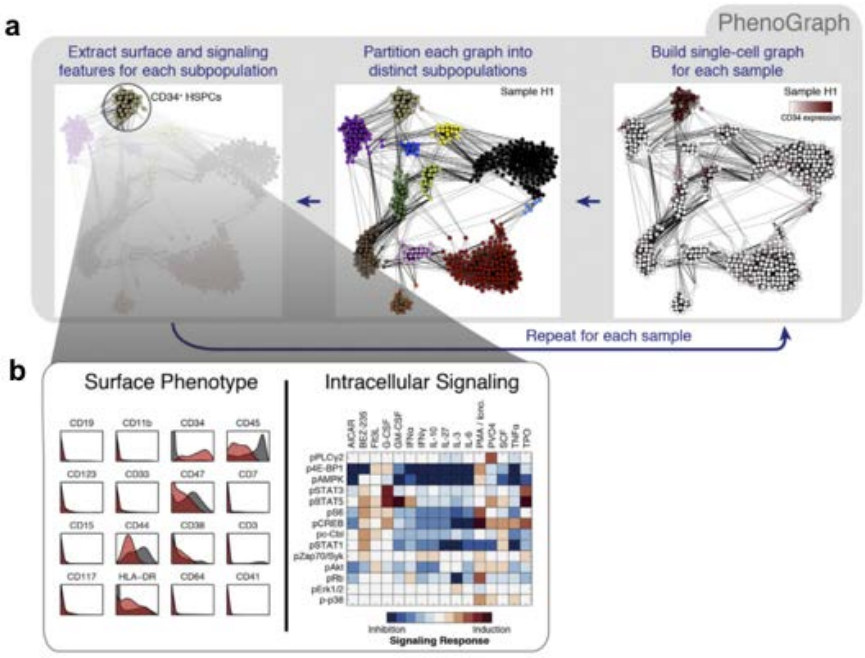

Figure 11. Overview of phenograph clustering. (a) PhenoGraph method for clustering high-dimensional single-cell data. Each node in the neighbor graph represents one of 500 random cells from a healthy donor (H1) colored by CD34 expression. CD34+ HSPCs form a dense subgraph and are automatically assigned to a single subpopulation. (b) HSPCs identified by PhenoGraph from donor H1. This subpopulation (red histograms) had a CD34+/CD45low phenotype relative to the other cells in the sample (gray histograms). Each PhenoGraph subpopulation contained cells from all perturbations, permitting analysis of 224 signaling responses. Figure and legend adapted from (Levine et al. 2015).

The reported application of PhenoGraph to high-dimensional data of human bone marrow derived from healthy donors as well as acute myeloid leukemia (AML) patients (Levine et al. 2015) suggests that this method is superior to previously available clustering methods, and can resolve sub-populations as rare as 1 in 2000 cells. In fact, one advantage distinguishing PhenoGraph from previous dimensionality reduction approaches is the addition of a second iteration process using the so-called Jaccard similarity coefficient. This computational step aids the identification of small cellular subsets (e.g. hematopoietic stem cells) that could potentially be obscured either by noise or by other larger cell populations.

1.6.5.5. FlowSOM – Self organizing high-dimensional data

Another method for clustering and visualization of cytometry data is FlowSOM (Van Gassen et al. 2015). It is based on the principle of self-organizing maps (SOMs) which is an unsupervised technique for clustering and dimensionality reduction (Kohonen 1990). The workflow is outlined in Figure 12. After optional preprocessing steps, a SOM is built from the input data. SOMs are a type of artificial neural network, consisting of a grid of nodes, in which each node represents a point in the multidimensional input space. New points are added and classified with the node that is the closest neighbor. The grid is trained in such a way that nearby nodes resemble each other more than nodes that are further away. As the next step, the SOM is visualized as a minimal spanning tree (also used in SPADE, see 1.6.5.1). Lastly, a metaclustering step is performed, employing consensus hierarchical clustering.

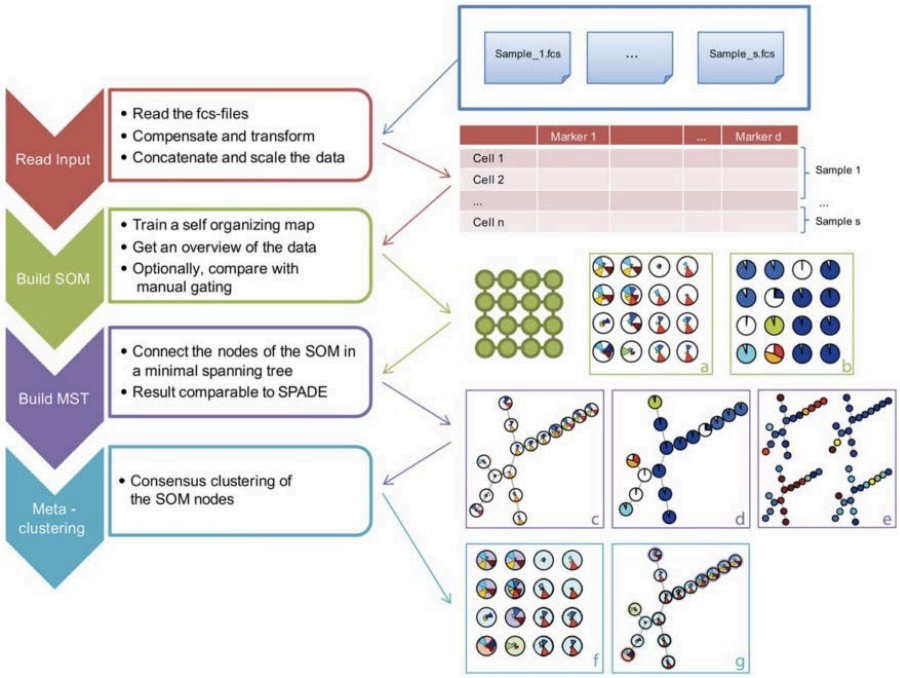

Figure 12. Overview of the four steps of the FlowSOM algorithm. (i) The fcs-files are read, compensated, transformed, concatenated and scaled, resulting in a matrix with a row for every cell, describing the measured marker values. (ii) A self-organizing map is trained on the matrix. The result is a grid of nodes, corresponding to cell clusters. Visualizations can be made showing the mean marker values of each node in star charts (a) or the concordance with a manual gating in pie charts (b). (iii) A minimal spanning tree is built, on which the same information can be visualized (c,d). We can also show mean marker values for specifically chosen markers, resulting in figures very similar to SPADE trees (e). (iv) A meta-clustering of the nodes is calculated, corresponding to an automatic gating procedure. This is indicated by the background color of the nodes, and can be both visualized in the grid (f) or the minimal spanning tree (g). Figure and legend adapted from (Van Gassen et al. 2015).

1.6.6. Practical considerations for automated data analysis

1.6.6.1. Quality control

The first practical aspect when starting to analyze high-dimensional data sets in an automated manner is to perform appropriate quality control (QC) and data pre-processing. While proper QC of both the instrument and acquired data should always be part of any standard cytometry analysis workflow, it becomes even more relevant with increasingly complex experiments. In brief, QC should at least include validation of both the instrument and reagents used (e.g. non-specific binding of antibody, spillover due to metal impurity), and for fluorescence-based flow cytometry, the assessment of signal stability over time and especially potential artifacts arising from improper compensation (reviewed in (Perfetto et al. 2006)).

1.6.6.2. Data transformation

In addition, automated analysis of high-dimensional data asks for dedicated pre-processing steps, especially data transformation. Epitope abundances measured by cytometry often follow normal distributions on a logarithmic scale (so called log-normal distribution) with the variance of different cell populations depending on their intensity. Therefore, obtaining a suitable representation of the data across its entire intensity range is crucial for visualization and particularly for automated analysis. To do so, different transformation methods can be employed (compared and reviewed in (Trotter 2007) and (Finak et al. 2010)). In the context of the aforementioned algorithms, the data are frequently transformed using a logicle or arcsinh transformation (Parks et al. 2006; Herzenberg et al. 2006). This transformation was introduced for flow cytometry data to allow negative values, which originate, on the one hand, from baseline subtractions and, on the other hand, from spectral overlap correction (compensation), while maintaining logarithmic like scaling for large parameter values.

1.6.6.3. Data normalization

Another important pre-processing step when performing automated analysis is data normalization. This standardization can be employed on multiple levels. In general, we here refer to normalization as the process of using internal or external control

values to express the acquired data on a common scale, thus improving comparability between multiple measurements. A first level of normalization is often to adjust measurements to differences that might occur in instrument sensitivity (over time or across different machines), and thus might influence measured values. In both, flow and mass cytometry, the addition of standardized beads with known signal intensity can be used for this purpose (Perfetto et al. 2006; Finck et al. 2013).

Further, in settings in which multiple samples with technical inter-sample variation (e.g. due to different cytometers, sample handling, staining process, etc.) should be included in the same automated analysis, per-channel basis normalization can help automated algorithms to identify respective cellular populations across many samples. Different approaches have been developed for this purpose, such as alignment of prominent landmark features or features of defined subpopulations (Hahne et al. 2010; Finak et al. 2014). In addition, to help match populations from multiple samples, normalization can also be applied in order to reduce differences in the contribution of markers and antibodies with different dynamic ranges. Large separations between positive and negative populations do not necessarily reflect the biological differences between those populations, therefore adjusting the range to a common scale might be desired. This can be done by normalizing the data on a per-channel basis e.g. to the z-score (also called standard score), thus expressing measured intensities as numbers of standard deviations above or below the mean. Alternatively, data points can also be scaled to any chosen channel-specific percentile of the dataset, thus expressing them in relation to the spread of the respective channel.

2. Aims of the study

2.1. Part I – Establishing the role of GM-CSF in MS

The first aim of this study was to reveal whether the preclinical finding that GM-CSF production by T_H cells plays a crucial role in the pathogenesis of autoimmune neuroinflammation would be applicable into MS in humans. Secondly, given that T_H cell-derived GM-CSF indeed shows involvement in MS, our next objective was to determine the factors regulating the production of GM-CSF in human T_H cells in order to better understand and possibly in the future interfere with the emergence of such pathogenic T_H cells. In addition, the genetic basis of MS was recently well established, however how this translates into pathogenic mechanisms resulting in the onset of neuroinflammatory disease remains elusive. It would thus be of great interest to examine genetic risk factors and their potential influence on GM-CSF production which would constitute one possible pathogenic mechanism in MS and thus aid our fundamental understanding of the disease.

2.2. Part II – High-dimensional analysis of T_H cell polarization in MS

Especially T_H cell differentiation and cytokine production were found to be critical mechanisms in the pathogenesis of MS, however the exact identity of the T_H cell polarization pattern and responsible cytokines underlying MS pathology are still under debate. Therefore, we wanted to extend our previous studies on the role of GM-CSF in MS by employing a high-dimensional and unbiased approach to reveal the breadth of cytokine production profiles of the entire T_H cell landscape in MS using mass cytometry. Specifically, in a first step we planned to establish a comprehensive panel of heavy-metal isotope-labelled antibodies against the most important cytokines, activation markers and chemokine receptors. Using this panel in combination with recently developed algorithms for unbiased analysis of high-dimensional data, our final aim was to identify distinct cellular profiles discriminating between different groups of MS and control patients.

3. Results – Part I

3.1. Regulation of GM-CSF production in human T_H cells

3.1.1. IL-2 induces the production of GM-CSF

To reveal the most potent inducer of GM-CSF production in human T_H cells, we activated (αCD3/αCD28, irradiated feeder cells) naïve T_H cells from healthy donors in the presence of IL-23, IL-1β and IL-6, which have been demonstrated to drive GM-CSF secretion in murine T_H cells (Codarri et al. 2011; El-Behi et al. 2011), or with IL-2. IL-23, IL-1β and IL-6 did not increase GM-CSF production by human T_H cells (Figure 13a,b). Importantly, we noticed that IL-2 was able to substantially increase the expression of GM-CSF by human T_H cells. Moreover, GM-CSF production observed without addition of exogenous cytokines was dependent on endogenously produced IL-2 (Figure 13c). Addition of TGF-β1 or TGF-β3 to induce IL-17A production negatively regulated GM-CSF secretion (Figure 13a,b and d-f), similar to what has been observed in murine T cells (El-Behi et al. 2011). The frequency of IL-2Rα$^+$ T_H cells was not affected by TGF-β (Figure 13f-h).

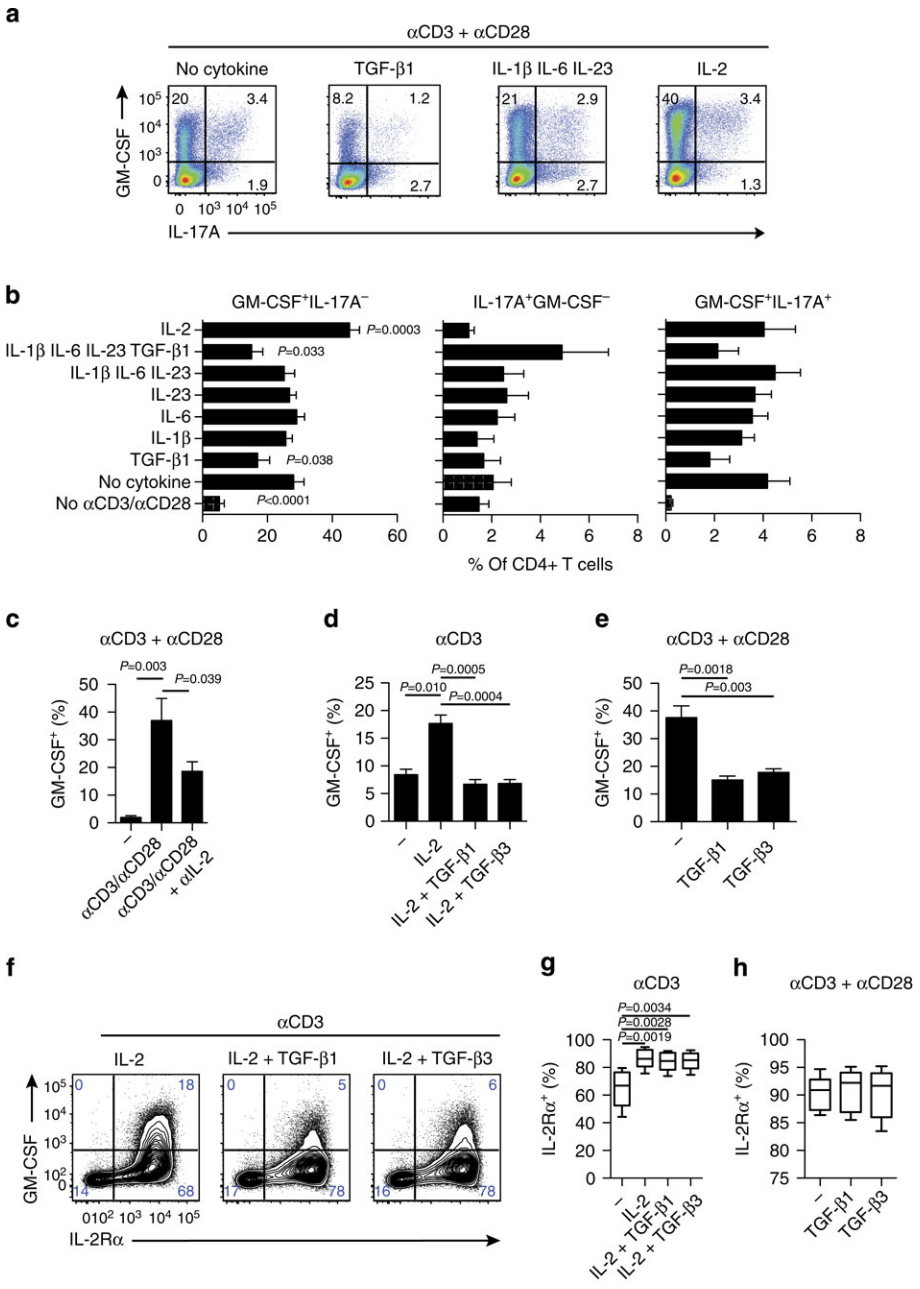

Figure 13. IL-2 drives GM-CSF secretion by human T_H cells. IL-2 drives GM-CSF secretion by human T_H cells. (a) Representative and (b) cumulative frequencies of sorted naïve T_H cells ($CD4^+CD45RO^-CD62L^+$), activated (αCD3/αCD28) in the presence of 10 ng ml^{-1} of the indicated cytokines. The frequency of $GM\text{-}CSF^+IL\text{-}17A^-$, $IL\text{-}17A^+GM\text{-}CSF^+$ and $GM\text{-}CSF^+IL\text{-}17A^+$ was determined by flow cytometry on day 7 (*n*=6). (c) Naïve T_H cells were activated (αCD3/αCD28) in the presence or absence of neutralizing IL-2 antibody (*n*=7). Data are combined from three independent experiments. (d-h) Naive T_H cells were activated as indicated in the presence or absence of the indicated TGF-β for 5 days (*n*=5). Shown are cumulative results of $GM\text{-}CSF^+$ T_H cells after αCD3 activation (d) or after αCD3/ αCD28 activation (e), representative flow cytometric results (f) and cumulative results of IL-2Rα expression on T_H cells after αCD3 activation (g) and after αCD3/ αCD28 activation (h). For all figures throughout, error bars show mean±s.e.m.

3.1.2. IL-2Rα engagement drives GM-CSF in human T_H cells

CD28 costimulation is a strong inducer of IL-2 production in T cells. To precisely control IL-2 levels, we activated naïve T_H cells with only αCD3 in the presence of irradiated feeder cells and the respective cytokines. Addition of IL-6 and IL-1β led to a moderate increase in the frequency of GM-CSF producing T_H cells, but only marginally affected the concentration of secreted GM-CSF (Figure 14a,b).

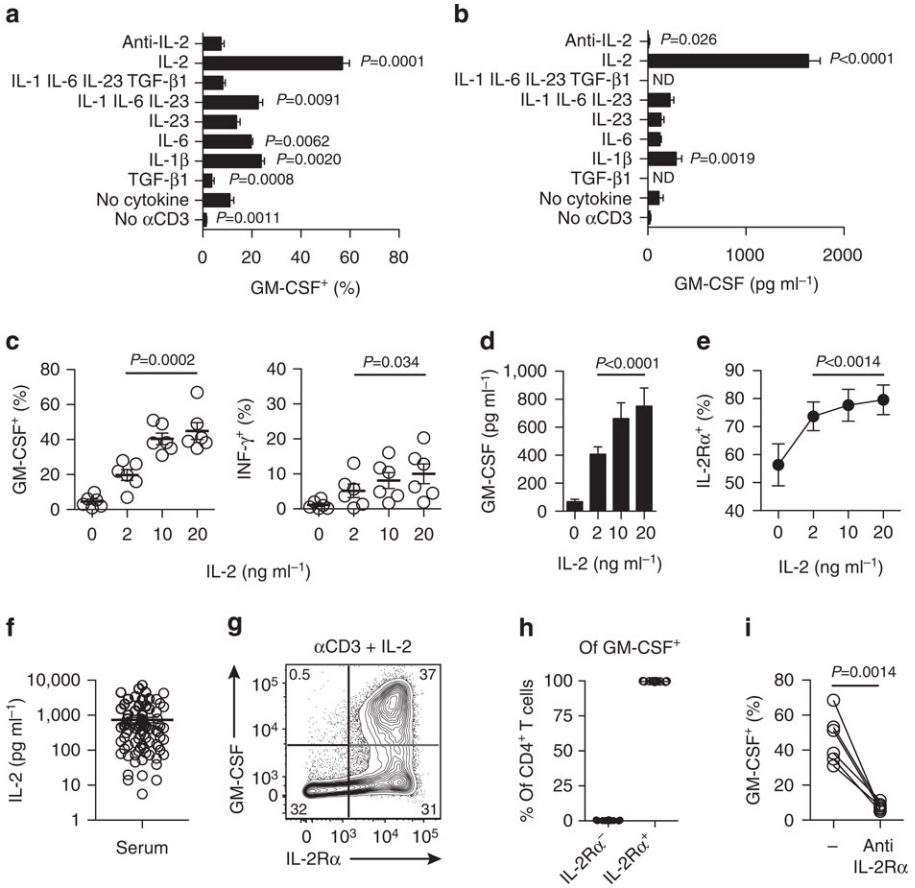

Figure 14. IL-2Rα is critical for the induction of GM-CSF. (a,b) Sorted naïve T_H cells ($CD4^+CD45RO^-CD25^{-/med}CD127^+$) were activated (αCD3) in the presence of 10 ng ml^{-1} of the indicated cytokine for 5 days (*n*=6). Shown are cumulative results of $GM\text{-}CSF^+$ in T_H cells (a) and the level of secreted GM-CSF in the cell culture supernatant (b). n.d. not detected. (c-e) Naïve T_H cells as in (a,b) were activated (αCD3) in the presence of the indicated concentration of IL-2 for 5 days. Shown are the frequency of $GM\text{-}CSF^+$ and IFN-γ+ T_H cells (c, *n*=6), GM-CSF levels in the cell culture supernatant (d, *n*=12) and the frequency of $IL\text{-}2R\alpha^+$ T_H cells (e, *n*=4). (f) GM-CSF levels in serum of healthy individuals was analyzed by ELISA (*n*=99). (g,h) Representative example (g) and cumulative results (h) of sorted naïve T_H cells which were activated (αCD3) in the presence of 10 ng ml^{-1} IL-2 and analyzed for GM-CSF secretion and IL-2Rα expression on day 5 (*n*=12). (i) Blocking of the IL-2Rα by monoclonal antibodies during the activation of naïve T_H cells in the presence of 10 ng ml^{-1} IL-2 for 5 days (*n*=6). Data are combined from three independent experiments. For all figures throughout, error bars show mean±s.e.m.

In contrast, IL-2 induced a strong increase in the frequency, as well as in the level of secreted GM-CSF. IL-2 promoted GM-CSF in a dose-dependent manner, in terms of

the frequency of cytokine producing T_H cells, as well as in the level of secreted cytokine (Figure 14c,d). Production of other cytokines such as IFN-γ was only mildly increased. Similar to the frequency of GM-CSF secreting cells, IL-2Rα$^+$ T_H cells increased depending on the IL-2 concentration (Figure 14e). Of note, the employed concentrations of recombinant IL-2 were within the range of IL-2 levels measured in the serum of healthy individuals (Figure 14f). After activation in the presence of IL-2, all GM-CSF producing T_H cells expressed the IL-2Rα (Figure 14g,h). This expression was critical for the induction of GM-CSF through IL-2, as shown by blocking of IL-2Rα with monoclonal antibodies, which drastically reduced GM-CSF secretion by T_H cells (Figure 14i). Together, this highlights the importance of the IL-2Rα for the induction of GM-CSF production by human T_H cells.

3.1.3. IL-2 drives GM-CSF production independent of proliferation

IL-2 is known to drive T_H cell expansion. We therefore tested whether this might contribute to the observed increase in the frequency of GM-CSF secreting T_H cells. We activated naïve T_H cells in the presence of IL-2, IL-7 or IL-15, cytokines known to promote T_H cell expansion (Figure 15a). IL-2 and IL-15 both induced strong GM-CSF production in T_H cells (Figure 15a,b). IL-7 strongly stimulated proliferation while it only slightly affected the frequency of GM-CSF secreting T_H cells, indicating that expansion *per se* is not sufficient to induce GM-CSF production (Figure 15a,b). Consequently, the frequency of GM-CSF secreting T_H cells did not correlate with the calculated percentage of divided cells (Figure 15c). To further support this, we determined the cell cycle state of GM-CSF secreting cells after activation of T_H cells in the presence of those cytokines. IL-2, IL-7 and IL-15 all induced proliferation (Figure 15d), however we found that the majority of GM-CSF secreting cells were not actively proliferating, thus demonstrating that proliferation is not essential for GM-CSF production (Figure 15e,f).

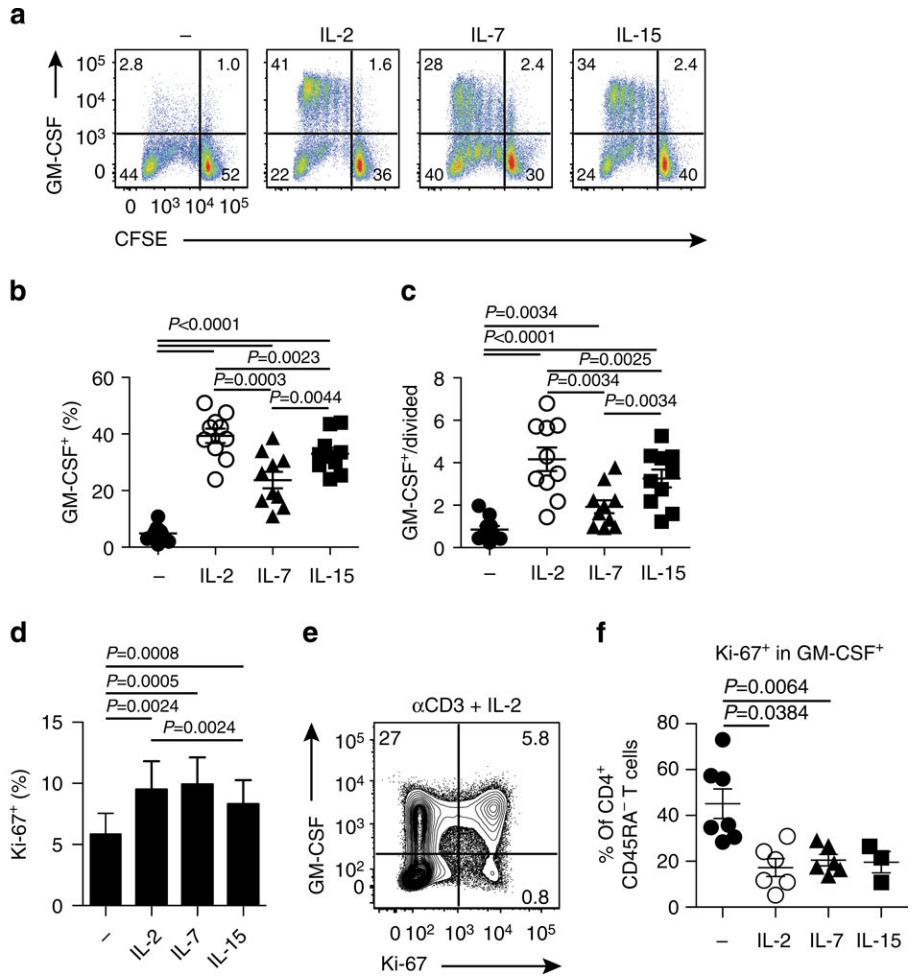

Figure 15. GM-CSF secretion is independent of proliferation. (a) Representative examples and (b) cumulative results of sorted naïve T_H cells which were activated (αCD3) in the presence of 10 ng ml^{-1} of IL-2, IL-7 or IL-15 and analyzed for GM-CSF expression and proliferation on day 5 (*n*=10). (c) Normalization of the frequency of GM-CSF secreting T_H cells by the calculated frequency of divided T_H cells (*n*=10). (d,e) Cumulative results (d) and representative example (e) of purified T_H cells which were activated (αCD3) in the presence of the indicated cytokines and analyzed for cell cycle state and GM-CSF production on day 2 (*n*=8). (f) Frequency of proliferating ($Ki\text{-}67^+$) T_H cells within the fraction of $GM\text{-}CSF^+$ T_H cells after activation in the presence of 10 ng ml^{-1} of the indicated cytokine for 4 days (*n*=7,6,6,3 respectively). Data are from one representative of two independent experiments. Each symbol represents a single individual. For all figures throughout, error bars show mean±s.e.m.

3.1.4. GM-CSF expression is regulated via STAT5

IL-2 and IL-15 both induce strong phosphorylation of STAT5. We investigated whether this signaling pathway is initiating GM-CSF induction in human T_H cells. Therefore, we stimulated T_H cells with different γ_c-cytokines or different IL-2 concentrations to induce varying levels of pSTAT5. The frequency of GM-CSF+ T_H cells closely correlated with STAT5 phosphorylation, indicating that pSTAT5 directly drives GM-CSF expression (Figure 16a,b). Using *in silico* analysis, we found the human GM-CSF (*CSF2*) promoter to contain a STAT5 binding site

(chr5:131,409,289-131,409,300). Further supporting this concept, we observed loss of IL-2-induced GM-CSF production on protein and mRNA level upon specific STAT5 inhibition (Nelson et al. 2011) in T_H cells (Figure 16c-e). GM-CSF production induced by endogenous IL-2 was similarly reduced by STAT5 inhibition.

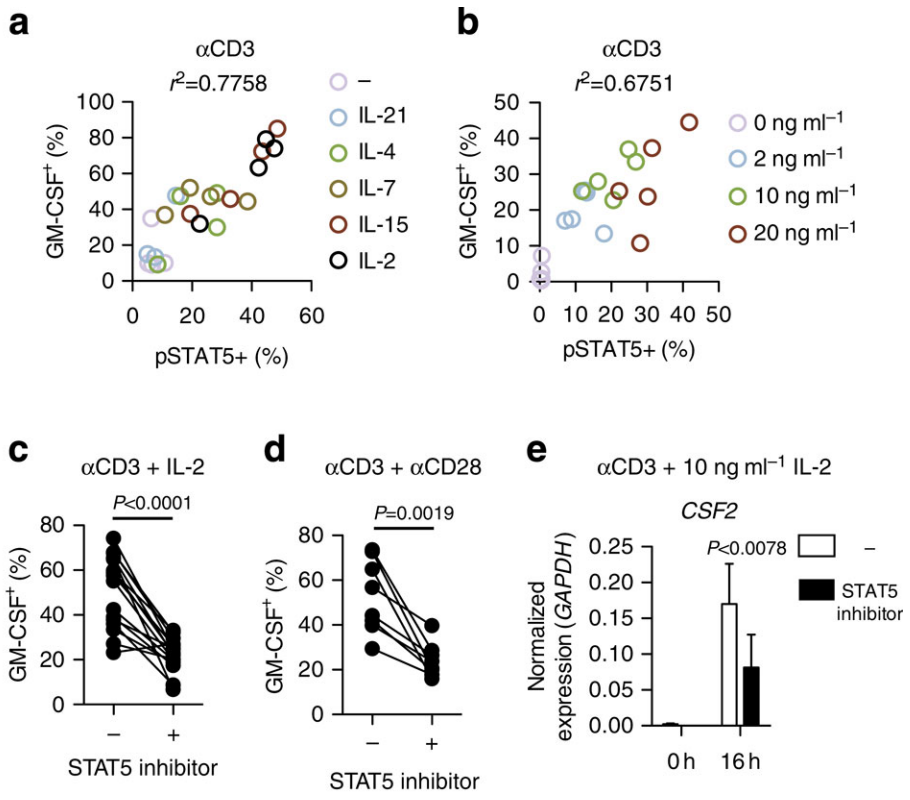

Figure 16. IL-2 induces GM-CSF via phosphorylation of STAT5. (a,b) Sorted naïve T_H cells ($CD4^+CD45RO^-CD25^{-/med}CD127^+$) were activated (αCD3) in the presence of the indicated cytokine for 5 days. GM-CSF secretion and STAT5 phosphorylation (10 min of restimulation with the indicated cytokine in the same concentration) were analyzed by flow cytometry on day 5. Shown are the frequencies of $GM\text{-}CSF^+$ vs. $pSTAT5^+$ T_H cells after stimulation in the presence of different γc-cytokines (a, *n*=4) and after stimulation with different IL-2 concentrations (b, *n*=5). (c,d) Naïve T_H cells as in (a,b) were activated with αCD3 + IL-2 (c, *n*=16) or αCD3/αCD28 (d, *n*=8) with or without inhibition of STAT5 phosphorylation (2.5 µg ml^{-1} pimozide). (e) Purified T_H cells were activated (αCD3) in the presence of IL-2 with or without the STAT5 inhibitor for 16 h before *CSF2* mRNA levels were analyzed by quantitative real-time PCR (*n*=8). Data are combined from two independent experiments. Each symbol represents a single individual. For all figures throughout, error bars show mean±s.e.m.

3.2. The influence of regulatory T cells

3.2.1. T_{reg} cells inhibit $GM\text{-}CSF^+$ T_H cells through IL-2 deprivation

T_{reg} cells are capable of regulating cytokine secretion by auto-aggressive T cells through various mechanisms (Vignali et al. 2008) and alterations in this suppression have been reported in MS patients (Viglietta et al. 2004; Carbone et al. 2014). We

found T_{reg} cells to suppress IL-2 induced GM-CSF production by conventional T_H cells (Figure 17a,b). This suppression functions mostly independently of TGF-β or IL-10, but rather through deprivation of IL-2 (Figure 17c). Regulation of IL-2 levels by T_{reg} cells thus has a major impact on the effector function of T_H cells through direct modulation of GM-CSF production.

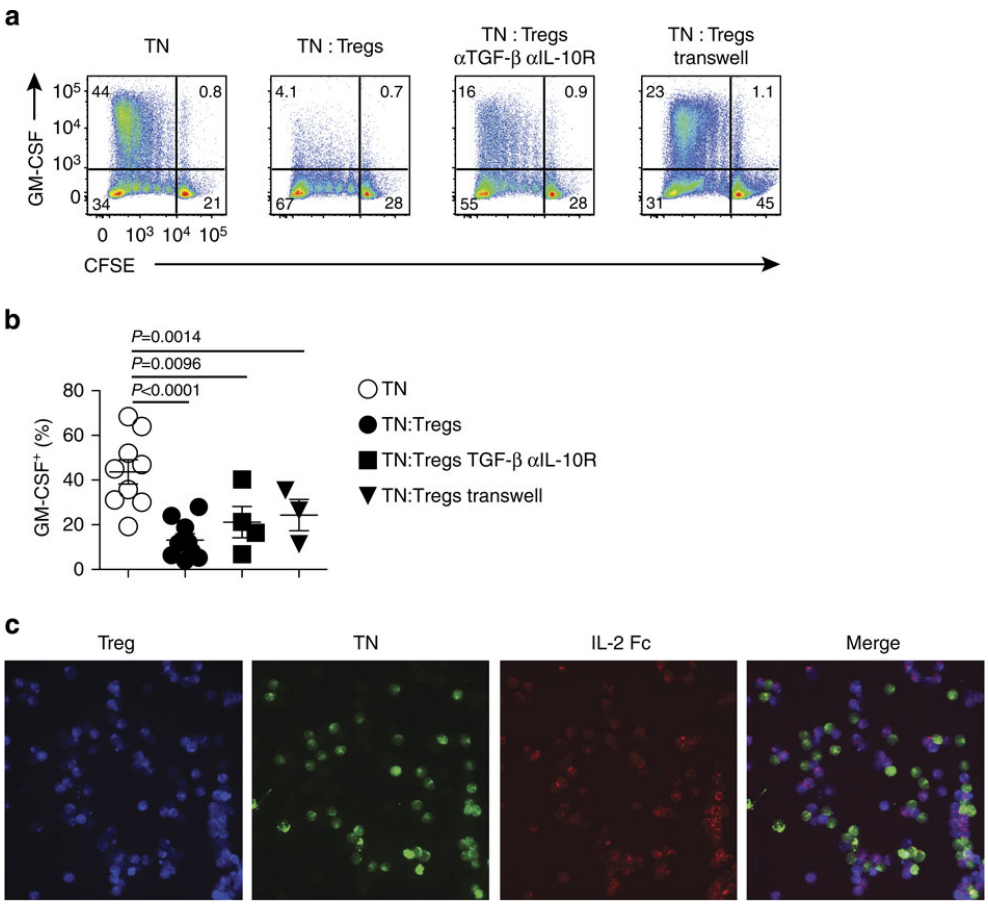

Figure 17. Regulatory T cells suppress GM-CSF production by deprivation of IL-2. (a,b) Sorted naïve (T_N) and regulatory T cells (T_{reg}) were co-cultured in a 1:1 ratio and activated (αCD3/αCD28) in the presence of 10 ng/ml IL-2 and the indicated blocking antibodies for 5 d (*n*=9,9,4,3 respectively). Shown are representative examples of GM-CSF secretion and CFSE dilution (a) and cumulative results of GM-CSF secretion (b). Data are combined from three independent experiments. (c) Fluorescent imaging of T_N (CFSE labelled) and T_{reg} cells (CellTrace Violet labelled) which were stimulated together with 10 ng/ml IL-2Fc for 10 min. Each symbol represents a single individual. For all figures throughout, error bars show mean±s.e.m.

3.3. GM-CSF expression in multiple sclerosis

3.3.1. GM-CSF secreting T_H cells are elevated in MS patients

GM-CSF is currently considered to be a promising therapeutic target in several autoimmune diseases such as rheumatoid arthritis (RA) (Burmester et al. 2013) and

MS (NCT01517282). Therefore, we quantified the *ex vivo* frequency of GM-CSF, IL-17A and IFN-γ secreting memory T_H cells in the peripheral blood of MS patients compared to OND patients (Table 1 - Table 3). We observed that untreated MS patients had a significantly higher frequency of GM-CSF producing memory T_H cells compared to OND patients (17.0% vs. 11.5%, Figure 18a,b).

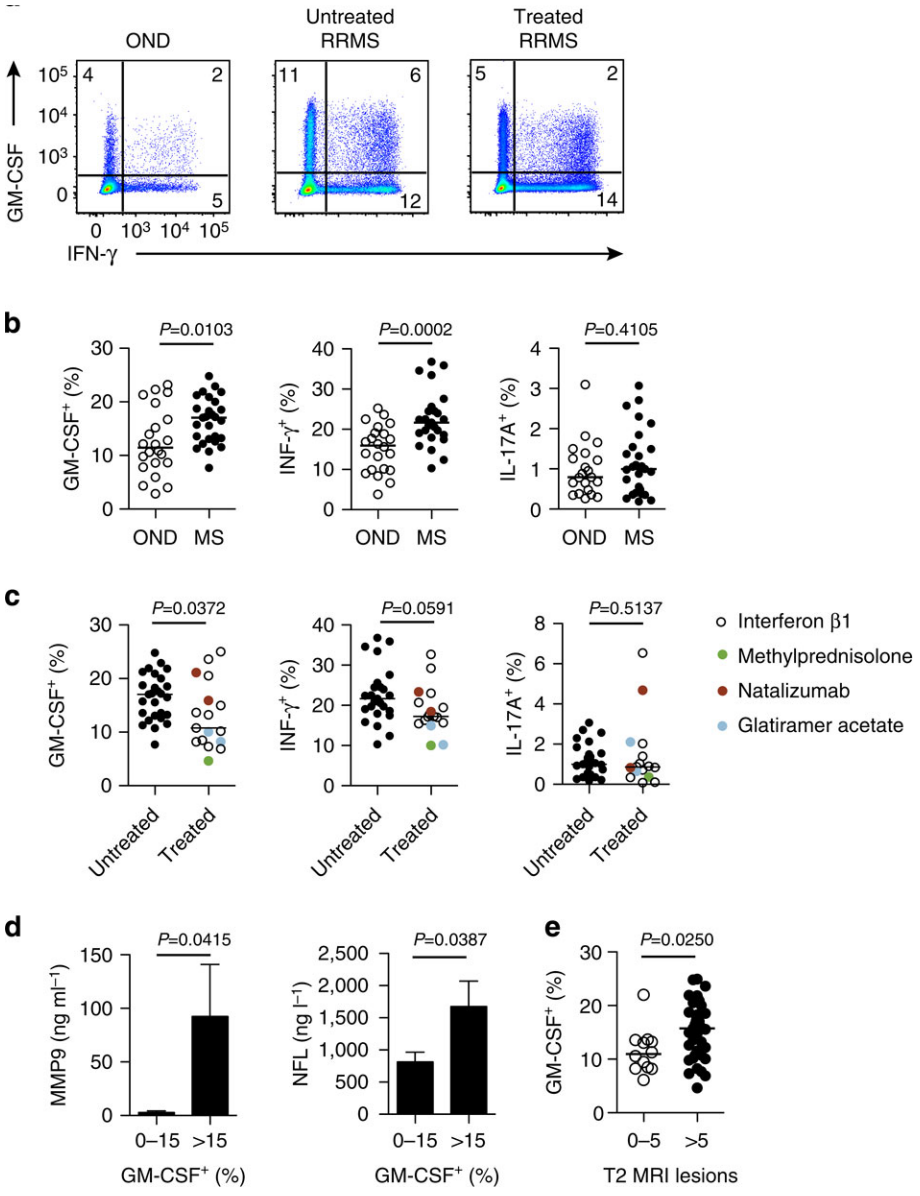

Figure 18. MS patients have elevated frequencies of GM-CSF secreting T_H memory cells. (a) Representative GM-CSF and IFN-γ production and (b) cumulative data from PBMCs of untreated RRMS patients and OND patients which were analyzed *ex vivo* (no previous *in vitro* culture) for the frequency of total GM-CSF$^+$, IFN-γ$^+$ and IL-17A$^+$ memory T_H cells by flow cytometry (OND *n*=22; MS *n*=27). (c) Effect of immune-modulatory treatment on the *ex vivo* frequency of peripheral GM-CSF$^+$, IFN-γ$^+$ (untreated *n*=27, treated *n*=17) and IL-17A$^+$ (untreated *n*=27, treated *n*=16) memory T_H cells. Data are combined from more than three independent experiments. (d) CFS serum levels of MMP9 and NFL in RRMS patients with a low (*n*=14) or high (*n*=14) frequency of GM-CSF$^+$ memory T_H cells. (e) *Ex vivo* frequency of GM-CSF$^+$ memory T_H cells in MS patients (RRMS/CIS) with 0-5 (*n*=12) vs. MS patients with >5 (*n*=39) T2 MRI lesions. Data are combined from more than three independent experiments. Each circle represents a single individual. (b,c,e) lines represent the median (d) error bars show mean±s.e.m.

A similar 1.5-fold increase (15.5% vs. 10.1%) was observed in an independent validation cohort of MS and OND patients, yet marginally above the statistical threshold (p=0.052, Figure 19a). Additionally, we could replicate the previously reported (Becher et al. 1999) increase in IFN-γ producing memory T_H cells in MS vs. OND (21.7% vs. 16.0%). In agreement with previous reports (Jamshidian et al. 2013), we observed only a modest increase (1.0% vs. 0.8%) in the frequency of IL-17A secreting T_H cells. Interestingly, patients treated with immune-modulatory drugs had a significantly reduced frequency of GM-CSF secreting T_H cells compared to untreated patients (10.8% vs. 17.0%, Figure 18a,c and Figure 19b). A similar effect of immuno-modulatory treatment, albeit less pronounced, was observed in the frequency of IFN-γ producing memory T_H cells (17.3% vs. 21.7%). We did not observe any significant difference in the percentage of IL-17A producing memory T_H cells upon therapy. The proportion of IL-2Rα$^+$ memory T_H cells did not significantly differ between the patient groups (Figure 19c). Taken together, GM-CSF$^+$ T_H cell frequencies are elevated in MS and decrease upon immune-modulatory therapy.

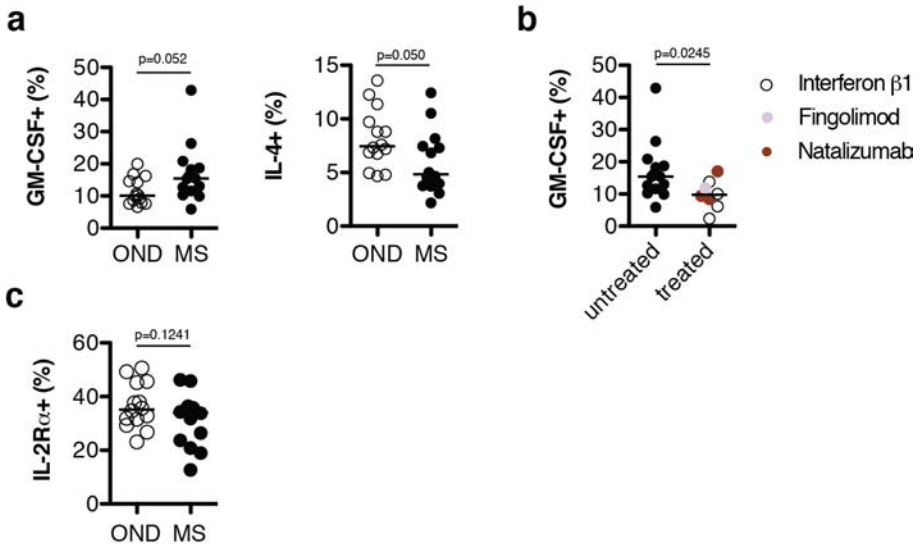

Figure 19. MS patients from an independent validation cohort have increased frequencies of GM-CSF producing T_H cells. (a-c) Frequency of cytokine secreting and IL-2Rα$^+$ memory T_H cells determined by flow cytometry without prior *in vitro* culture (MS *n*=14, OND *n*=14, treated MS *n*=8). Shown are cytokine production in OND vs. MS patients (a) as well as in untreated vs. treated MS patients (b) and the frequency of IL-2Rα$^+$ memory T_H cells in OND vs. MS patients (c). Data are combined from three independent experiments. Each symbol represents a single individual. For all figures throughout, lines represent the median.

3.3.2. GM-CSF$^+$ T_H cells coincide with biomarkers for disease severity

Furthermore, we analyzed whether increased GM-CSF production by T_H cells is associated with cerebrospinal fluid (CSF) biomarkers of disease progression and severity such as matrix metalloproteinase 9 (MMP9), an indicator of brain-blood barrier integrity (Ram et al. 2006), as well as neurofilament-light chain (NFL), a marker for neuronal damage (Lycke et al. 1998). MS patients with an elevated frequency (above a median of 15.3%) of GM-CSF secreting T_H cells had strongly elevated CSF levels of MMP9 (2.9 vs. 92.4 ng ml^{-1}, Figure 18d) as well as NFL (810 vs. 1677 ng L^{-1}), compared to MS patients with a low (below median) frequency of GM-CSF producing T_H cells. Additionally, we observed an increase in GM-CSF producing T_H cells in MS patients with more T2 MRI lesions (Figure 18e). Taken together, these observations indicate that patients with higher proportions of GM-CSF producing T_H cells may have a more severe MS phenotype.

3.4. Genetic modulation of GM-CSF production

3.4.1. *IL2RA* risk alleles convey an elevated frequency of GM-CSF$^+$ T_H cells

Given the relationship between MS and the frequency of GM-CSF$^+$ T_H cells, together with the role of IL-2 in the regulation of GM-CSF, we tested whether MS-associated *IL2RA* polymorphisms modulate GM-CSF production and thereby increase the risk of MS in healthy individuals (Table 4). In agreement with previous reports (Dendrou et al. 2009), we observed increased surface expression of IL-2Rα on naïve T_H cells in individuals with rs2104286 risk (A/A) vs. protective alleles (A/G or G/G, Figure 20a). We analyzed whether this risk allele-mediated increase in IL-2 responsiveness of naïve T_H cells translates into corresponding frequencies of GM-CSF-producing memory T_H cells. *In vitro* stimulation (αCD3 and 10 ng ml^{-1}) of sorted naïve T_H cells with rs2104286 risk alleles resulted in higher frequencies of GM-CSF producing memory T_H cells when compared to T_H cells carrying protective alleles (Figure 20b). Additionally, sorted IL-2Rα$^{\blacksquare}$ naïve T_H cells produced higher levels of GM-CSF after activation in the presence of IL-2 compared their IL-2Rα$^-$ counterpart (Figure 20c). We next analyzed whether this modulation of GM-CSF production also occurs *in vivo* and observed that individuals with rs2104286 risk alleles had a substantially increased

number of GM-CSF producing memory T_H cells compared to individuals with protective alleles (Figure 20d). The frequency of IFN-γ and IL-17A secreting memory T_H cells was not affected by rs2104286.

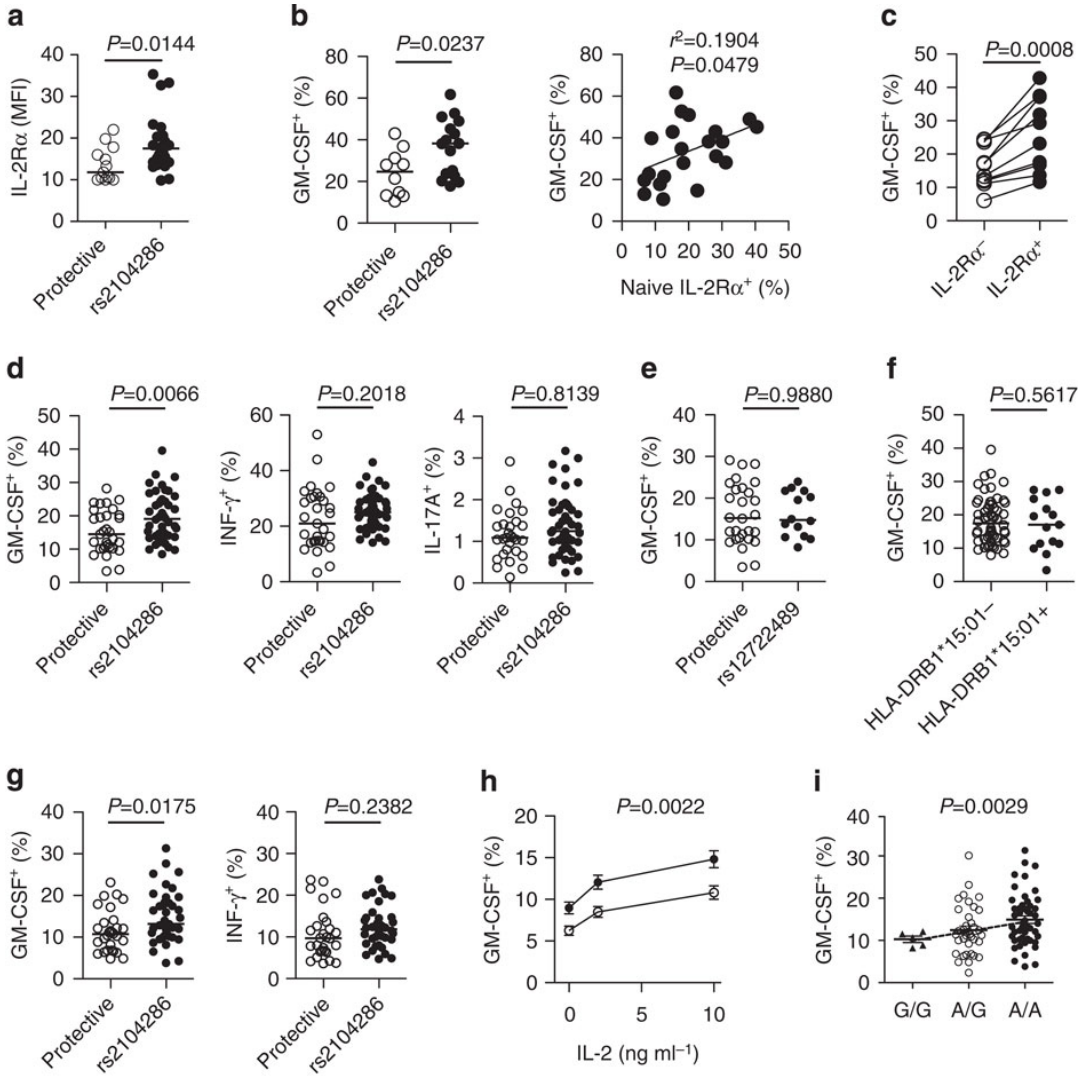

Figure 20. MS-associated *IL2RA* risk alleles augment GM-CSF producing T_H cells. (a) *Ex vivo* surface expression of IL-2Rα on naïve T_H cells from healthy individuals with a protective (G/G or A/G) or risk *IL2RA* genotype (A/A) at rs2104286, determined by flow cytometry (protective *n*=14, rs2104286 *n*=25). Data are combined from more than three independent experiments. (b) Sorted naïve T_H cells were activated *in vitro* (αCD3) in the presence of 10 ng ml^{-1} IL-2 and then analyzed for GM-CSF expression by flow cytometry on day 5 (protective *n*=10, rs2104286 *n*=16). Data are combined from more than three independent experiments. (c) Naïve T_H cells were sorted according to IL-2Rα expression and then activated (αCD3) for 5 days in the presence of 10 ng ml^{-1} IL-2 (*n*=10). Data are combined from two independent experiments. (d) PBMCs from healthy individuals were analyzed *ex vivo* (without previous *in vitro* culture) for the frequency of GM-CSF$^+$, IFN-γ$^+$ and IL-17A$^+$ memory T_H cells (protective *n*=31, rs2104286 *n*=46). (e) Individuals with rs2104286 protective alleles were further analyzed for *ex vivo* GM-CSF expression with regard to rs12722489 (protective *n*=28, rs12722489 *n*=14). (f) *Ex vivo* frequency of GM-CSF$^+$ T_H cells with regard to HLA-DRB1*15:01 alleles (HLA-DRB1*15:01$^-$ *n*=58, HLA-DRB1*15:01$^+$ *n*=15). Data are combined from more than three independent experiments. (g,h) Purified T_H cells were cultured in the presence of 0-10 ng ml^{-1} IL-2 (no αCD3) for 4 days. Shown are the frequency of GM-CSF$^+$ and IFN-γ$^+$ T_H cells at 10 ng ml^{-1} IL-2 (protective *n*=28, rs2104286 *n*=40, g) and the frequency of GM-CSF$^+$ T_H cells at IL-2 concentrations from 0-10 ng ml^{-1} (protective *n*=30, rs2104286 *n*=34, h). (i) Gene-dosage effect of rs2104286 on the frequency of GM-CSF$^+$ T_H cells, cultured as in (g,h), assuming a linear gene-phenotype relation (G/G n=5, A/G n=33, A/A n=45). Data are combined from more than three independent experiments. Each symbol represents a single individual. (a-g) lines represent the median, (h,i) error bars show mean±s.e.m.

Several SNPs have been identified within the *IL2RA* locus, including rs12722489, which is in modest linkage disequilibrium with rs2104286. Recent data show that of these two, only rs2104286 increases the risk to develop MS (Beecham et al. 2013). Accordingly, rs12722489 did not alter the frequency of GM-CSF producing T_H cells, demonstrating that the observed increase in GM-CSF production by rs2104286 is a specific consequence of risk-driving genetic variants and not other *IL2RA* SNPs (Figure 20e). Furthermore, we found the strongest genetic association with MS, HLA-DRB1*15:01, to have no influence on the frequency of GM-CSF expressing T_H cells (Figure 20f), indicating that modulation of GM-CSF expression is not a general mechanism of MS-associated risk genes. Additionally, HLA-DRB1*15:01 has been reported to enhance autologous T cell proliferation (Mohme et al. 2013), further indicating that elevated proliferation is largely disconnected from the observed increase in GM-CSF production.

3.4.2. *IL2RA*-influence on GM-CSF is preserved upon IL-2R engagement

To directly assess the impact of the *IL2RA* SNP rs2104286 on IL-2R signaling, we additionally measured GM-CSF secretion after stimulating T_H cells with IL-2 in the absence of TCR-engagement. Individuals with MS-associated risk alleles again showed a significantly higher number of GM-CSF secreting T_H cells compared to donors carrying protective alleles (Figure 20g). As observed also immediately *ex vivo*, the frequency of IFN-γ secreting T_H cells did not differ significantly between groups upon IL-2 stimulation. The increased frequency of GM-CSF producing T_H cells in individuals with rs2104286 risk alleles was maintained at different IL-2 concentrations (Figure 20h). Lastly, we observed a gene-dosage effect of the MS-associated rs2104286 risk allele on the frequency of IL-2 stimulated GM-CSF secreting T_H cells (Figure 20i).

3.5. GM-CSF expression by cytotoxic T cells

We found that GM-CSF production by $CD8^+$ T cells is not modulated by MS-associated risk genes or by MS disease (Figure 21a-c). This specificity therefore underlines the importance of GM-CSF production by human T_H cells in the context of MS pathology.

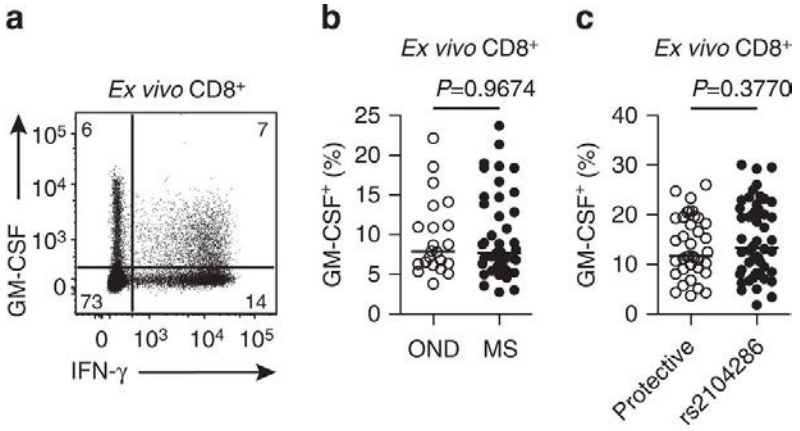

Figure 21. GM-CSF production by $CD8^+$ T cells is not altered in the context of MS. (a-c) The frequency of cytokine secreting $CD8^+$ T cells determined by flow cytometry without prior *in vitro* culture. Shown are a representative GM-CSF and IFN-γ secretion profile of $CD8^+$ T cells (a), cumulative frequencies of GM-CSF secreting $CD8^+$ T cells from untreated MS (*n*=27) vs. OND patients (*n*=22; b) and cumulative frequencies of GM-CSF secreting $CD8^+$ T cells with a protective (G/G or A/G) or risk *IL2RA* genotype (A/A) at rs2104286 (protective *n*=37, rs2104286 *n*=52; c). Data are combined from more than three independent experiments. Each circle represents a single individual. Throughout all figures lines represent the median.

4. Results – Part II

4.1. Establishing a mass cytometry workflow

4.1.1. Design of the metal-metal isotope labeled antibody panel

In order to extend our previous studies on the role of GM-CSF and other cytokines in MS, we employed high-dimensional mass cytometry to further explore the breadth of cytokine production profiles, focusing on T_H cells but also investigating other immune cell lineages. We designed a panel of heavy-metal isotope-labeled antibodies against 36 antigens with a total of 46 measured parameters measured per cell (Figure 22). Comprising a broad range of lineage markers, this panel was designed to identify all major immune populations ($CD4^+$ T cells, $CD8^+$ T cells, γδT cells, B cells, NK cells and monocytes) found in human PBMCs.

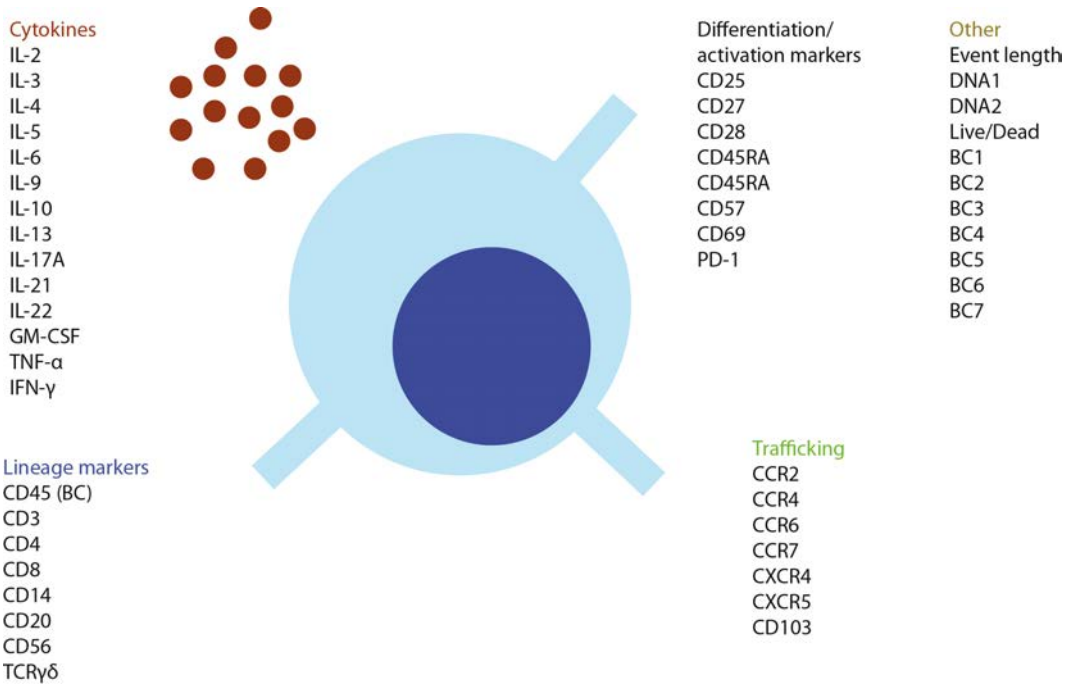

Figure 22. Antibody panel for mass cytometric exploration of T_H cell polarization. Antigens were chosen based on their importance in defining cellular subsets and lineages or based on prior reports indicating a possible involvement in MS. Monoclonal anti-human antibodies against the listed antigens were then obtained either pre-conjugated to heavy-metal isotopes or as purified antibodies which were then conjugated in house. Clones, suppliers and metal isotopes for all antibodies are listed in Table 6. The indicated categories were used in the analysis for differential weighing and categorical one-dimensional t-SNE.

In order to perform an in-depth analysis of the T_H cell subsets, we included a wide range of cytokines currently implicated in the pathogenesis of MS (Navikas and Link 1996; Becher and Segal 2011; Amedei et al. 2012) as well as other cytokines that have been suggested to define or contribute to a separate T_H cell lineage (Sallusto and Lanzavecchia 2009; O'Shea and Paul 2010). Additionally, we included multiple chemokine receptors which were shown to be differentially expressed on various T_H cell subsets (Appay et al. 2008; Mahnke et al. 2013), as well as maturation and activation markers, providing further insight into the state of immune activation. All antibodies were purchased either in purified form and then conjugated (see section 6.11.1) or obtained pre-conjugated to heavy-metal isotopes. Next, we established a staining protocol, optimized for the simultaneous detection of intracellular cytokines, as well as delicate surface markers such as chemokine receptors (see section 6.11). In short, we first stimulated the cells with PMA/ionomycin for 4h in the presence of a golgi-inhibitor. Next, we performed staining against surface markers and chemokine receptors simultaneously at 37°C (Berhanu et al. 2003) before fixation with 1.6% PFA and intracellular staining at 4°C for 1h. Using this protocol, we were able to obtain an optimal combination of surface marker, chemokine receptor and cytokine stainings (Figure 23a-c).

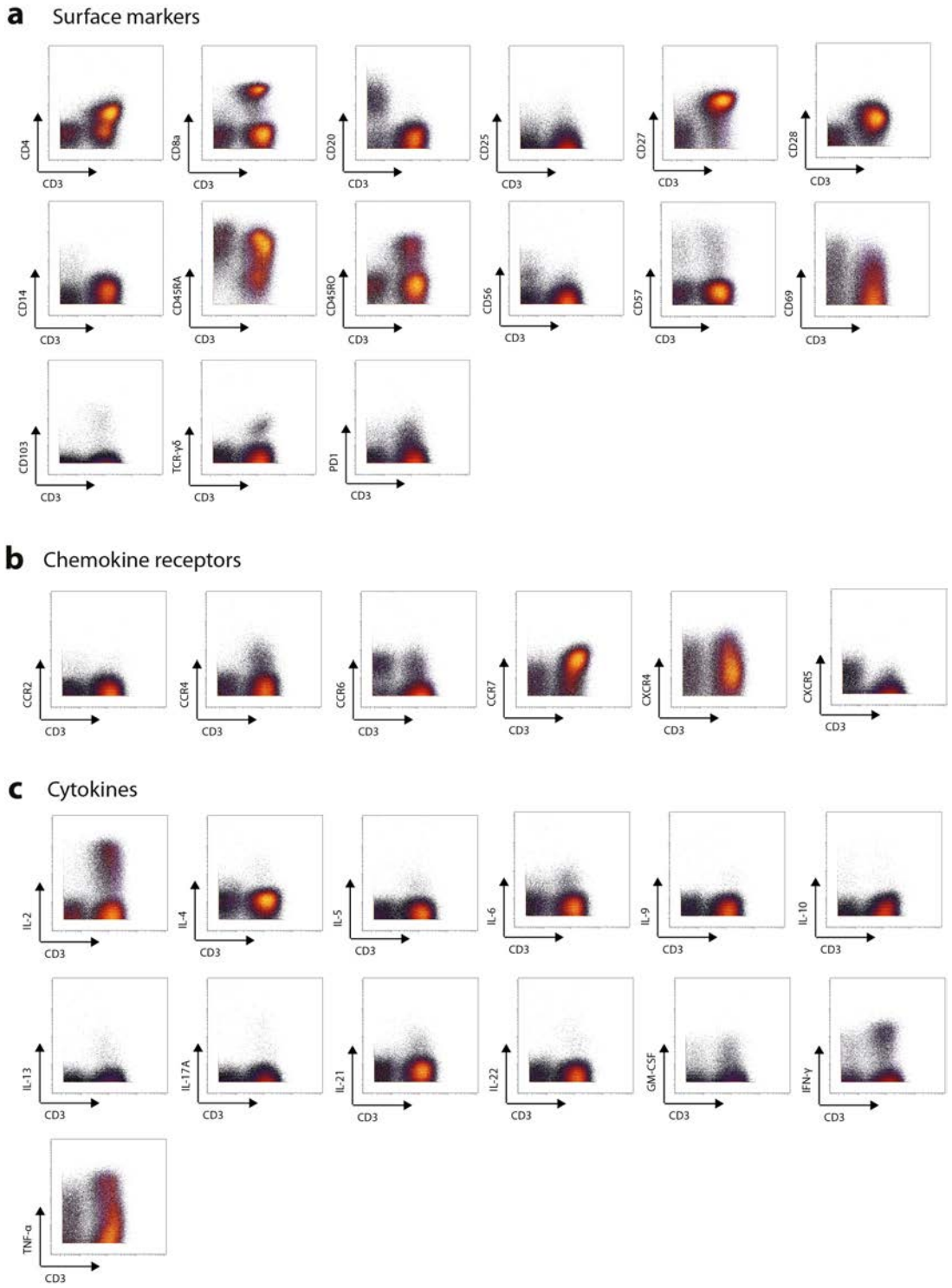

Figure 23. Cytokine and surface marker staining of human PBMCs using mass cytometry. Human PBMCs form healthy donors were stained with the antibodies against (a) surface markers, (b) chemokine receptors and (c) cytokines as listed in Table 6 and acquired on a CyTOF2 mass cytometer. Data was exported as fcs-files and uploaded to the cytobank website (www.cytobank.org). Plots shown are gated in live, single cells.

4.1.2. Establishing live cell barcoding

The availability of numerous channels also facilitates the use of mass-tag cell barcoding techniques without having to sacrifice the detection of other potentially important parameters. For this, cells are labeled with a specific combination of heavy-metal isotope-conjugated antibodies (Figure 24a). Subsequently, multiple barcoded samples can be combined and stained simultaneously within the same reaction tube, thereby virtually eliminating inter-sample staining variability and deviations during the acquisition process. Additionally, barcoding drastically reduces the number of undetected duplets. After acquisition, individual samples can be debarcoded by automatically gating on the specific combination of isotopes (Zunder et al. 2015). We established a barcoding scheme using a total of seven differently conjugated α-CD45 antibodies allowing for up to 35 unique combinations with a 7-choose-3 barcoding scheme (depicted for a 6-choose-2 scheme in Figure 24a,b).

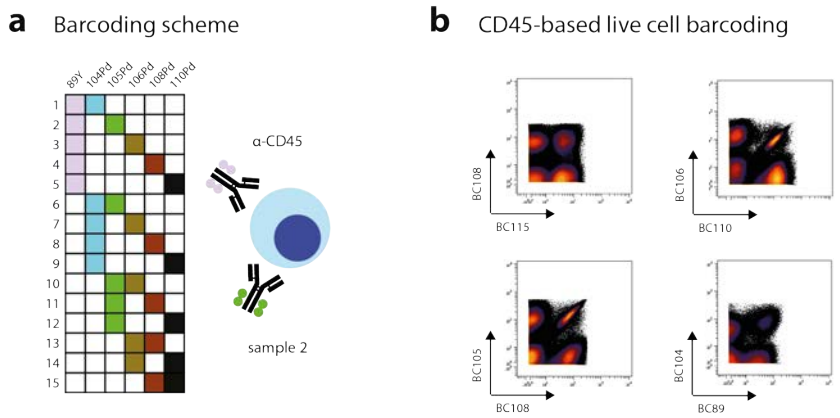

Figure 24. CD45-based live cell barcoding for mass cytometry. (a) Barcoding scheme for a 15-sample barcoding with a 6-choose-2 pattern. Alternatively, we employed a 7-choose-3 pattern with which we were able to barcode up to 35 samples. These patterns ensure that no duplets of cells from different samples are mistaken as another barcode. (b) Representative sample stainings of the seven α-CD45 antibodies used. Samples were then identified using an automated gating software (Zunder et al. 2015).

4.2. High-dimensional analysis of immune populations in MS patients

4.2.1. Algorithm-guided definition of immune lineages

After having established a comprehensive panel, the according staining protocol and the barcoding method, we used these techniques to explore the breadth of cytokine production profiles and immune activation in different groups of MS and control

patients (see Table 5). In order to compare the results obtained from different cohorts, we performed the analysis on all samples together and only later assigned individual cells back to their original files. Our first aim was to identify the major PBMC populations, namely $CD45RA^{high}CD45RO^{low}$ and $CD45RA^{low}CD45RO^{high}$ $CD4^+$ and $CD8^+$ T cells, B cells, NK cells, γδT cells and monocytes in order to investigate their modulation in MS. To do so, we employed the recently established FlowSOM algorithm (see section 1.6.5.5), which identifies cellular populations in a more unbiased and automated way by using the information provided from all measured channels instead of relying on strict two-dimensional gating (Figure 25a-d).

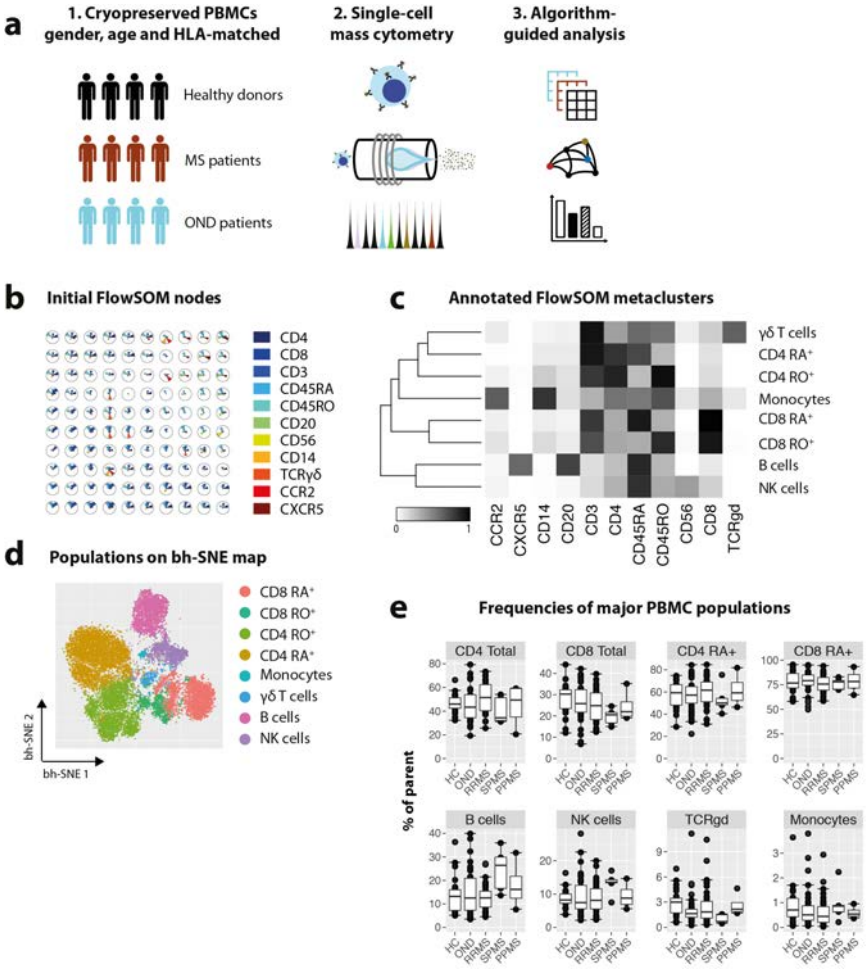

Figure 25. Algorithm-guided analysis of immune populations in MS. (a) PBMCs from healthy controls (HC n = 28), other neurological diseases (OND n = 36), relapse-remitting MS (RRMS n = 40), secondary-progressive MS (SPMS n = 5) and primary-progressive MS (PPMS n = 4) donors were analyzed using the mass cytometry panel described in section 4.1. (b) The FlowSOM algorithm was used to assign all cells to an artificial neuronal network consisting of 100 initial nodes. The mean expression of all indicated markers is represented by the height of each part. (c) Nodes as in (b) were metaclustered (k = 8) and manually annotated based on the expression level of several lineage-associated markers. (d) The Barnes-Hut (BH) implementation of the t-SNE algorithm was used to visualize the dataset on a two-dimensional map. Annotated metaclusters from (c) are overlayed as a color-dimension. (e) The frequency of all populations was compared in the control vs. different groups of MS patients. All frequencies are given as % of total PBMCs, except $CD4^+$ RA^+ and $CD8^+$ RA^+ are given as percent of their respective parent. Boxplots represent the 25th to 75th percentile with a black horizontal line indicating the median.

FlowSOM first assigns all cells to nodes (Figure 25b) and subsequently merges similar nodes into metaclusters (Figure 25c). All markers were used as input for the algorithm, however since our aim was to define major immune populations, we increased the contribution of all lineage markers (see section 6.12.2). The number of metaclusters (k = 8) was suggested by the FlowSOM algorithm based on a variance-measurement within the clusters. Based on the mean expression level of several lineage markers, the resulting eight metaclusters were then annotated as meaningful immunological populations. Additionally, the combined dataset was subjected to dimensionality reduction and visualization via t-SNE (Figure 25d), using the same increased contribution of lineage markers as above. Comparing the FlowSOM metaclustering results with the t-SNE projection showed a suitable correlation with the visually separate populations provided by t-SNE, thus further supporting the accuracy of the obtained populations. In a last step, the frequencies of all identified populations were compared between the groups of MS and control patients. Apart from an increased frequency of B cells in SPMS patients (26.4 ± 6.2% median ± s.e.m.), which was accompanied by a slight decrease in $CD4^+$ and $CD8^+$ T cells, no overt modifications were observed on the population level.

4.2.2. Defined cytokine-producing T_H cell populations expand in MS

Having automatically defined the major immune populations found in human PBMCs, we wanted to perform a more detailed analysis of their cytokine production, differentiation and activation markers and trafficking profiles in different groups of MS patients (Figure 26). First, we manually analyzed the production of GM-CSF, IFN-γ and IL-17A by $CD45RO^+$ T_H cells, which all three have been implicated in MS pathogenesis. As with conventional flow cytometry (see section 3.3.1), we found that GM-CSF (8.8 ± 0.8% vs. 5.7 ± 0.8%, median ± s.e.m.) and to a lesser extend IFN-γ (15.6 ± 2.0% vs. 13.7 ± 1.7%, median ± s.e.m.), but not IL-17A production (1.6 ± 0.2% vs. 1.6 ± 0.2% median ± s.e.m.) were increased in RRMS versus OND patients (Figure 26a,b). IL-17A production however seemed to be increased in PPMS vs. OND patients (3.9 ± 0.7% vs. 1.6 ± 0.2%, median ± s.e.m.). Additionally, in order to validate that mass cytometry can be a useful tool to study cytokine production by various immune cells, we analyzed whether the frequencies of cytokine positive cells

(obtained from the same patients) correlate when analyzed by mass versus flow cytometry (Figure 26c). Reassuringly, the two methods displayed a tight correlation, even with several years passing between the respective experiments.

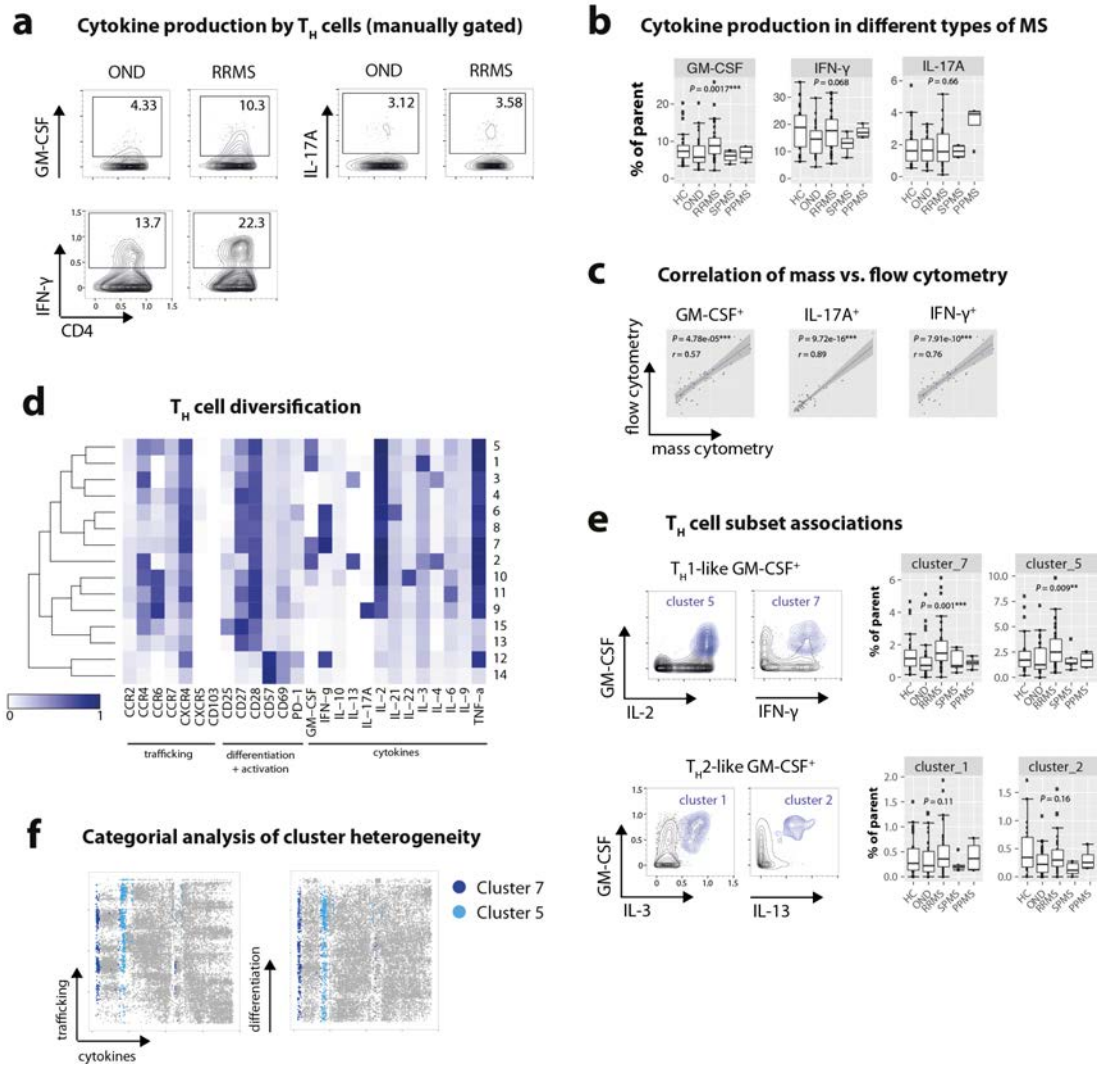

Figure 26. Fine mapping of altered memory T_H cell polarization in MS. (a,b) Manual gating on GM-CSF, IFN-γ and IL-17A-producing T_H in HC (n = 28), OND (n = 36), RRMS (n = 40), SPMS (n = 5) and PPMS (n = 4) confirms increased production of GM-CSF and IFN-γ in MS using mass cytometry. (c) Correlation of the frequencies of GM-CSF, IL-17A and IFN-γ-producing $CD45RO^+$ T_H cells from the same donors obtained with mass versus flow cytometry. The correlation co-efficient and the P-value were calculated using a linear regression model. (d) Co-expression of various cytokines, trafficking-associated antigens, and differentiation markers was assessed by clustering $CD45RA^-CD45RO^+$ T_H cells using the FlowSOM algorithm with increased weighing for cytokine markers and subsequent metaclustering (k = 15). The heatmap shows median expression levels of all analyzed markers across all samples. (d) Cytokine production profiles of indicated clusters (blue) and full $CD45RA^-CD45RO^+$ T_H cells (black) and their respective frequencies in different groups of control and MS patients. (e) The t-SNE algorithm was used to project cells from all samples onto three different categorical axes, using the markers indicated in (c) as respective inputs. The expanded GM-CSF-producing clusters were overlayed in blue. Boxplots represent the 25th to 75th percentile with a black horizontal line indicating the median. All P-values were calculated using a non-parametric Mann-Whitney-Wilcoxon test. Multiple comparisons corrections were performed with the Benjamini-Hochberg approach. *** = significant with false discovery rate (FDR) < 5%, ** = significant with FDR < 10%, * = significant with FDR < 15%.

IFN-γ has been known for decades to be the signature cytokine of the T_H1 lineage, however, recently also other subsets have been shown to produce IFN-γ (see section 1.3.1). GM-CSF has also been associated with multiple T_H cell subsets. On the one hand, GM-CSF is driven by T_H1 polarizing cytokines and on the other hand, it was initially described to be associated with the T_H2 lineage. Therefore, we wanted to examine if the increased GM-CSF production in MS patients is due to the expansion of a specifically defined GM-CSF producing subset, co-expressing a particular set of cytokines and associated trafficking and differentiation profiles. To do so, $CD45RO^+CD4^+$ cells from all samples were clustered using the FlowSOM algorithm and increasing the weight of cytokines in this clustering (Figure 26d). Multiple known T_H cell lineages could be identified, such as T_H1-like populations (cluster 7, 8), T_H2 (cluster 1, 2, 3), T_H17 (cluster 9), T_H22 (cluster 10), T_{FH} (cluster 6) and T_{REG} (cluster 15) populations. We did not detect a distinct cluster corresponding to T_H9 cells. Also, $CD103^+$ cells were present but not distinct enough in their overall marker expression profile to form a separate cluster.

GM-CSF production was prominent in four different clusters, with co-expression of IFN-γ (cluster 7) or co-expression of T_H2 cytokines IL-3 and IL-4 (cluster 2) or IL-13 (cluster 1). In RRMS patients, we found that specifically those GM-CSF producing subsets were expanded, which were associated with the T_H1 lineage (cluster 7 ~1.9 fold increase in RRMS vs. OND, cluster 7 ~1.8 fold). This was not the case with $GM\text{-}CSF^+$ clusters co-expressing T_H2-like cytokines (clusters 1 and 2; Figure 26e). Lastly, we analyzed whether the specifically expanded clusters 5 and 7 display an exclusive trafficking or maturation/activation profile. As described previously (Cheng et al. 2015), we employed the categorical t-SNE-based dimensionality reduction algorithm with three distinct sets of input dimensions, based on a broad categorization of the markers into cytokines, trafficking/homing and differentiation/activation (Figure 26f). We found that both clusters had a very defined cytokine production profile, as it was intended by weighing cytokine markers during the clustering, however their trafficking and differentiation profiles were quite heterogeneous.

4.2.3. Cytotoxic T cells in MS

Although T_H cells are thought to be the main pathogenic mediators in MS, we wanted to make use of the high-dimensional power of mass cytometry which allows for the analysis of multiple cell types within the same experiment. Thus, we also investigated the polarization profiles of $CD8^+$ cytotoxic T cells (T_C) cells. As with $CD4^+$ T cells, we first analyzed cytokine production of $CD45RO^+CD8^+$ T cells by manual gating (Figure 27a). Comparing MS and control patients, we found a tendency for increased production of IFN-γ in RRMS vs. OND patients (57.6 ± 2.5% vs. 47.6 ± 5.1% median ± s.e.m.), which was however not statistically significant ($P = 0.16$, Figure 27b).

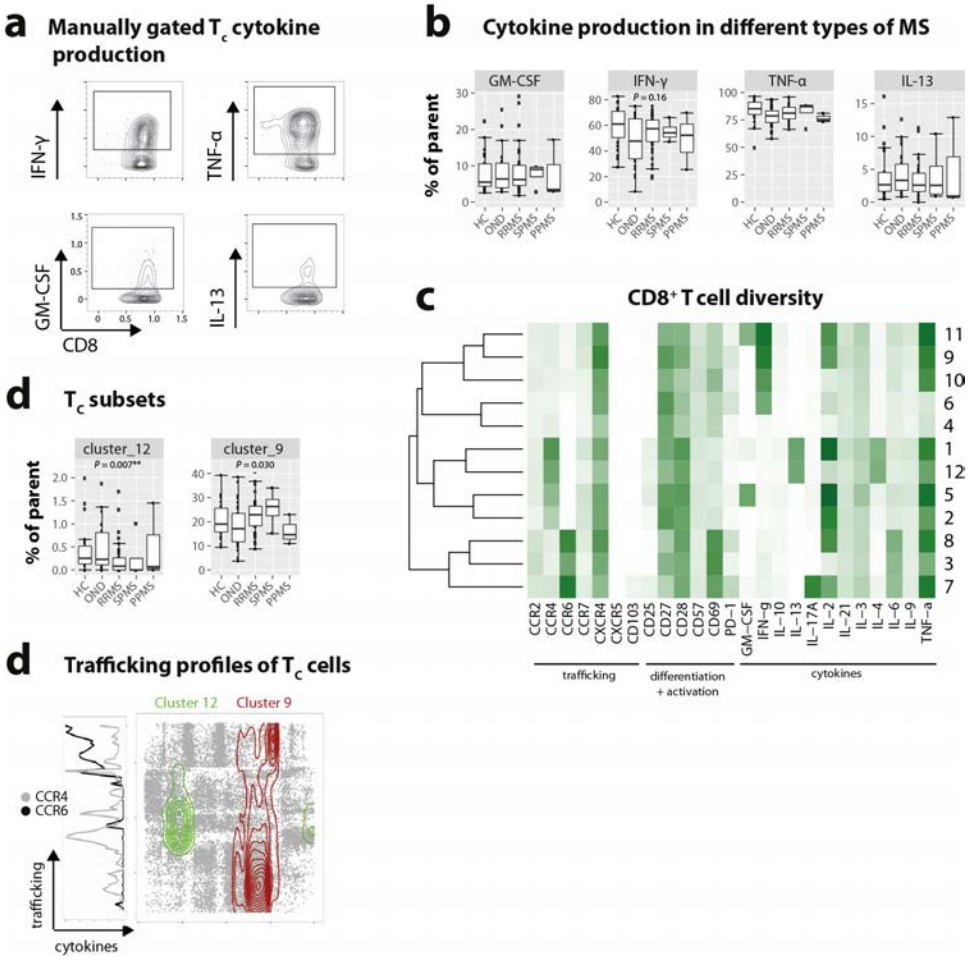

Figure 27. Modulation of $CD45RO^+$ cytotoxic T cells in MS. (a) The frequency of cytokine-positive $CD45RO^+CD8^+$ cells was determined by manual gating. (b) Cumulative result of manually gated cytokine positive cells in HC (n = 28), OND (n = 36), RRMS (n = 40), SPMS (n = 5) and PPMS (n = 4). (c) The FlowSOM algorithm was used to define T_C subsets. As before, the contribution of cytokine markers was increased. (d) Frequency of clusters as defined in (c) in MS vs. control patients. (d) Categorical, one-dimensional t-SNE was used to further explore the trafficking profile of differentially modulated clusters 9 and 13. Vertical histograms represent the normalized median intensity across the trafficking profile. Boxplots represent the 25th to 75th percentile with a black horizontal line indicating the median. All P-values were calculated using a non-parametric Mann-Whitney-Wilcoxon test. Multiple comparisons corrections were performed with the Benjamini-Hochberg approach. *** = significant with FDR < 5%, ** = significant with FDR < 10%, * = significant with FDR < 15%.

Extending this preliminary analysis, we wanted to examine whether a particular T_C subset, which is not only defined by the production of a single cytokine but by the whole set of (T_C-relevant) antigens analyzed, would be specifically modulated in MS. Again we made use of the FlowSOM algorithm to automatically define T_C sub-populations with a focus on cytokine expression patterns (Figure 27c). We found clusters corresponding to multiple, previously described T_C subsets also in terms of their expression of chemokine receptor expression profiles. Analyzing their potential role in different groups of MS patients, we found that two clusters were specifically modulated in their frequency in RRMS patients. A small population of T_C cells co-producing IL-13 and IL-4 (cluster 12) was specifically decreased in RRMS vs. OND patients (0.23 ± 0.13% vs. 0.08 ± 0.04% median ± s.e.m.) whereas a substantial cluster co-expressing TNF-α, IL-2 and IFN-γ was increased (22.9 ± 1.3% vs. 17.2 ± 2.8% median ± s.e.m.). Furthermore, exploring the trafficking profile of these clusters we found that while cluster 12 seemed to have a more homogeneous trafficking profile with high expression of CCR4, cluster 9 comprised $CCR4^-CCR6^-$ but also $CCR4^-CCR6^+$ cells (Figure 27d).

4.2.4. B cells and NK cells in MS

Besides the investigation of $CD4^+$ and $CD8^+$ T cells, the broad nature of our panel also allows the investigation of further immune cell populations in MS. Especially B cells were recently shown to be more important players in MS pathogenesis then previously appreciated (see section 1.3.4). We were able to analyze several maturation and activation markers, as well as cytokines expressed by B cells. The frequencies of GM-CSF, IL-6, IL-10 and TNF-α producing B cells were however not significantly modulated in our cohort of MS patients (Figure 28a). Likewise, there was no major modulation of the expression levels of investigated chemokine receptors or maturation markers on B cells (data not shown).

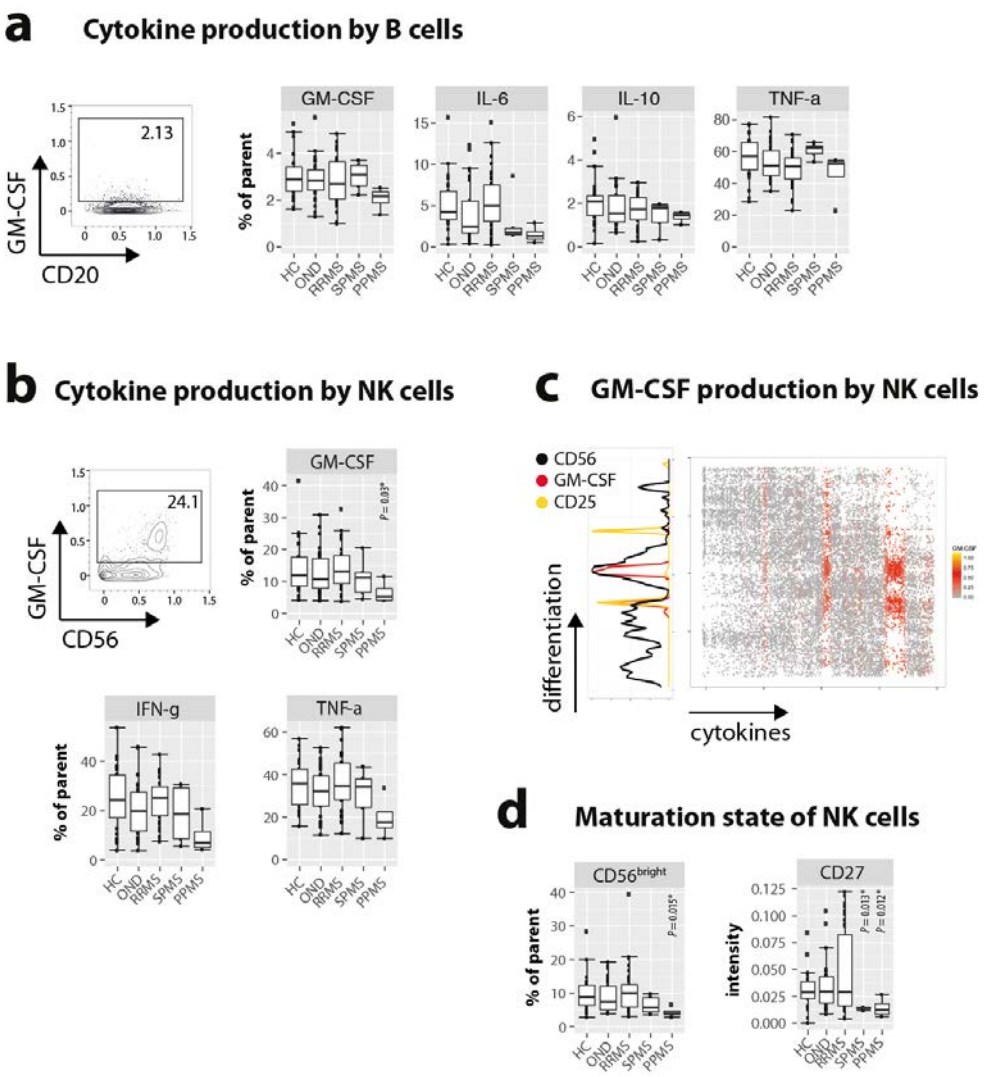

Figure 28. Cytokine-production profiles of additional immune populations in MS. (a) B cells were manually analyzed for the frequency GM-CSF, IL-6, IL-10 and TNF-α positive cells in various groups of control and MS patients. HC (n = 28), OND (n = 36), RRMS (n = 40), SPMS (n = 5) and PPMS (n = 4). (b) Cytokine production by NK cells was analyzed analogously. (c) Categorical, one-dimensional t-SNE analysis was used to further characterize the GM-CSF producing NK cell subset. Vertical histograms represent the normalized median intensity of CD56 (black), CD25 (yellow) and GM-CSF (red) across the trafficking dimension. On the plot, GM-CSF expression is shown as a color dimension from grey (low) to red to yellow (high). (d) The frequency of $CD56^{bright}$ NK cells was determined by manual gating. All P-values were calculated using a non-parametric Mann-Whitney-Wilcoxon test. Multiple comparisons corrections were performed with the Benjamini-Hochberg approach. *** = significant with FDR < 5%, ** = significant with FDR < 10%, * = significant with FDR < 15%.

NK cells might also contribute to some degree to pathogenic and/or regulatory mechanisms in MS (see section 1.3.6). To investigate their possible modulation in different subsets of MS patients, we examined NK cell maturation and cytokine production based on the available markers. We did not detect a significant modulation of NK cell cytokine production in RRMS patients compared to OND patients (Figure 28b). However, the few examined PPMS patients showed a decrease in a GM-CSF producing population in comparison to OND patients (5.3 ± 2.1% vs. 10.7 ± 2.2%

median ± s.e.m.). Further investigations using categorical t-SNE dimensionality reduction demonstrated that the GM-CSF^{+} NK cells can be divided into two distinct populations based on their differentiation marker profile (Figure 28c). Specifically, we found a GM-CSF producing population of CD56^{bright} cells and a separate population of CD25^{+} but CD56^{dim} NK cells (Clausen et al. 2003; Gasteiger et al. 2013). Accompanying the decreased GM-CSF production in PPMS patients, the frequency of CD56^{bright} cells was also reduced in PPMS versus OND patients (3.9 ± 0.9% vs. 7.4 ± 1.0%, median ± s.e.m., Figure 28d). Additionally, we found a down regulation of the median CD27 expression on NK cells in PPMS patients (~3-fold decrease of median intensity), further supporting modulated NK cell maturation and differentiation in this progressive form of MS and again demonstrating how a broad analysis using mass cytometry can reveal unexpected phenotypes on otherwise overlooked immune populations.

5. Discussion

5.1. The role of GM-CSF in MS and other autoimmune diseases

The molecular signature and functional properties of auto-aggressive T cells in chronic inflammatory disease remain a subject of intense research (Becher and Segal 2011). GM-CSF has emerged as a major pro-inflammatory mediator in several preclinical models of autoimmune disease. For instance, T cells deficient of GM-CSF fail to transfer disease in an animal model of MS. Thus GM-CSF has, in contrast to other cytokines such as IL-17A or IFN-γ, a non-redundant function in the development of autoimmune neuro-inflammation (Codarri et al. 2011). Of note, a recent phase II clinical trial showed therapeutic efficacy of GM-CSF neutralization in RA patients (Behrens et al. 2014) and a phase Ib trial in MS patients has just been completed, demonstrating the urgent need for a better understanding of the role of this cytokine in autoimmunity (Constantinescu et al. 2015).

Supporting the involvement of GM-CSF in MS, we here report increased frequencies of GM-CSF producing T_H cells in MS compared to control patients. In addition, we found increased levels of CSF biomarkers of MS disease progression and severity, as well as the number of MRI lesions, to correspond with GM-CSF expression in these patients. Interestingly, immuno-modulatory therapy in MS coincided with a reduction in the frequency of GM-CSF (but not IL-17A or IFN-γ) secreting T cells. This is not likely due to a direct impact of therapeutic interventions on GM-CSF production, but rather that therapy-induced reduction in disease activity leads to a normalization of GM-CSF frequencies in T_H cells.

5.2. The regulation of GM-CSF by IL-2 signaling

In contrast to mice, where numerous cytokines have been proposed to initiate GM-CSF transcription (Codarri et al. 2011; El-Behi et al. 2011), we observed that in humans, IL-2 is a particularly strong driver of GM-CSF production. As we could show, activation of STAT5 seems to play a crucial role in this process, which has now also been confirmed by further studies in humans as well as in mice (Noster et al. 2014; Sheng et al. 2014). Also in agreement with others, we found the GM-CSF-

inducing capacity of IL-2 to be independent of the effect IL-2 has on proliferation (Noster et al. 2014).

5.3. The genetic influence on GM-CSF production

GWA studies firmly link polymorphisms in the *IL2RA* locus (rs2104286) with the risk to develop MS. However, the mechanism by which this polymorphism confers risk has been elusive. Here we found a significantly increased propensity of T_H cells from individuals carrying *IL2RA* risk alleles to secrete GM-CSF. Rs2104286 is an intronic SNP, which has been shown to regulate mRNA expression of IL-2Rα (Dendrou et al. 2009). We here confirm that individuals with rs2104286 risk alleles have increased levels of surface IL-2Rα on naïve T_H cells. This elevated responsiveness of naïve T_H cells from healthy individuals with risk alleles results in a higher propensity to develop GM-CSF-expressing effector T_H cells. This finding mechanistically links a prominent genetic risk factor with the production of the pro-inflammatory cytokine GM-CSF by T_H cells, extending previous studies exploring possible pathogenic mechanisms of *IL2RA* SNPs (Lowe et al. 2007; Maier et al. 2009b; Maier et al. 2009a; Dendrou et al. 2009). We did not find any modulation of cytokine production by T_H cells with regard to the strongest genetic risk factor of MS, the HLA-DRB1*15:01, nor with regard to other polymorphisms in cytokine receptors such as the *IL7R*. Together, this further underlines the specificity of the observed modulation by the *IL2RA* and contributes to the emerging picture in which non-HLA variants influence the threshold of immune activation and the subsequent differentiation profile, whereas HLA variants rather define the tissue specificity of the immune attack (Dendrou et al. 2015).

5.4. Mass cytometry for the in-depth analysis of clinical phenotypes

This thesis also constitutes one of the first reports in which the relatively new technology of mass cytometry is used to perform a more comprehensive analysis of immune states, especially cytokine production, and their pertubations in autoimmunity (Nair et al. 2015). To ensure that mass cytometry in combination with automated algorithms for high-dimensional data analysis are a suitable tool, we

compared our results obtained from conventional flow cytometry with the outcome of our mass cytometric experiments we found a tight correlation between the two techniques (Nicholas et al. 2015). Mass cytometry has faced the drawback of reduced sensitivity in comparison to traditional flow cytometry (Bendall et al. 2012), however near-future hardware improvements will render these differences negligible. Nevertheless, also the existing configuration was sufficient to clearly identify cytokine positive cells and to determine the profile of chemokine receptor expression. Thus, the high-dimensional ability of mass cytometry is so far only rivaled by single-cell RNA sequencing (Wu et al. 2014).

5.5. Algorithm-guided data analysis

Furthermore, we here employed automated algorithms in order to perform a more unbiased and automated analysis. This has been shown to be especially valuable when looking at high-dimensional associations of markers where strict two-dimensional gating might miss important phenotypes (Lugli et al. 2010; Pedreira et al. 2013; Chester and Maecker 2015). Several algorithms have been shown to perform equally well and in many cases even superior when compared to manual gating (Aghaeepour et al. 2013; Kvistborg et al. 2015). Also, as shown above, the automatically defined populations corresponded well to expected immune populations and they were coherent with visually distinct clusters on a t-SNE map. Additionally, analysis of cytokine co-expression would not have been possible without using clustering algorithms. Given the examined 13 cytokines, there are 2^{13} = 8'192 possible combinations, even without using any additional information provided by trafficking or activation profiles. While the biologically relevant number of actual populations might be considerably lower, this clearly underlines the advantage of unbiased and automated analysis approaches. Since we were especially interested in cytokine-production this also provided the rationale to differentially weigh cytokine markers in the analysis. This approach resulted in clusters more homogeneous in terms of their cytokine expression profile while still making use of the information provided by other markers. Together, this enabled us to automatically define subpopulations of which the majority could be easily attributed with previously described biological functions and to study their possible modulation MS.

5.6. GM-CSF producing T_H cells comprise several subsets

Having established this tool set, we could firstly confirm the increase in GM-CSF producing T_H cells in RRMS patients, which we also found by flow cytometry in combination with manual gating, thus validating our approach and its clinical relevance on an additional layer. Next, using algorithm-guided subdivision of T_H cells, we found that GM-CSF producing T_H cells are a heterogeneous population, comprising multiple subsets as defined by co-expression with other cytokines as well as specific profiles of trafficking and differentiation markers. More specifically, GM-CSF production was observed by T_H1, T_H2 and also other T_H cells. However, we found that T_H1-associated clusters constituted the largest fraction of GM-CSF producing T_H cells. We believe that this comprehensive analysis can help understand and consolidate contradictory reports in which GM-CSF production has been reported to be associated with and driven by T_H17 (Codarri et al. 2011; El-Behi et al. 2011), T_H2 and T_H1-inducing cytokines (Kruger et al. 1996; Noster et al. 2014). A possible explanation is that *in vitro* skewing towards these lineages is likely to result in associated GM-CSF production. However, as we have shown above, IL-2 is by far the most potent of these factors and congruently, we found clinically important *in vivo* relevance of the IL-2 pathway through the influence of *IL2RA* genetic variants.

We here demonstrated that both, IFN-γ as well as GM-CSF production are increased in MS patients and that these two cytokines are substantially co-expressed in human T_H cells. The finding that double-positive, but also GM-CSF$^+$ and IFN-γ$^-$ populations are increased in MS supports the notion of an independent pathogenic role of GM-CSF, also in the absence of IFN-γ.

5.7. Modulation of further immune populations in MS

Making use of the high-dimensional power of mass cytometry and thus the ability to analyse multiple populations simultaneously, we also analsyed the differentiation and cytokine profile of CD8$^+$ T cells, NK cells as well as B cells in MS. Consistent with our flow cytometry analysis, high-dimensional mass cytometry did not reveal modulation of GM-CSF production by CD8$^+$ T cells in RRMS, although this has been reported by others (Rasouli et al. 2015). Instead we found a population of IFN-γ and

TNF-α co-producing T_C cells to be increased in RRMS patients, whereas a T_C2-like population was decreased. This finding is consistent with the general modulation of these cytokines in MS, however the functional relevance of their production by $CD8^+$ T cells will remain debated. Nevertheless, this again underlines the ability of mass cytometry to perform comprehensive clinical studies in which multiple cell types can be investigated simultaneously.

5.8. Conclusions

This study resolves and integrates findings obtained in preclinical models with human disease by providing a direct link between a genetic risk trait in MS pathogenesis, IL-2R signaling, and a feature of pathogenic T cells, namely GM-CSF production. Additionally, we demonstrate the usefulness of mass cytometry in combination with automated algorithms for the analysis of clinical phenotypes of various immune populations simultaneously. We here made use of this abilty for the precise characterization of the pathogenic profile of T_H cells and its modulation in MS.

Taken together, we hope that this report can contribute to our knowledge of T_H biology in general, and that it might advance our important understanding of the role of these cells and their specific subsets in the pathogenesis of autoimmune disease.

We are looking forward to see GM-CSF neutralization moving forward in clinical trials and hope that our findings might soon contribute to benefit patients with MS and other autoimmune diseases.

6. Methods

6.1. Healthy donor and patient samples for GM-CSF studies

6.1.1. Human PBMC samples

Healthy donors were recruited via the blood donation center Zurich, Switzerland with approval of the cantonal ethics committee Zurich. MS and OND patient samples (Table 1 - Table 3) were collected at the neurological clinics at Karolinska University Hospitals Solna and Huddinge. MS and OND samples for validation were collected at the Nottingham University Hospitals, UK. Informed consent was collected from all participants. DNA was isolated using the DNeasy blood and tissue kit (Qiagen). SNPs and the HLA-DRB1*15:01 (rs3135388, (de Bakker et al. 2006; Hafler et al. 2007)) genotype were determined using TaqMan SNP Genotyping Assays (Life technologies). Flow cytometric experiments and analysis was performed blinded with regard to disease and genotype.

6.1.2. Characterization of patient cohorts

Table 1. Clinical diagnosis/characterization of MS and OND patients in cohort 1

OND patients	Detailed clinical characteristics	n
	Psychosis	14
	Paresthesia	4
	Narcolepsy	1
	Benign tumor in brain	1
	Lesions on peroneal nerve	1
	Visual disturbance	1
MS patients		
	RRMS remission	40
	RRMS relapse	4

Abbreviations: OND = other neurological disease (non-inflammatory), MS = multiple sclerosis, RRMS = relapse-remitting MS.

Table 2. Clinical diagnosis/characterization of MS patients in cohort 2

OND patients	Detailed clinical characteristics	n
	Epileptic disorder	6
	Cerebrovascular disease	2
	Headache	2
	Cranial nerve palsy	1
	Neurodegenerative disease	1
	Non-epileptic attack	1
	Spasmus facialis	1
MS patients		
	RRMS	18
	SPMS	3
	PPMS	1

Abbreviations: MS = multiple sclerosis, RRMS = relapse-remitting MS, SPMS = secondary-progressive MS, PPMS = primary-progressive MS.

Table 3. Demographic characteristics of MS and OND patients

Cohort 1		n	Age mean (range)	Sex (Female:Male)
	MS	44	35.0 (17-56)	32:12
	OND	22	40.0 (17-72)	11:11
Cohort 2				
	MS	22	43.9 (24-65)	13:9
	OND	14	57.3 (30-75)	7:7

Abbreviations: MS = multiple sclerosis, OND = other neurological diseases

6.1.3. Characterization of healthy donors

Table 4. Demographic and genotypic characteristics of healthy donors

	n	Age mean (range)	Sex (Female:Male)
total	221	47.1 (21-69)	160:61
G/G	11	48.6 (33-65)	5:6
A/G	73	48.8 (24-68)	52:21
A/A	137	46.0 (21-69)	103:34

G = protective allele at rs2104286, A = risk allele at rs2104286. Inclusion criteria were 20-69 years. Samples for different assays were chosen randomly and blinded with regard to sex, age and genotype.

6.2. PBMC isolation, cryopreservation and thawing

PBMCs were isolated by density gradient centrifugation using Lympholyte-H (Cedarlanes). PBMCs were cryopreserved in sterile-filtered FCS (Biochrom) + 10% DMSO (Applichem) at a final concentration of 2.5 x 10^6 ml^{-1} and stored in liquid nitrogen. Cyrovials were thawed in a 37 °C water bath and washed twice by drop-wise addition of 37 °C RPMI-1640 (PAN biotech) with 10% FCS.

6.3. *In vitro* culture

6.3.1. Regulation of GM-CSF production

To address the regulation of GM-CSF, sorted naïve T_H cells were stimulated for 5 days with 1 μg ml^{-1} anti-human CD3 (OKT3, Bioexcel) antibody with or without 1 μg ml^{-1} anti-human CD28 (CD28.2, BD Pharmingen) and 10 ng ml^{-1} of one of the following cytokines: IL-1β, IL-6, IL-23, IL-2, IL-4, IL-7, IL-9, IL-15, IL-21 and TGF-β1 (all from PeproTech). Proliferation was assessed by labeling cells with 5 μM CFSE. Where indicated, 10 μg ml^{-1} of anti-human IL-2Rα (Basiliximab, Novartis) was added to the culture on day 0. To simultaneously analyze GM-CSF production and STAT5 phosphorylation, T_H cells were cultured as described above. For inhibition of STAT5 phosphorylation, 2.5 μg ml^{-1} pimozide (Sigma) was added at day

0 and flow cytometric readouts were performed at day 5. For IL-2 restimulation of PBMCs obtained from healthy donors, $CD4^+$ T cells were purified by MACS separation (Miltenyi Biotech), as suggested by the supplier. IL-2 was added in concentrations ranging from 0–10 ng ml^{-1} and T_H cells were cultured for 4 days at 37°C.

6.3.2. Impact of regulatory T cells

The impact of T_{reg} cells on GM-CSF production was determined by co-culture of sorted naïve (labeled with CFSE, eBiosciences) and regulatory T_H cells (labeled with CellTrace Violet, Lifetechnologies) at a 1:1 ratio for 5 days. The cells were stimulated with 10 ng ml^{-1} IL-2 and anti-CD3 plus anti-CD28 antibodies. Where indicated, 10 μg ml^{-1} anti-TGF-β and anti-IL-10R (Biolegend) were added to the culture at day 0.

6.4. *Ex vivo* restimulation of PBMCs

The frequency of cytokine secreting cells was determined after short restimulation using 50 ng ml^{-1} PMA and 500 ng ml^{-1} ionomycin in the presence of a protein transport inhibitor (Golgiplug, BD) for 4 hours at 37 °C.

6.5. Flow Cytometry

6.5.1. Flow cytometry and cell sorting

To sort naïve T_H cells ($CD4^+CD127^+CD25^{-/med}CD45RO^-$) from healthy donors, total PBMCs were stained with anti-human CD4 APC-Cy7 (RPA-T4, 1/100, BD Pharmingen), CD25 APC (BC96, 1/50, eBioscience), CD127 FITC (eBioRDR5, 1/50, eBioscience) and CD45RO ECD (HI100, 1/100, Beckman Coulter). T_{reg} cells were defined as $CD4^+CD127^-CD25^{high}$ and excluded from the naïve T_H cell population. Anti-human monoclonal antibodies used for *ex vivo* surface staining were PacificBlue-conjugated CD4 (RPA-T4, 1/200, Biolegend), Brilliant Violet™ 785-conjugated CD8 (RPA-T8, 1/200, Biolegend), APC-conjugated CD25 (BC96, 1/50, eBiosciences) and PE-Cy7-conjugated CD45RA (HI100, 1/200, Biolegend).

6.5.2. Intracellular cytokine staining

Intracellular cytokine staining was performed using anti-human PE-conjugated GM-CSF (BVD2-21C11, 1/200, BD Biosciences), Alexa Fluor 488-conjugated or PE-Cy7-conjugated IFN-γ (4S.B3, both 1/200, Biolegend or eBiosciences), APC-Cy7-conjugated IL-17A (BL168, 1/200, Biolegend) and AlexaFluor 488-conjugated IL-4 (8D4-8, 1/50, Biolegend). Dead cells were excluded using the LIVE/DEAD® fixable dead cell stain kit (Invitrogen).

6.5.3. STAT5 phosphorylation and Ki-67 staining

Respective cell populations were stimulated for 10 min at 37°C with 10 ng ml^{-1} of the indicated cytokine. Cells were then fixed in 1.6% PFA and permeabilzed in methanol on ice for 30 min. Subsequently, anti-human APC-conjugated CD4 (RPA-T4, 1/20, Biolegend) and PE or APC-conjugated pSTAT5 (47, both 1/20, BD Biosciences and C71E5, Cell signaling technology, respectively) were used for staining. Cell cycle analysis was performed using FITC-conjugated anti-human Ki-67 (35/Ki-67, 1/20, BD Biosciences).

6.5.4. Acquisition and analysis

FACS acquisition and sorting were performed on LSR-Fortessa (BD) and Aria III (BD), respectively. Analysis was performed using the FlowJo software (Tree star) in combination with Prism (GraphPad).

6.6. Quantitative Real-Time PCR

RNA was isolated with the PureLink™ RNA Micro Kit and cDNA was obtained using SuperScript® III reverse transcriptase (both Life Technologies). qPCR was then performed using the *CSF2* and *GAPDH* TaqMan gene expression assay (Life Technologies) and read on a CFX384 Touch Real-Time PCR Detection System (BioRad).

6.7. Microscopy

Sorted naïve T_H cells (CFSE labeled) and T_{reg} cells (CellTrace Violet labeled) were placed on cover slide, pretreated with poly-l-lysine, and allowed to rest for 30 min. 10 ng ml^{-1} IL-2Fc (Sigma) was added for 10 min before cells were washed and fixed with 1:1 aceton:methanol for 12h at -20 °C. IL-2Fc was then stained with APC-conjugated anti-human IgG antibodies (G18-145, BD Biosciences). Fluorescent imaging was performed using an inverted fluorescent microscope with a 40x objective (IX81, Olympus).

6.8. ELISA

Cytokine levels of cell culture supernatants and human serum was analyzed by ELISA as suggested by the supplier (all Mabtech). CFS levels of MMP9 and NFL were determined as previously described (Khademi et al. 2013).

6.9. Statistical analysis

All statistical tests were performed using the R statistical software package or Prism 5 (GraphPad). Differences between two groups were analyzed using a two-sided t-test, accounting for different variances by Welch`s correction if indicated. Non-gaussian distributions were compared by the nonparametric Mann-Whitney test. Analysis of variance (ANOVA) was used to compare more than two groups and regression analysis was used to test for correlations between genotype and flow cytometric data, controlling for age and sex. Gene-dosage effects were analyzed by linear regression, assuming a linear genotype-phenotype correlation. We estimated the sample size considering the variation and mean of the distribution.

6.10. Healthy donor and patient samples for mass cytometry studies

6.10.1. Recruitment of patients

PBMC samples of MS and control patients (Table 5) were collected at the neurological clinics at Karolinska University Hospitals Solna and Huddinge, Sweden. Informed consent was collected from all participants. Mass cytometric experiments and initial analysis was performed blinded with regard to disease and genotype.

Table 5. MS and control patient samples for mass cytometry experiments

Cohort Part 1	**n**	**Age mean (range)**	**Sex (Female:Male)**
HD	20	40 (26-55)	8:12
OND	24	40.5 (21-74)	15:9
PPMS	4	52.8 (43-66)	2:2
RRMS	17	38.2 (22-55)	11:6
SPMS	5	56 (49-60)	2:3
Cohort Part 2			
HD	8	26.9 (20-36)	6:2
OND	11	30.8 (20-39)	5:6
RRMS	20	34.1 (17-55)	15:5

Abbreviations: OND = other neurological disease (non-inflammatory), MS = multiple sclerosis, RRMS = relapse-remitting MS, PPMS = primary-progressive MS, SPMS = secondary-progressive.

6.11. Mass cytometry

6.11.1. Antibody conjugation and validation

Monoclonal anti-human antibodies (Table 6) were purchased either pre-conjugated to heavy-metal isotopes from Fluidigm or in purified form and conjugated in house using the Maxpar™ X8 chelating polymer kit (Fluidigm) according to the manufacturer's instructions. In short, carrier protein was washed away and the purified antibody was partially reduced for 25 min at 37°C and lastly conjugated by

addition of isotope-loaded metal-chelating polymers. Following conjugation, the antibody protein concentration was determined by nanodrop (Thermo Scientific). Successful conjugation and sufficient staining signal of the antibody was then validated by staining cryopreserved PBMCs from various healthy donors and determining the specific signal above background (negative biological control populations or unstimulated cells).

6.11.2. Live cell barcoding

Samples were *ex vivo* re-activated as described above (see section 6.4). In order to reduce inter-sample staining variability, minimize sample-handling time and reduce antibody consumption, we made use of the live cell barcoding approach (Mei et al. 2015). Therefore, isothiocyanobenzyl-EDTA (p-SCN-EDTA; Dojindo) was loaded with five different palladium isotopes and one indium isotope (^{104}Pd, ^{105}Pd, ^{106}Pd, ^{108}Pd, ^{110}Pd, ^{115}In all from Trace Sciences International) as described (Zunder et al. 2015) and subsequently used to label anti-human CD45 (Biolegend) as suggested (Mei et al. 2015). To further increase the number of possible samples with a unique barcode, pre-conjugated ^{89}Y-CD45 (Fluidigm) was used as an additional barcoding reagent. To obtain robust barcoding results with even staining intensity on all samples, a 6-choose-2 scheme (or 7-choose-3) was used, resulting in 15 (or 35) specific combinations of heavy-metal labeled CD45 antibodies.
PBMCs from MS and control patients were labeled with metal-tagged CD45 antibodies after *ex vivo* re-activation at 37 °C for 25 min in cell staining medium (CSM; RPMI-1640, 4% FCS) on a rotating shaker (500 rpm). Samples were washed twice in CSM and combined into a single reaction vessel for further staining steps.

6.11.3. Surface staining for mass cytometry

Following live cell barcoding, the combined sample was centrifuged, supernatant was aspirated and cells were resuspended in 500 µL of surface antibody solution (Table 6) in CSM. Cells were stained for 20 min at 37 °C on a rotating shaker (500 rpm) to optimize chemokine receptor staining (Berhanu et al. 2003). Dead cells were excluded by adding 1 mL of 2.5 µM cisplatin (Sigma) in PBS at the end of the staining period

and incubating for 2 min on ice (Fienberg et al. 2012). Afterwards, the sample was once washed once with PBS/BSA (PBS, 0.5% bovine serum albumin (BSA; Sigma).

Table 6. Antibodies and other staining-reagents used for mass cytometry.

Isotope	Metal	Antigen	Clone	Supplier	Category
89	Y	BC89	HI30	Fluidigm	barcoding
104	Pd	BC104	HI30	Biolegend	barcoding
105	Pd	BC105	HI30	Biolegend	barcoding
106	Pd	BC106	HI30	Biolegend	barcoding
108	Pd	BC108	HI30	Biolegend	barcoding
110	Pd	BC110	HI30	Biolegend	barcoding
115	In	BC115	HI30	Biolegend	barcoding
141	Pr	CCR6	G034E3	Fluidigm	surface
142	Nd	IL-4	MP4-25D2	Fluidigm	ICS
143	Nd	CCR2	K036C2	Biolegend	surface
144	Nd	CD57	HCD57	Biolegend	surface
145	Nd	CD4/CD4	RPA-T4/OKT4	Fluidigm/Biolegend	surface
146	Nd	CD8a	RPA-T8/SK1	Fluidigm	surface
147	Sm	CD56	NCAM16.2	BD	surface
148	Nd	IL-17A	BL168	Fluidigm	ICS
149	Sm	IL-3	BVD8-3G11	Biolegend	ICS
150	Nd	IL-22	22URTI	Fluidigm	ICS
151	Eu	CD103	Ber-ACT8	Fluidigm	surface
152	Sm	TCRγδ	11F2	Fluidigm	surface
153	Eu	CD25	M-A251	Biolegend	surface
154	Sm	IL-6	MQ2-13A5	Biolegend	ICS
155	Gd	IL-9	MH9A4	Biolegend	ICS
156	Gd	IL-13	JES10-5A2	Biolegend	ICS
158	Gd	CCR4	205410	Fluidigm	surface
159	Tb	GM-CSF	BVD2-21C11	Fluidigm	ICS
160	Gd	CD69	FN50	Biolegend	surface
161	Dy	CD20	2H7	Biolegend	surface
162	Dy	CD27	O323	Biolegend	surface
163	Dy	CD14	M5E2	Biolegend	surface
164	Dy	CD45RO	UCHL1	Fluidigm	surface
165	Ho	IFN-γ	B27	Fluidigm	ICS
166	Er	IL-10	JES3-9D7	Fluidigm	ICS
167	Er	CCR7	G043H7	Fluidigm	surface
168	Er	TNF-α	MAb11	Biolegend	ICS
169	Tm	CD45RA	HI100	Fluidigm	surface
170	Er	CD3	UCHT-1	Fluidigm	surface
171	Yb	CXCR5	51505	Fluidigm	surface
172	Yb	IL-21	3A3-N2	Fluidigm	ICS
173	Yb	CXCR4	12G5	Fluidigm	surface
174	Yb	CD28	CD28.2	Biolegend	surface
175	Lu	PD-1	EH12.2H7	Fluidigm	surface
176	Yb	IL-2	MQ1-17H12	Biolegend	ICS
191	Ir	DNA1		Fluidigm	other
193	Ir	DNA2		Fluidigm	other
195	Pt	Dead		Sigma	other

6.11.4. Intracellular cytokine staining for mass cytometry

Surface-stained cells were fixed by resuspending them in 1.6% paraformaldehyde (PFA; Electron Microscopy Sciences) for 25 min at 4 °C on a rotary shaker (500 rpm). Afterwards, the sample was washed twice with permeabilization buffer (PBS, 0.5% saponin, 2% BSA, 0.01% sodium azide, all Sigma), the supernatant was aspirated and the sample was resuspended in 500 µL of intracellular antibody mixture (Table 6) in permeabilization buffer for 1 h at 4 °C on a rotary shaker (500 rpm). The sample was washed with permeabilization buffer, the supernatant was aspirated and the cells were resuspended in 500 µL of iridium intercalator solution (Fluidigm) over night. Next, the sample was washed twice with PBS/BSA, once with ddH_2O, resuspended at 0.5-1 x 10^6 cells mL^{-1} and filtered through a cell strainer cap (Falcon) before acquisition.

6.11.5. Acquisition on CyTOF2 mass cytometer and bead normalization

Samples were acquired on a CyTOF2 mass cytometer (DVS Sciences/Fluidigm). Quality control and tuning processes were performed on a daily basis before acquisition. Data from different days was normalized by adding 5-element beads (Fluidigm) to the sample immediately before acquisition and using the matlab-based normalization software as described previously (Finck et al. 2013). Only events with event length between 10 and 100 were exported.

6.12. Algorithm-guided data analysis

6.12.1. Data pre-processing

Prior to downstream analysis, live cells were exported by manual gating on event length, DNA (^{191}Ir and ^{193}Ir) and live cells (^{195}Pt) using FlowJo (Treestar). Next, cells were assigned to their initial samples using debarcoding software (Zunder et al. 2015). Bead-normalized files were then transformed using an inverse hyperbolic sine (arcsinh) function with a cofactor of 5 (Bendall et al. 2011) using the R environment (R Development Core Team 2008). In order to improve comparability of samples acquired on different days and to equalize the contribution of each marker in

subsequent automated data analysis steps, we performed a percentile normalization step (Levine et al. 2015) and thereby normalized all data to the 99.5th percentile (99.995th percentile for low expressed cytokines) of the combined (barcoded) sample. This preserves inter-sample variability in maximum expression values which might be biologically relevant.

6.12.2. FlowSOM clustering

Following pre-processing, all samples from all cohorts were down sampled to a maximum of 100'000 cells/sample, combined into one file and subjected to the FlowSOM clustering algorithm in order to identify meaningful immunological populations (see section 1.6.5.5). We choose FlowSOM over other clustering options (see section 1.6.5) for several reasons: *(1)* in our hands it identified clusters which efficiently represented immune populations that we expected to be present based on prior biological knowledge, *(2)* its availability within the R environment which enabled us to perform large parts of the analysis in a streamlined way, *(3)* it was able to perform clusterings within a few minutes on a standard desktop computer enabling us to run it multiple times and thus compare the influence of different input parameters, especially the *k*-value used in the meta-clustering step. FlowSOM was run on the combined sample to facilitate the identification of small populations which could be overlooked when clustering is performed on each single sample. After the initial clustering step, resulting nodes were subjected to meta-clustering. The respective *k*-value was chosen manually and in a way so that we were still able to identify all populations which were expected to be present, based on general biological knowledge. To make use of the whole, high-dimensional data, all analyzed markers were used for this clustering analysis. However, we adjusted the weighing of the input markers according to our scientific question, *e.g.* for the identification of PBMC populations we increased the scale for all lineage markers from 0-1 to 0-2. Likewise, for the analysis of cytokine co-production by different immune subsets, we increased the weighing for all cytokines accordingly.

6.12.3. t-SNE dimensionality reduction

In order to visualize the high-dimensional data and to perform a quality control of the FlowSOM clustering we additionally performed t-SNE dimensionality reduction (see section 1.6.5.2), creating a two-dimensional plot of all cells, and compared whether the visually distinct populations obtained from t-SNE correspond to the populations defined by the FlowSOM algorithm. In case we performed weighing for the clustering algorithm, the same scales were also used for t-SNE visualization. Again, the combined sample was used and further down sampled to 20'000 cells to avoid overcrowding. Two-dimensional t-SNE was then run using the Rtsne package in R with a predefined random seed to ensure reproducibility.

Another analysis approach of using a categorical, one-dimensional variant of the t-SNE algorithm was recently shown to be helpful in the precise analysis of immune subpopulations (Cheng et al. 2015). We employed to same principle by categorizing our panel into lineage, differentiation and activation, trafficking and cytokine antigens and using these categorical t-SNE dimensions to further explore immune subpopulations. When using these categorized sets of input markers, no weighing was necessary.

6.12.4. Statistical analysis of mass cytometry experiments

In order to compare the frequency of algorithm-defined populations between the different groups of MS and control patients, we made use of the non-parametric Mann-Whitney-Wilcoxon test. All pairwise tests were calculated between OND and the respective population of MS patients. Multiple comparisons correction for all populations analyzed in the respective experiment was performed with the Bonferroni-Hochberg correction. The level of significance with the respective false-discovery rate is indicated with the initial *P*-value.

References

Aghaeepour N, Finak G, Hoos H, et al (2013) Critical assessment of automated flow cytometry data analysis techniques. Nat Methods 10:228–38. doi: 10.1038/nmeth.2365

Amedei A, Prisco D, D'Elios MM (2012) Multiple sclerosis: the role of cytokines in pathogenesis and in therapies. Int J Mol Sci 13:13438–60. doi: 10.3390/ijms131013438

Amir ED, Davis KL, Tadmor MD, et al (2013) viSNE enables visualization of high dimensional single-cell data and reveals phenotypic heterogeneity of leukemia. Nat Biotechnol 31:545–52. doi: 10.1038/nbt.2594

Appay V, van Lier RAW, Sallusto F, Roederer M (2008) Phenotype and function of human T lymphocyte subsets: consensus and issues. Cytometry A 73:975–83. doi: 10.1002/cyto.a.20643

Ascherio A, Munger KL (2007) Environmental risk factors for multiple sclerosis. Part II: Noninfectious factors. Ann Neurol 61:504–513. doi: 10.1002/ana.21141

Ascherio A, Munger KL, Lünemann JD (2012) The initiation and prevention of multiple sclerosis. Nat Rev Neurol. doi: 10.1038/nrneurol.2012.198

Bach J-F (2002) The effect of infections on susceptibility to autoimmune and allergic diseases. N Engl J Med 347:911–20. doi: 10.1056/NEJMra020100

Bandura DR, Baranov VI, Ornatsky OI, et al (2009) Mass Cytometry: Technique for Real Time Single Cell Multitarget Immunoassay Based on Inductively Coupled Plasma Time-of-Flight Mass Spectrometry. Anal Chem 81:6813–6822. doi: 10.1021/ac901049w

Baranov VI, Quinn Z, Bandura DR, Tanner SD (2002) A Sensitive and Quantitative Element-Tagged Immunoassay with ICPMS Detection. Anal Chem 74:1629–1636. doi: 10.1021/ac0110350

Becher B, Giacomini PS, Pelletier D, et al (1999) Interferon-gamma secretion by peripheral blood T-cell subsets in multiple sclerosis: correlation with disease phase and interferon-beta therapy. Ann Neurol 45:247–50.

Becher B, Schlitzer A, Chen J, et al (2014) High-dimensional analysis of the murine myeloid cell system. Nat Immunol. doi: 10.1038/ni.3006

Becher B, Segal BM (2011) T(H)17 cytokines in autoimmune neuro-inflammation. Curr Opin Immunol 23:707–12. doi: 10.1016/j.coi.2011.08.005

Beecham AH, Patsopoulos NA, Xifara DK, et al (2013) Analysis of immune-related loci identifies 48 new susceptibility variants for multiple sclerosis. Nat Genet. doi: 10.1038/ng.2770

Behrens F, Tak PP, Østergaard M, et al (2014) MOR103, a human monoclonal antibody to granulocyte-macrophage colony-stimulating factor, in the treatment

of patients with moderate rheumatoid arthritis: results of a phase Ib/IIa randomised, double-blind, placebo-controlled, dose-escalation trial. Ann Rheum Dis 74:1058–64. doi: 10.1136/annrheumdis-2013-204816

Ben-Nun A, Wekerle H, Cohen IR (1981) The rapid isolation of clonable antigen-specific T lymphocyte lines capable of mediating autoimmune encephalomyelitis. Eur J Immunol 11:195–9. doi: 10.1002/eji.1830110307

Bendall SC, Nolan GP, Roederer M, Chattopadhyay PK (2012) A deep profiler's guide to cytometry. Trends Immunol 33:323–32. doi: 10.1016/j.it.2012.02.010

Bendall SC, Simonds EF, Qiu P, et al (2011) Single-cell mass cytometry of differential immune and drug responses across a human hematopoietic continuum. Science 332:687–96. doi: 10.1126/science.1198704

Benham H, Rehaume LM, Hasnain SZ, et al (2014) Interleukin-23 mediates the intestinal response to microbial β-1,3-glucan and the development of spondyloarthritis pathology in SKG mice. Arthritis Rheumatol (Hoboken, NJ) 66:1755–67. doi: 10.1002/art.38638

Berhanu D, Mortari F, De Rosa SC, Roederer M (2003) Optimized lymphocyte isolation methods for analysis of chemokine receptor expression. J Immunol Methods 279:199–207. doi: 10.1016/S0022-1759(03)00186-8

Bielekova B, Richert N, Howard T, et al (2004) Humanized anti-CD25 (daclizumab) inhibits disease activity in multiple sclerosis patients failing to respond to interferon beta. Proc Natl Acad Sci U S A 101:8705–8. doi: 10.1073/pnas.0402653101

Blink SE, Miller SD (2009) The contribution of gammadelta T cells to the pathogenesis of EAE and MS. Curr Mol Med 9:15–22.

Bloomgren G, Richman S, Hotermans C, et al (2012) Risk of Natalizumab-Associated Progressive Multifocal Leukoencephalopathy. N Engl J Med 366:1870–1880. doi: 10.1056/NEJMoa1107829

Bodenmiller B, Zunder ER, Finck R, et al (2012) Multiplexed mass cytometry profiling of cellular states perturbed by small-molecule regulators. Nat Biotechnol 30:858–67. doi: 10.1038/nbt.2317

Bonneville M, O'Brien RL, Born WK (2010) Gammadelta T cell effector functions: a blend of innate programming and acquired plasticity. Nat Rev Immunol 10:467–78. doi: 10.1038/nri2781

Booss J, Esiri MM, Tourtellotte WW, Mason DY (1983) Immunohistological analysis of T lymphocyte subsets in the central nervous system in chronic progressive multiple sclerosis. J Neurol Sci 62:219–32.

Bruggner R V, Bodenmiller B, Dill DL, et al (2014) Automated identification of stratifying signatures in cellular subpopulations. Proc Natl Acad Sci U S A 111:E2770–7. doi: 10.1073/pnas.1408792111

Burdach S, Zessack N, Dilloo D, et al (1991) Differential regulation of lymphokine production by distinct subunits of the T cell interleukin 2 receptor. J Clin Invest

87:2114–21.

Burmester GR, Feist E, Sleeman MA, et al (2011) Mavrilimumab, a human monoclonal antibody targeting GM-CSF receptor-α, in subjects with rheumatoid arthritis: a randomised, double-blind, placebo-controlled, phase I, first-in-human study. Ann Rheum Dis 70:1542–9. doi: 10.1136/ard.2010.146225

Burmester GR, Weinblatt ME, McInnes IB, et al (2013) Efficacy and safety of mavrilimumab in subjects with rheumatoid arthritis. Ann Rheum Dis 72:1445–52. doi: 10.1136/annrheumdis-2012-202450

Cai Y, Shen X, Ding C, et al (2011) Pivotal role of dermal IL-17-producing γδ T cells in skin inflammation. Immunity 35:596–610. doi: 10.1016/j.immuni.2011.08.001

Campbell IK, Rich MJ, Bischof RJ, et al (1998) Protection from collagen-induced arthritis in granulocyte-macrophage colony-stimulating factor-deficient mice. J Immunol 161:3639–44.

Carbone F, De Rosa V, Carrieri PB, et al (2014) Regulatory T cell proliferative potential is impaired in human autoimmune disease. Nat Med 20:69–74. doi: 10.1038/nm.3411

Carrieri PB, Provitera V, De Rosa T, et al (1998) Profile of cerebrospinal fluid and serum cytokines in patients with relapsing-remitting multiple sclerosis: a correlation with clinical activity. Immunopharmacol Immunotoxicol 20:373–82. doi: 10.3109/08923979809034820

Carswell R (1838) Pathological anatomy: illustrations of the elementary forms of disease. Longman, Orme, Brown, Green and Longman, London

Cepok S, Jacobsen M, Schock S, et al (2001) Patterns of cerebrospinal fluid pathology correlate with disease progression in multiple sclerosis. Brain 124:2169–76.

Chanvillard C, Jacolik RF, Infante-Duarte C, Nayak RC (2013) The role of natural killer cells in multiple sclerosis and their therapeutic implications. Front Immunol 4:63. doi: 10.3389/fimmu.2013.00063

Cheng Y, Wong MT, van der Maaten L, Newell EW (2015) Categorical Analysis of Human T Cell Heterogeneity with One-Dimensional Soli-Expression by Nonlinear Stochastic Embedding. J Immunol. doi: 10.4049/jimmunol.1501928

Chester C, Maecker HT (2015) Algorithmic Tools for Mining High-Dimensional Cytometry Data. J Immunol 195:773–9. doi: 10.4049/jimmunol.1500633

Clausen J, Vergeiner B, Enk M, et al (2003) Functional significance of the activation-associated receptors CD25 and CD69 on human NK-cells and NK-like T-cells. Immunobiology 207:85–93. doi: 10.1078/0171-2985-00219

Codarri L, Gyülvészi G, Tosevski V, et al (2011) RORγt drives production of the cytokine GM-CSF in helper T cells, which is essential for the effector phase of autoimmune neuroinflammation. Nat Immunol 12:560–7. doi: 10.1038/ni.2027

Cohen JA, Barkhof F, Comi G, et al (2010) Oral fingolimod or intramuscular

interferon for relapsing multiple sclerosis. N Engl J Med 362:402–15. doi: 10.1056/NEJMoa0907839

Cohen JA, Coles AJ, Arnold DL, et al (2012) Alemtuzumab versus interferon beta 1a as first-line treatment for patients with relapsing-remitting multiple sclerosis: a randomised controlled phase 3 trial. Lancet (London, England) 380:1819–28. doi: 10.1016/S0140-6736(12)61769-3

Comi G, Filippi M, Wolinsky JS (2001) European/Canadian multicenter, double-blind, randomized, placebo-controlled study of the effects of glatiramer acetate on magnetic resonance imaging--measured disease activity and burden in patients with relapsing multiple sclerosis. European/Canadian Gla. Ann Neurol 49:290–7.

Compston A, Coles A (2008) Multiple sclerosis. Lancet 372:1502–17. doi: 10.1016/S0140-6736(08)61620-7

Constantinescu CS, Asher A, Fryze W, et al (2015) Randomized phase 1b trial of MOR103, a human antibody to GM-CSF, in multiple sclerosis. Neurol Neuroimmunol Neuroinflammation 2:e117–e117. doi: 10.1212/NXI.0000000000000117

Costa ES, Pedreira CE, Barrena S, et al (2010) Automated pattern-guided principal component analysis vs expert-based immunophenotypic classification of B-cell chronic lymphoproliferative disorders: a step forward in the standardization of clinical immunophenotyping. Leukemia 24:1927–1933. doi: 10.1038/leu.2010.160

Crotty S (2011) Follicular helper CD4 T cells (TFH). Annu Rev Immunol 29:621–63. doi: 10.1146/annurev-immunol-031210-101400

Croxford AL, Lanzinger M, Hartmann FJ, et al (2015) The Cytokine GM-CSF Drives the Inflammatory Signature of CCR2+ Monocytes and Licenses Autoimmunity. Immunity 1–13. doi: 10.1016/j.immuni.2015.08.010

de Bakker PIW, McVean G, Sabeti PC, et al (2006) A high-resolution HLA and SNP haplotype map for disease association studies in the extended human MHC. Nat Genet 38:1166–72. doi: 10.1038/ng1885

De Rosa SC, Herzenberg LA, Roederer M (2001) 11-color, 13-parameter flow cytometry: identification of human naive T cells by phenotype, function, and T-cell receptor diversity. Nat Med 7:245–8. doi: 10.1038/84701

Dendrou CA, Fugger L, Friese MA (2015) Immunopathology of multiple sclerosis. Nat Rev Immunol. doi: 10.1038/nri3871

Dendrou CA, Plagnol V, Fung E, et al (2009) Cell-specific protein phenotypes for the autoimmune locus IL2RA using a genotype-selectable human bioresource. Nat Genet 41:1011–5. doi: 10.1038/ng.434

Di Palma S, Bodenmiller B (2015) Unraveling cell populations in tumors by single-cell mass cytometry. Curr Opin Biotechnol 31:122–9. doi: 10.1016/j.copbio.2014.07.004

Ebers GC (1998) Randomised double-blind placebo-controlled study of interferon β-1a in relapsing/remitting multiple sclerosis. Lancet 352:1498–1504. doi: 10.1016/S0140-6736(98)03334-0

Edelson BT, Bradstreet TR, KC W, et al (2011) Batf3-dependent CD11b(low/-) peripheral dendritic cells are GM-CSF-independent and are not required for Th cell priming after subcutaneous immunization. PLoS One 6:e25660. doi: 10.1371/journal.pone.0025660

El-Behi M, Ciric B, Dai H, et al (2011) The encephalitogenicity of T(H)17 cells is dependent on IL-1- and IL-23-induced production of the cytokine GM-CSF. Nat Immunol 12:568–75. doi: 10.1038/ni.2031

Eyerich S, Eyerich K, Pennino D, et al (2009) Th22 cells represent a distinct human T cell subset involved in epidermal immunity and remodeling. J Clin Invest 119:3573–85. doi: 10.1172/JCI40202

Fiehn C, Wermann M, Pezzutto A, et al (1992) [Plasma GM-CSF concentrations in rheumatoid arthritis, systemic lupus erythematosus and spondyloarthropathy]. Zeitschrift für Rheumatol 51:121–6.

Fienberg HG, Simonds EF, Fantl WJ, et al (2012) A platinum-based covalent viability reagent for single-cell mass cytometry. Cytom Part A 81 A:467–475. doi: 10.1002/cyto.a.22067

Finak G, Bashashati A, Brinkman R, Gottardo R (2009) Merging mixture components for cell population identification in flow cytometry. Adv Bioinformatics 247646. doi: 10.1155/2009/247646

Finak G, Jiang W, Krouse K, et al (2014) High-throughput flow cytometry data normalization for clinical trials. Cytometry A 85:277–86. doi: 10.1002/cyto.a.22433

Finak G, Perez J-M, Weng A, Gottardo R (2010) Optimizing transformations for automated, high throughput analysis of flow cytometry data. BMC Bioinformatics 11:546. doi: 10.1186/1471-2105-11-546

Finck R, Simonds EF, Jager A, et al (2013) Normalization of mass cytometry data with bead standards. Cytometry A 83:483–94. doi: 10.1002/cyto.a.22271

Fox RJ, Miller DH, Phillips JT, et al (2012) Placebo-controlled phase 3 study of oral BG-12 or glatiramer in multiple sclerosis. N Engl J Med 367:1087–97. doi: 10.1056/NEJMoa1206328

Fulwyler MJ (1965) Electronic Separation of Biological Cells by Volume. Science (80-) 150:910–911. doi: 10.1126/science.150.3698.910

Gasteiger G, Hemmers S, Bos PD, et al (2013) IL-2-dependent adaptive control of NK cell homeostasis. J Exp Med 210:1179–87. doi: 10.1084/jem.20122571

Genser B, Cooper PJ, Yazdanbakhsh M, et al (2007) A guide to modern statistical analysis of immunological data. BMC Immunol 8:27. doi: 10.1186/1471-2172-8-27

Gentleman RC, Carey VJ, Bates DM, et al (2004) Bioconductor: open software development for computational biology and bioinformatics. Genome Biol 5:R80. doi: 10.1186/gb-2004-5-10-r80

Gödhe W (1968) Automatisches Meß-und Zählgerät für die Teilchen einer Dispersion. DE1815352.

Greter M, Helft J, Chow A, et al (2012) GM-CSF Controls Nonlymphoid Tissue Dendritic Cell Homeostasis but Is Dispensable for the Differentiation of Inflammatory Dendritic Cells. Immunity 36:1031–1046. doi: 10.1016/j.immuni.2012.03.027

Guilliams M, De Kleer I, Henri S, et al (2013) Alveolar macrophages develop from fetal monocytes that differentiate into long-lived cells in the first week of life via GM-CSF. J Exp Med 210:1977–92. doi: 10.1084/jem.20131199

Guilliams M, Ginhoux F, Jakubzick C, et al (2014) Dendritic cells, monocytes and macrophages: a unified nomenclature based on ontogeny. Nat Rev Immunol 14:571–8. doi: 10.1038/nri3712

Hafler DA, Compston A, Sawcer S, et al (2007) Risk alleles for multiple sclerosis identified by a genomewide study. N Engl J Med 357:851–62. doi: 10.1056/NEJMoa073493

Hahne F, Khodabakhshi AH, Bashashati A, et al (2010) Per-channel basis normalization methods for flow cytometry data. Cytom Part A 77:121–131. doi: 10.1002/cyto.a.20823

Haines JL, Terwedow HA, Burgess K, et al (1998) Linkage of the MHC to familial multiple sclerosis suggests genetic heterogeneity. The Multiple Sclerosis Genetics Group. Hum Mol Genet 7:1229–34.

Hamilton JA (2008) Colony-stimulating factors in inflammation and autoimmunity. Nat Rev Immunol 8:533–44. doi: 10.1038/nri2356

Hartung H-P, Gonsette R, König N, et al Mitoxantrone in progressive multiple sclerosis: a placebo-controlled, double-blind, randomised, multicentre trial. Lancet (London, England) 360:2018–25. doi: 10.1016/S0140-6736(02)12023-X

Hauser SL, Waubant E, Arnold DL, et al (2008) B-cell depletion with rituximab in relapsing-remitting multiple sclerosis. N Engl J Med 358:676–88. doi: 10.1056/NEJMoa0706383

Hazenberg BP, Van Leeuwen MA, Van Rijswijk MH, et al (1989) Correction of granulocytopenia in Felty's syndrome by granulocyte-macrophage colony-stimulating factor. Simultaneous induction of interleukin-6 release and flare-up of the arthritis. Blood 74:2769–70.

Hercus TR, Dhagat U, Kan WLT, et al (2013) Signalling by the βc family of cytokines. Cytokine Growth Factor Rev 24:189–201. doi: 10.1016/j.cytogfr.2013.03.002

Herzenberg LA, Tung J, Moore WA, et al (2006) Interpreting flow cytometry data: a guide for the perplexed. Nat Immunol 7:681–5. doi: 10.1038/ni0706-681

Hume DA (2006) The mononuclear phagocyte system. Curr Opin Immunol 18:49–53. doi: 10.1016/j.coi.2005.11.008

Huseby ES, Liggitt D, Brabb T, et al (2001) A pathogenic role for myelin-specific CD8(+) T cells in a model for multiple sclerosis. J Exp Med 194:669–76.

Jamshidian A, Shaygannejad V, Pourazar A, et al (2013) Biased Treg/Th17 balance away from regulatory toward inflammatory phenotype in relapsed multiple sclerosis and its correlation with severity of symptoms. J Neuroimmunol 262:106–12. doi: 10.1016/j.jneuroim.2013.06.007

Kamentsky LA, Melamed MR, Derman H (1965) Spectrophotometer: new instrument for ultrarapid cell analysis. Science 150:630–1.

Kappos L, Li D, Calabresi PA, et al (2011) Ocrelizumab in relapsing-remitting multiple sclerosis: a phase 2, randomised, placebo-controlled, multicentre trial. Lancet (London, England) 378:1779–87. doi: 10.1016/S0140-6736(11)61649-8

Khademi M, Dring AM, Gilthorpe JD, et al (2013) Intense inflammation and nerve damage in early multiple sclerosis subsides at older age: a reflection by cerebrospinal fluid biomarkers. PLoS One 8:e63172. doi: 10.1371/journal.pone.0063172

Kohonen T (1990) The self-organizing map. Proc IEEE 78:1464–1480.

Kruger M, Van Gool S, Peng XH, et al (1996) Production of granulocyte-macrophage colony-stimulating factor by T cells is regulated by B7 and IL-1 beta. Immunology 88:49–54.

Kvistborg P, Gouttefangeas C, Aghaeepour N, et al (2015) Thinking outside the gate: single-cell assessments in multiple dimensions. Immunity 42:591–2. doi: 10.1016/j.immuni.2015.04.006

LeVine AM, Reed JA, Kurak KE, et al (1999) GM-CSF-deficient mice are susceptible to pulmonary group B streptococcal infection. J Clin Invest 103:563–9. doi: 10.1172/JCI5212

Levine JH, Simonds EF, Bendall SC, et al (2015) Data-Driven Phenotypic Dissection of AML Reveals Progenitor-like Cells that Correlate with Prognosis. Cell. doi: 10.1016/j.cell.2015.05.047

Lin C-C, Bradstreet TR, Schwarzkopf EA, et al (2014) Bhlhe40 controls cytokine production by T cells and is essential for pathogenicity in autoimmune neuroinflammation. Nat Commun 5:3551. doi: 10.1038/ncomms4551

Lo K, Brinkman RR, Gottardo R (2008) Automated gating of flow cytometry data via robust model-based clustering. Cytometry A 73:321–32. doi: 10.1002/cyto.a.20531

Lou X, Zhang G, Herrera I, et al (2007) Polymer-based elemental tags for sensitive bioassays. Angew Chemie - Int Ed 46:6111–6114. doi: 10.1002/anie.200700796

Lowe CE, Cooper JD, Brusko T, et al (2007) Large-scale genetic fine mapping and genotype-phenotype associations implicate polymorphism in the IL2RA region

in type 1 diabetes. Nat Genet 39:1074–82. doi: 10.1038/ng2102

Lucchinetti C, Brück W, Parisi J, et al (2000) Heterogeneity of multiple sclerosis lesions: implications for the pathogenesis of demyelination. Ann Neurol 47:707–17.

Lugli E, Roederer M, Cossarizza A (2010) Data analysis in flow cytometry: the future just started. Cytometry A 77:705–13. doi: 10.1002/cyto.a.20901

Lujan E, Zunder ER, Ng YH, et al (2015) Early reprogramming regulators identified by prospective isolation and mass cytometry. Nature 521:352–356. doi: 10.1038/nature14274

Lycke JN, Karlsson J-E, Andersen O, Rosengren LE (1998) Neurofilament protein in cerebrospinal fluid: a potential marker of activity in multiple sclerosis. J Neurol Neurosurg Psychiatry 64:402–404. doi: 10.1136/jnnp.64.3.402

Maaten L Van Der, Hinton G (2008) Visualizing Data using t-SNE. J Mach Learn Res 9:2579–2605. doi: 10.1007/s10479-011-0841-3

Maecker HT, McCoy JP, Nussenblatt R (2012) Standardizing immunophenotyping for the Human Immunology Project. Nat Rev Immunol 12:191–200. doi: 10.1038/nri3158

Magliozzi R, Howell O, Vora A, et al (2007) Meningeal B-cell follicles in secondary progressive multiple sclerosis associate with early onset of disease and severe cortical pathology. Brain 130:1089–104. doi: 10.1093/brain/awm038

Mahnke YD, Brodie TM, Sallusto F, et al (2013) The who's who of T-cell differentiation: human memory T-cell subsets. Eur J Immunol 43:2797–809. doi: 10.1002/eji.201343751

Maier LM, Anderson DE, Severson CA, et al (2009a) Soluble IL-2RA levels in multiple sclerosis subjects and the effect of soluble IL-2RA on immune responses. J Immunol 182:1541–7.

Maier LM, Lowe CE, Cooper J, et al (2009b) IL2RA genetic heterogeneity in multiple sclerosis and type 1 diabetes susceptibility and soluble interleukin-2 receptor production. PLoS Genet 5:e1000322. doi: 10.1371/journal.pgen.1000322

Majonis D, Herrera I, Ornatsky O, et al (2010) Synthesis of a functional metal-chelating polymer and steps toward quantitative mass cytometry bioassays. Anal Chem 82:8961–9. doi: 10.1021/ac101901x

Marusic S, Miyashiro JS, Douhan J, et al (2002) Local delivery of granulocyte macrophage colony-stimulating factor by retrovirally transduced antigen-specific T cells leads to severe, chronic experimental autoimmune encephalomyelitis in mice. Neurosci Lett 332:185–9.

McFarlin DE, McFarland HF (1982a) Multiple sclerosis (first of two parts). N Engl J Med 307:1183–8. doi: 10.1056/NEJM198211043071905

McFarlin DE, McFarland HF (1982b) Multiple sclerosis (second of two parts). N

Engl J Med 307:1246–51. doi: 10.1056/NEJM198211113072005

McQualter JL, Darwiche R, Ewing C, et al (2001) Granulocyte macrophage colony-stimulating factor: a new putative therapeutic target in multiple sclerosis. J Exp Med 194:873–82.

McWilliams IL, Rajbhandari R, Nozell S, et al (2015) STAT4 controls GM-CSF production by both Th1 and Th17 cells during EAE. J Neuroinflammation 12:128. doi: 10.1186/s12974-015-0351-3

Mei HE, Leipold MD, Schulz AR, et al (2015) Barcoding of Live Human Peripheral Blood Mononuclear Cells for Multiplexed Mass Cytometry. J Immunol 194:2022–31. doi: 10.4049/jimmunol.1402661

Metcalf D (2008) Hematopoietic cytokines. Blood 111:485–91. doi: 10.1182/blood-2007-03-079681

Miller DH, Leary SM (2007) Primary-progressive multiple sclerosis. Lancet Neurol 6:903–12. doi: 10.1016/S1474-4422(07)70243-0

Mohme M, Hotz C, Stevanovic S, et al (2013) HLA-DR15-derived self-peptides are involved in increased autologous T cell proliferation in multiple sclerosis. Brain 136:1783–98. doi: 10.1093/brain/awt108

Moutsianas L, Jostins L, Beecham AH, et al (2015) Class II HLA interactions modulate genetic risk for multiple sclerosis. Nat Genet 47:1107–1113. doi: 10.1038/ng.3395

Naegele M, Tillack K, Reinhardt S, et al (2012) Neutrophils in multiple sclerosis are characterized by a primed phenotype. J Neuroimmunol 242:60–71. doi: 10.1016/j.jneuroim.2011.11.009

Naim I, Datta S, Rebhahn J, et al (2014) SWIFT-scalable clustering for automated identification of rare cell populations in large, high-dimensional flow cytometry datasets, part 1: algorithm design. Cytometry A 85:408–21. doi: 10.1002/cyto.a.22446

Nair N, Mei HE, Chen S-Y, et al (2015) Mass cytometry as a platform for the discovery of cellular biomarkers to guide effective rheumatic disease therapy. Arthritis Res Ther 17:127. doi: 10.1186/s13075-015-0644-z

Navikas V, Link H (1996) Review: cytokines and the pathogenesis of multiple sclerosis. J Neurosci Res 45:322–33. doi: 10.1002/(SICI)1097-4547(19960815)45:4<322::AID-JNR1>3.0.CO;2-B

Nelson E a., Walker SR, Weisberg E, et al (2011) The STAT5 inhibitor pimozide decreases survival of chronic myelogenous leukemia cells resistant to kinase inhibitors. Blood 117:3421–3429. doi: 10.1182/blood-2009-11-255232

Newell EW, Sigal N, Bendall SC, et al (2012) Cytometry by time-of-flight shows combinatorial cytokine expression and virus-specific cell niches within a continuum of CD8+ T cell phenotypes. Immunity 36:142–52. doi: 10.1016/j.immuni.2012.01.002

Nicholas KJ, Greenplate AR, Flaherty DK, et al (2015) Multiparameter analysis of stimulated human peripheral blood mononuclear cells: A comparison of mass and fluorescence cytometry. Cytometry A. doi: 10.1002/cyto.a.22799

Noster R, Riedel R, Mashreghi M-F, et al (2014) IL-17 and GM-CSF expression are antagonistically regulated by human T helper cells. Sci Transl Med 6:241ra80. doi: 10.1126/scitranslmed.3008706

O'Connor P, Wolinsky JS, Confavreux C, et al (2011) Randomized trial of oral teriflunomide for relapsing multiple sclerosis. N Engl J Med 365:1293–303. doi: 10.1056/NEJMoa1014656

O'Shea JJ, Paul WE (2010) Mechanisms underlying lineage commitment and plasticity of helper CD4+ T cells. Science 327:1098–102. doi: 10.1126/science.1178334

Okada Y, Wu D, Trynka G, et al (2014) Genetics of rheumatoid arthritis contributes to biology and drug discovery. Nature 506:376–81. doi: 10.1038/nature12873

Oksenberg JR, Baranzini SE, Sawcer S, Hauser SL (2008) The genetics of multiple sclerosis: SNPs to pathways to pathogenesis. Nat Rev Genet 9:516–26. doi: 10.1038/nrg2395

Openshaw H, Stuve O, Antel JP, et al (2000) Multiple sclerosis flares associated with recombinant granulocyte colony-stimulating factor. Neurology 54:2147–50.

Ornatsky O, Bandura D, Baranov V, et al (2010) Highly multiparametric analysis by mass cytometry. J Immunol Methods 361:1–20. doi: 10.1016/j.jim.2010.07.002

Pantelyushin S, Haak S, Ingold B, et al (2012) Rorγt+ innate lymphocytes and γδ T cells initiate psoriasiform plaque formation in mice. J Clin Invest 122:2252–2256. doi: 10.1172/JCI61862

Parks DR, Roederer M, Moore WA (2006) A new "Logicle" display method avoids deceptive effects of logarithmic scaling for low signals and compensated data. Cytometry A 69:541–51. doi: 10.1002/cyto.a.20258

Pedreira CE, Costa ES, Lecrevisse Q, et al (2013) Overview of clinical flow cytometry data analysis: recent advances and future challenges. Trends Biotechnol 31:415–25. doi: 10.1016/j.tibtech.2013.04.008

Perfetto SP, Ambrozak D, Nguyen R, et al (2006) Quality assurance for polychromatic flow cytometry. Nat Protoc 1:1522–30. doi: 10.1038/nprot.2006.250

Perfetto SP, Chattopadhyay PK, Roederer M (2004) Seventeen-colour flow cytometry: unravelling the immune system. Nat Rev Immunol 4:648–55. doi: 10.1038/nri1416

Pfender N, Martin R (2014) Daclizumab (anti-CD25) in Multiple Sclerosis. Exp Neurol. doi: 10.1016/j.expneurol.2014.04.015

Polman CH, O'Connor PW, Havrdova E, et al (2006) A randomized, placebo-controlled trial of natalizumab for relapsing multiple sclerosis. N Engl J Med

354:899–910. doi: 10.1056/NEJMoa044397

Ponomarev ED, Shriver LP, Maresz K, et al (2007) GM-CSF production by autoreactive T cells is required for the activation of microglial cells and the onset of experimental autoimmune encephalomyelitis. J Immunol 178:39–48.

Pugliatti M, Rosati G, Carton H, et al (2006) The epidemiology of multiple sclerosis in Europe. Eur J Neurol 13:700–722. doi: 10.1111/j.1468-1331.2006.01342.x

Qiu P, Simonds EF, Bendall SC, et al (2011) Extracting a cellular hierarchy from high-dimensional cytometry data with SPADE. Nat Biotechnol 29:886–91. doi: 10.1038/nbt.1991

Quinn J, Fisher PW, Capocasale RJ, et al (2007) A statistical pattern recognition approach for determining cellular viability and lineage phenotype in cultured cells and murine bone marrow. Cytometry A 71:612–24. doi: 10.1002/cyto.a.20416

R Development Core Team (2008) R: A Language and Environment for Statistical Computing. Vienna, Austria

Ram M, Sherer Y, Shoenfeld Y (2006) Matrix metalloproteinase-9 and autoimmune diseases. J Clin Immunol 26:299–307. doi: 10.1007/s10875-006-9022-6

Rasouli J, Ciric B, Imitola J, et al (2015) Expression of GM-CSF in T Cells Is Increased in Multiple Sclerosis and Suppressed by IFN- Therapy. J Immunol. doi: 10.4049/jimmunol.1403243

Riise T, Nortvedt MW, Ascherio A (2003) Smoking is a risk factor for multiple sclerosis. Neurology 61:1122–4.

Ritz SA, Stämpfli MR, Davies DE, et al (2002) On the generation of allergic airway diseases: from GM-CSF to Kyoto. Trends Immunol 23:396–402. doi: 10.1016/S1471-4906(02)02278-0

Rochman Y, Spolski R, Leonard WJ (2009) New insights into the regulation of T cells by gamma(c) family cytokines. Nat Rev Immunol 9:480–90. doi: 10.1038/nri2580

Romagnani S (2000) T-cell subsets (Th1 versus Th2). Ann Allergy Asthma Immunol 85:9–18; quiz 18, 21. doi: 10.1016/S1081-1206(10)62426-X

Rose JW (2012) Anti-CD25 Immunotherapy: Regulating the Regulators. Sci Transl Med 4:145fs25.

Rumble JM, Huber AK, Krishnamoorthy G, et al (2015) Neutrophil-related factors as biomarkers in EAE and MS. J Exp Med 212:23–35. doi: 10.1084/jem.20141015

Sadovnick AD (2012) Genetic background of multiple sclerosis. Autoimmun Rev 11:163–6. doi: 10.1016/j.autrev.2011.05.007

Sakagami T, Uchida K, Suzuki T, et al (2009) Human GM-CSF autoantibodies and reproduction of pulmonary alveolar proteinosis. N Engl J Med 361:2679–81. doi: 10.1056/NEJMc0904077

Sallusto F, Lanzavecchia A (2009) Heterogeneity of CD4+ memory T cells: Functional modules for tailored immunity. Eur J Immunol 39:2076–2082. doi: 10.1002/eji.200939722

Salou M, Nicol B, Garcia A, Laplaud D-A (2015) Involvement of CD8(+) T Cells in Multiple Sclerosis. Front Immunol 6:604. doi: 10.3389/fimmu.2015.00604

Sawcer S, Hellenthal G, Pirinen M, et al (2011) Genetic risk and a primary role for cell-mediated immune mechanisms in multiple sclerosis. Nature 476:214–9. doi: 10.1038/nature10251

Schmitt E, Klein M, Bopp T (2014) Th9 cells, new players in adaptive immunity. Trends Immunol 35:61–8. doi: 10.1016/j.it.2013.10.004

Shekhar K, Brodin P, Davis MM, Chakraborty AK (2014) Automatic Classification of Cellular Expression by Nonlinear Stochastic Embedding (ACCENSE). Proc Natl Acad Sci U S A 111:202–7. doi: 10.1073/pnas.1321405111

Sheng W, Yang F, Zhou Y, et al (2014) STAT5 programs a distinct subset of GM-CSF-producing T helper cells that is essential for autoimmune neuroinflammation. Cell Res 24:1387–402. doi: 10.1038/cr.2014.154

Sinha S, Boyden AW, Itani FR, et al (2015) CD8(+) T-Cells as Immune Regulators of Multiple Sclerosis. Front Immunol 6:619. doi: 10.3389/fimmu.2015.00619

Sonderegger I, Iezzi G, Maier R, et al (2008) GM-CSF mediates autoimmunity by enhancing IL-6-dependent Th17 cell development and survival. J Exp Med 205:2281–94. doi: 10.1084/jem.20071119

Sörensen T, Baumgart S, Durek P, et al (2015) immunoClust--An automated analysis pipeline for the identification of immunophenotypic signatures in high-dimensional cytometric datasets. Cytometry A 87:603–15. doi: 10.1002/cyto.a.22626

Su D, Shen M, Li X, Sun L (2013) Roles of γδ T cells in the pathogenesis of autoimmune diseases. Clin Dev Immunol 2013:985753. doi: 10.1155/2013/985753

Sun D, Whitaker JN, Huang Z, et al (2001) Myelin antigen-specific CD8+ T cells are encephalitogenic and produce severe disease in C57BL/6 mice. J Immunol 166:7579–87.

Tanner SD, Baranov VI, Ornatsky OI, et al (2013) An introduction to mass cytometry: fundamentals and applications. Cancer Immunol Immunother 62:955–65. doi: 10.1007/s00262-013-1416-8

Thacker EL, Mirzaei F, Ascherio A (2006) Infectious mononucleosis and risk for multiple sclerosis: A meta-analysis. Ann Neurol 59:499–503. doi: 10.1002/ana.20820

Trotter J (2007) Alternatives to log-scale data display. Curr Protoc Cytom Chapter 10:Unit10.16. doi: 10.1002/0471142956.cy1016s42

van der Maaten L (2014) Accelerating t-SNE using Tree-Based Algorithms. J Mach

Learn Res 15:3221–3245.

Van Gassen S, Callebaut B, Van Helden MJ, et al (2015) FlowSOM: Using self-organizing maps for visualization and interpretation of cytometry data. Cytometry A. doi: 10.1002/cyto.a.22625

Viglietta V, Baecher-Allan C, Weiner HL, Hafler DA (2004) Loss of functional suppression by CD4+CD25+ regulatory T cells in patients with multiple sclerosis. J Exp Med 199:971–9. doi: 10.1084/jem.20031579

Vignali DAA, Collison LW, Workman CJ (2008) How regulatory T cells work. Nat Rev Immunol 8:523–32. doi: 10.1038/nri2343

Vladimirova O, Lu FM, Shawver L, Kalman B (1999) The activation of protein kinase C induces higher production of reactive oxygen species by mononuclear cells in patients with multiple sclerosis than in controls. Inflamm Res 48:412–6.

Wicks IP, Roberts AW (2015) Targeting GM-CSF in inflammatory diseases. Nat Rev Rheumatol. doi: 10.1038/nrrheum.2015.161

Wiendl H, Gross CC (2013) Modulation of IL-2Rα with daclizumab for treatment of multiple sclerosis. Nat Rev Neurol. doi: 10.1038/nrneurol.2013.95

Wilder ME, Cram LS (1977) Differential fluorochromasia of human lymphocytes as measured by flow cytometry. J Histochem Cytochem 25:888–91.

Wu AR, Neff NF, Kalisky T, et al (2014) Quantitative assessment of single-cell RNA-sequencing methods. Nat Methods 11:41–6. doi: 10.1038/nmeth.2694

Yamasaki R, Lu H, Butovsky O, et al (2014) Differential roles of microglia and monocytes in the inflamed central nervous system. J Exp Med jem.20132477–. doi: 10.1084/jem.20132477

Yona S, Jung S (2010) Monocytes: subsets, origins, fates and functions. Curr Opin Hematol 17:53–59. doi: 10.1097/MOH.0b013e3283324f80

Zhang B, Yamamura T, Kondo T, et al (1997) Regulation of experimental autoimmune encephalomyelitis by natural killer (NK) cells. J Exp Med 186:1677–87.

Zielinski CE, Mele F, Aschenbrenner D, et al (2012) Pathogen-induced human T(H)17 cells produce IFN-γ or IL-10 and are regulated by IL-1β. Nature. doi: 10.1038/nature10957

Zunder ER, Finck R, Behbehani GK, et al (2015) Palladium-based mass tag cell barcoding with a doublet-filtering scheme and single-cell deconvolution algorithm. Nat Protoc 10:316–333. doi: 10.1038/nprot.2015.020

Acknowledgements

Firstly, I would like to very much thank Burkhard Becher for inviting me into his lab, for the scientific freedom and trust, for providing a thriving scientific environment and for his enduring support. I really learned a lot in these four years and it motivated me to go on.

Additionally, I am very grateful to my PhD committee members Roland Martin and Christian Münz. I received plenty of support, help and useful comments from both of them.

This work would not have been possible without Tomas Olsson and his colleagues who provided most of the patient samples used in these studies and of course without all the patients and healthy people willing to donate their blood for research.

Further, I want to thank Laura Codarri who provided the basis for many aspects of my PhD work and who taught me a lot when I arrived in the lab. Vinko and Florian introduced me to the advanced world of cytometry and were always there to answer questions. Thanks also to Andy who always kept me up to date with the world of mouse immunology. Additionally, I want to thank Ines for helping me to organize everything. Edoardo and Ekaterina were very valuable with experiments and spotting the little mistakes in this thesis.

I also want to mention especially my family and friends here, who always provided me with the necessary backing and support in so many ways. And, of course, Dunja who made my life here in Zurich so much more joyful.

Curriculum Vitae

Name: Felix Jerg Hartmann
Born 03.03.1986 in Stuttgart, Germany
Email: hartmann.immunology@gmail.com
Phone:+49-151-44244353
Web: researchgate.net/profile/Felix_Hartmann

EDUCATION & EMPLOYMENT

August 2015 - present	Staff Scientist Mass Cytometry *(15%)* Mass Cytometry Facility University of Zurich, Zurich, Switzerland
January 2012 - present	PhD Thesis "Pathogenic Mediators in Multiple Sclerosis – The Role of GM-CSF and other T_H Cell Cytokines" Prof. B. Becher, Inflammation Research Institute of Experimental Immunology, University of Zurich, Zurich, Switzerland
September 2009 - December 2011	M.Sc. Molecular Biotechnology (grade average 1.1) Master thesis "HER2-Specific Regulatory T Cells in Breast Cancer Patients" Prof. P. Beckhove, Translational Immunology German Cancer Research Center (dkfz) and University of Heidelberg, Heidelberg, Germany
April 2010 - September 2010	Research internship "Exploring the Anti-Inflammatory Potential of Regulatory T-bodies in Inflammation-Associated Cancer" Prof. Z. Eshhar, Department of Immunology Weizmann Institute of Science, Rehovot, Israel
October 2006 - August 2009	B.Sc. Molecular Biotechnology (grade average 1.5) Bachelor thesis "Toxicity of Bioenhancers and Liposomal Formulations for Peroral Application in the Caco-Cell Model" Prof. G. Fricker, Pharmaceutical Technology & Pharmacology Institute of Pharmacy and Molecular Biotechnology University of Heidelberg, Heidelberg, Germany
September 1996 - June 2006	German University Entrance Qualification (Abitur) grade average 1.1 Otto-Hahn-Gymnasium, Ludwigsburg, Germany

AREA OF RESEARCH

My primary research interest is to understand the pathogenic mechanisms underlying autoimmune diseases such as multiple sclerosis, type 1 diabetes, rheumatoid arthritis or narcolepsy. Additionally, I am studying basic T cell functions, their modulation by genetic and environmental factors and their interaction with other immune cells.
Regarding these subjects, we recently demonstrated that a multiple sclerosis-associated genetic risk factor modulates T_H cell production of the pathogenic cytokine GM-CSF. Additionally, we could show that elevated production of this cytokine is linked to MS disease severity (Hartmann et. al (2014). *Nat. Commun.*) Currently, we are employing high-dimensional mass cytometry analysis to reveal cytokine production patterns by T_H cell subsets and their divergence under several inflammatory conditions.

GRANTS AND AWARDS

January 2016	Pfizer Research Prize, Pfizer Foundation, Switzerland
October 2015	Poster Prize, MS Researcher Meeting, Switzerland
April 2015	Research grant, Swiss Multiple Sclerosis Society, Switzerland
April 2014	Research grant, Swiss Multiple Sclerosis Society, Switzerland
October 2013	Presentation Award, Conference on Autoimmunity, Corfu, Greece
January 2012-2014	PhD fellowship, van Riemsdijk Foundation for MS research, Switzerland

MEMBERSHIPS

Since 2014	German Society of Immunology (DGfI)

PRESENTATIONS AND POSTERS

2015 MS Researcher meeting of the Swiss MS Society, Berne, Switzerland (poster)

2015 European Congress of Immunology (ECI), Vienna, Austria (poster)

2015 NIF Winter School on Advanced Immunology, Singapore (oral presentation and poster)

2014 World Immune Regulation Meeting (WIRM), Davos, Switzerland (poster)

2014 Young Investigators in MS meeting, Grindelwald, Switzerland (oral presentation)

2013 6th International Conference on Autoimmunity, Corfu, Greece (oral presentation)

2013 MS Researcher meeting of the Swiss MS Society, Berne, Switzerland (poster)

2013 Young Investigators in MS meeting, Grindelwald, Switzerland (oral presentation)

2012 MS Researcher meeting Swiss MS Society, Geneva, Switzerland (oral presentation)

SCIENTIFIC PUBLICATIONS

Felix Jerg Hartmann
Inflammation Research
Institute of Experimental Immunology
University of Zurich, Zurich, Switzerland
hartmann.immunology@gmail.com

Mair F*, **Hartmann FJ***, Mrdjen D, Tosevski V, Krieg C & Becher B (2016). The end of gating? An introduction to automated analysis of high dimensional cytometry data. *European Journal of Immunology*. ***contributed equally**

Croxford AL, Lanzinger M, **Hartmann FJ**, Pelczar P, Clausen B, Jung S, Greter M & Becher B (2015). GM-CSF Drives the Inflammatory Signature of $CCR2^{+}$ Myeloid Cells and Licences Autoimmune Inflammation. *Immunity*.

Hartmann FJ, Khademi M, Aram J, Ammann S, Kockum I, Constantinescu C, Gran B, Piehl F, Olsson T, Codarri L & Becher B (2014). Multiple Sclerosis-associated *IL2RA* Polymorphism Controls GM-CSF Production in Human T_H Cells. *Nature Communications.*

Schmidt HH, Ge Y, **Hartmann FJ**, Conrad H, Klug F, Nittel S, Bernhard H, Domschke C, Schuetz F, Sohn C, Beckhove P (2013). HLA Class II tetramers reveal tissue-specific regulatory T cells that suppress T-cell responses in breast carcinoma patients. *Oncoimmunology*.

Parmentier J, **Hartmann FJ**, Fricker G (2010). In vitro evaluation of liposomes containing bio-enhancers for the oral delivery of macromolecules. *European journal of pharmaceutics and biopharmaceutics*.